Max-Planck-Institut für Kolloid- und Grenzflächenforschung

Abteilung für Kolloidchemie

Self-assembly behavior in hydrophilic block copolymers

Dissertation

zur Erlangung des akademischen Grades
„doctor rerum naturalium"
(Dr. rer. nat)
in der Wissenschaftsdisziplin „Polymer- und Kolloidchemie"

eingereicht an der
Mathematisch-Naturwissenschaftlichen Fakultät
der Universität Potsdam

von

Clara Valverde Serrano

geboren am 02.10.1984 in Murcia (Spanien)

Potsdam, Mai 2011

Abstract

Block copolymers are receiving increasing attention in the literature. Reports on amphiphilic block copolymers have now established the basis of their self assembly behavior: aggregate sizes, morphologies and stability can be explained from the absolute and relative block lengths, the nature of the blocks, the architecture and also solvent selectiveness. In water, self-assembly of amphiphilic block copolymers is assumed to be driven by the hydrophobic. The motivation of this thesis is to study the influence on the self-assembly in water of A-*b*-B type block copolymers (with A hydrophilic) of the variation of the hydrophilicity of B from non-soluble (hydrophobic) to totally soluble (hydrophilic).

Glucose-modified polybutadiene-*block*-poly(N-isopropylacrylamide) copolymers were prepared and their self-assembly behavior in water studied. The copolymers formed vesicles with an asymmetric membrane with a glycosylated exterior and poly(N-isopropylacrylamide) on the inside. Above the low critical solution temperature (LCST) of poly(N-isopropylacrylamide), the structure collapsed into micelles with a hydrophobic PNIPAM core and glycosylated exterior. This collapse was found to be reversible. As a result, the structures showed a temperature-dependent interaction with L-lectin proteins and were shown to be able to encapsulate organic molecules.

Several families of double hydrophilic block copolymers (DHBC) were prepared. The blocks of these copolymers were biopolymers or polymer chimeras used in aqueous two-phase partition systems. Copolymers based on dextran and poly(ethylene glycol) blocks were able to form aggregates in water. Dex_{6500}-*b*-PEG_{5500} copolymer spontaneously formed vesicles

with PEG as the "less hydrophilic" barrier and dextran as the solubilizing block. The aggregates were found to be insensitive to the polymer's architecture and concentration (in the dilute range) and only mildly sensitive to temperature. Variation of the block length, yielded different morphologies. A longer PEG chain seemed to promote more curved aggregates following the inverse trend usually observed in amphiphilic block copolymers. A shorter dextran promoted vesicular structures as usually observed for the amphiphilic counterparts. The linking function was shown to have an influence of the morphology but not on the self-assembly capability in itself. The vesicles formed by dex_{6500}-b-PEG_{5500} showed slow kinetics of clustering in the presence of Con A lectin. In addition both dex_{6500}-b-PEG_{5500} and its crosslinked derivative were able to encapsulate fluorescent dyes. Two additional dextran-based copolymers were synthesized, dextran-b-poly(vinyl alcohol) and dextran-b-poly(vinyl pyrrolidone). The study of their self-assembly allowed to conclude that ATPS is a valid source of inspiration to conceive DHBCs capable of self-assembling. In the second part the principle was extended to polypeptide systems with the synthesis of a poly(N-hydroxyethylglutamine)-$block$-poly(ethylene glycol) copolymer. The copolymer that had been previously reported to have emulsifying properties was able to form vesicles by direct dissolution of the solid in water. Last, a series of thermoresponsive copolymers were prepared, dextran-b-$PNIPAM_m$. These polymers formed aggregates below the LCST. Their structure could not be unambiguously elucidated but seemed to correspond to vesicles. Above the LCST, the collapse of the PNIPAM chains induced the formation of stable objects of several hundreds of nanometers in radius that evolved with increasing temperature. The cooling of these solution below LCST restored the initial aggregates.

This self-assembly of DHBC outside any stimuli of pH, ionic strength, or temperature has only rarely been described in the literature. This work constituted the first formal attempt to frame the phenomenon. Two reasons were accounted for the self-assembly of such systems: incompatibility of the polymer pairs forming the two blocks (enthalpic) and a considerable solubility difference (enthalpic and entropic). The entropic contribution to the positive Gibbs free energy of mixing is believed to arise from the same loss of conformational entropy that is responsible for *"the hydrophobic effect"* but driven by a competition for water of the two blocks. In that sense this phenomenon should be described as the "***hydrophilic effect***".

Table of Contents

Chapter 1:   Introduction

"In order to assemble into vesicular objects, block copolymers need to have at least two incompatible blocks that have a different solubility in the liquid where vesicle formation takes place."

Napoli A., Sebok D., Senti D., and Meier W. [1]

The study of self-assembly involving low molecular weight surfactants into colloidal structures is now a mature field of supramolecular chemistry. Besides being well-established in industrial applications, the principles of their self-assembly are now well-understood. The study of the role of the hydrophilic "head" and the hydrophobic "tail" allows the straight-forward prediction of the solution behavior and therefore also the design of given surfactants for a given application. More recently, block copolymers have received increasing attention due to the fact that their assemblies have potential applications in drug delivery and other

medical applications, imaging and sensing and even catalysis. In the literature, reports on amphiphilic block copolymers have now established the basis of the self assembly behavior: aggregate sizes, morphologies, stability can be explained from the absolute and relative block lengths, the nature of the blocks, architecture and also solvent selectiveness.

In water, self-assembly of amphiphilic block copolymers is assumed to be driven by the hydrophobic effect, an entropic effect, that promotes the segregation of the hydrophobic block and water to overcome the loss of conformational entropy. In a classic amphiphilic system, in the dilute regime, this segregation will lead to different aggregates such as micelles, worm-like micelles, vesicles…(Figure 1.1).
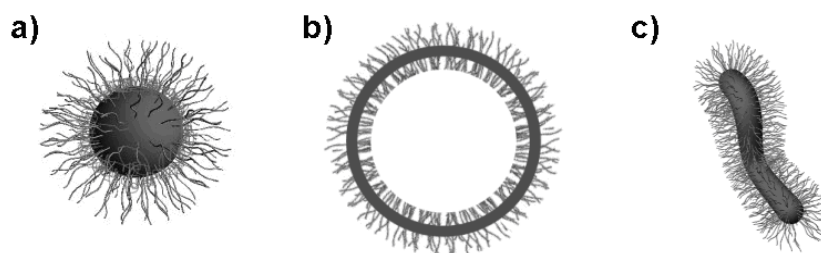
Figure 1.1: Example of structures that can be formed by block copolymers in selective solvent. a) micelles b) vesicles c) rod-like micelles. Reproduced from [29].

The morphology of these structures is typically predicted and controlled by fixing the absolute and the relative length of the blocks. More complexity can be introduced by deviating from this simple models by varying the hydrophilic/hydrophobic balance in these polymers. The underlying motivation of this thesis is to study the influence in the self-assembly in water of block copolymers of the A-*b*-B type (A hydrophilic) with the hydrophilicity of B varying from non-soluble (hydrophobic) to totally soluble (hydrophilic).

Chapter 2 deals with the basic principles on which the thesis is built. First a brief introduction to aqueous two-phase partition systems and cell microcompartmentation is given. Briefly, some basic principles concerning structure formation of block copolymers are addressed as well as a quick view on the polymerization techniques and associated tools used in this work.

Biomacromolecules crowd the interior and exterior of cells giving raise to a variety of physico-chemical phenomena that direct a certain number of structural and functional characteristics of cells including phase separation. This phase separation is analogous to the aqueous phase separation exploited in aqueous two-phase partition systems (ATPS) techniques in biological sciences that uses polymer-polymer-water ternary systems. From this point of view, microcompartmentation and ATPS can be used as inspiration to develop new block copolymers potentially able to microphase separate in water. Ideal candidates are block copolymers made of biopolymers or polymer chimeras known to phase separate in ATPS systems. The covalent link between the two blocks should introduce compatibility, but if the incompatibility remains high enough and solubility difference is strong, phase separation could take place leading to the formation of self-assembled aggregates as we know them. **Chapter 3** deals thus with the synthesis, characterization and study of aggregates formed by double hydrophilic block copolymers (DHBC) engineered to self-assemble outside any stimuli of pH, ionic strength, or temperature (see Appendix III for a comprehensive review of literature examples). Several block copolymers systems inspired from ATPS and microcompartmentation in cells are studied. The introductory paragraph of the chapter attempts to present the basic thermodynamic background backing the potential microphase separation of hydrophilic$_1$-hydrophilic$_2$ block copolymers. Both entropic and enthalpic reasons can be advanced to suggest such behavior in well chosen polymer pairs. The parameters leading to $\Delta G_m > 0$ are considered and translated to practical terms first with a quick study of a poly(ethylene glycol)/dextran/water system and later to the dextran-block-poly(ethylene glycol) copolymer in water system. A family of dextran-*b*-PEG copolymers is thus studied and the characterization of the colloids introduced with a continuous comparison with the behavior of amphiphilic copolymer systems. Different conditions of temperature and concentration are tested as well as the variation of structural parameters known to affect the self-assembly process and phase diagram of copolymers: block lengths, linking units and architecture. Because dextran is a highly relevant molecule in the biological context, this system was preliminary tested for its interaction with L-lectin type of proteins and encapsulation properties. Two additional dextran-based systems were synthesized, dextran-*block*-poly(vinyl alcohol) and dextran-*block*-poly(vinyl pyrrolidone) to help prove the validity of ATPS as a source of inspiration to engineer such systems. In the

second part of the chapter, a polypeptide system based on poly(N-hydroxyethyl glutamine) was studied and a thermoresponsive synthetic system based on Poly(N-isopropylacrylamide) helped extend and complexify this particular self-assembly behavior of double hydrophilic block copolymers.

In **Chapter 4**, hydrophilically modified amphiphilic polymers were studied. Inspired by the glucose-modified polybutadiene-block-poly(ethylene glycol) previously reported,[2] glucose-modified polybutadiene-block-poly(N-isopropylacrylamide) thermoresponsive polymers were prepared. Their self-assembly behaviour at room temperature and above the low critical solution temperature of poly(N-isopropylacrylamide) were studied. Their temperature-dependent interaction with L-lectin proteins and encapsulation properties were tested.

Chapter 2:   Basic Principles

2.1   ATPS and microcompartmentation in cells

2.1.1 Aqueous two phase systems (ATPS)

ATPS is a liquid-liquid extraction technique. When two polymers or a salt and a polymer are mixed together at appropriate concentrations and at a particular temperature, phase separation can occur. Since the bulk of both phases is water, they constitute mild but physico-chemically differentiated environments where biomaterials can be driven to a preferential phase according to their characteristics such as isoelectric point, surface hydrophobicity and molar mass (Figure 2.1).[3]-[5] This phenomenon has been exploited for the recovery and partial purification of biological material including proteins, genetic material, nanoparticles, low molecular weight molecules, and even cell organelles and cells.[6] Besides the general advantages associated with liquid-liquid extraction techniques (short phase separation time, scalability, low-cost…), ATPS techniques show an enhanced attractiveness when compared

with classic organic solvent extraction associated with the fact that it assures protein stability, suppresses the use of VOCs, and most components can be recycled.

ATPS can be classified into four groups according to the chemical entities causing the phase separation. The first one is constituted of two nonionic polymers in a polymer-polymer-solvent ternary system. This category comprises the most widely studied system dextran/ poly(ethylene glycol) (PEG) as well as PEG/polyvinyl alcohol (PEG/PVOH), dextran/ polypropylene glycol (PPG)… The second one is constituted of a nonionic polymer and a polyelectrolyte where the most studied systems are dextran sulfate-based systems (dextran sulfate/ PEG, dextran sulfate/ PPG, but also carboxymethylcellulose/ methycellulose,…). The third is constituted of two polyelectrolytes such as dextran sulfate/ carboxymethyldextran or carboxymethylcellulose/ carboxymethyldextran). The fourth category is constituted by a nonionic polymer and a low-molecular weight compound, typically a kosmotropic salt (PEG/ ammonium sulfate, PEG/ phosphate ...). A slightly dated list of polymer systems capable of phase separation in aqueous media was given in Boris Y. Zaslavsky in his excellent book on the topic.[7]
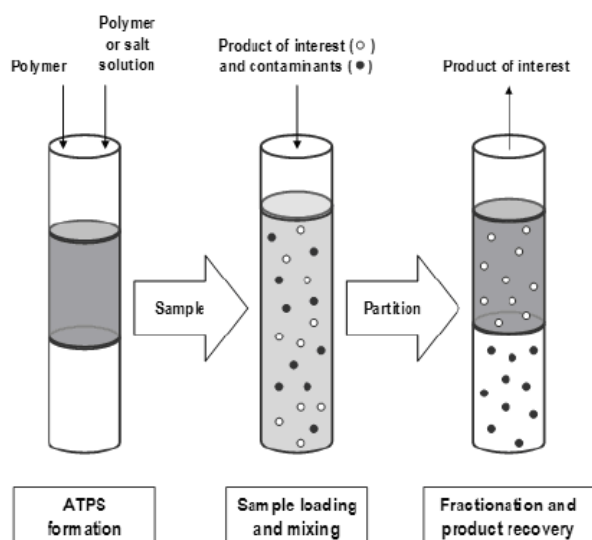
Figure 2.1: Simplified representation of the fractionation of bioparticles in aqueous two-phase processes. Reproduced from [6].

The phase separation in these systems can always be described by a phase diagram called coexistence curve or binodal (Figure 2.2). Under the binodal we find the homogenous region,

and above the binodal the biphasic region.[8] This phase diagram also provides information such as the composition of the coexisting phases and the tie-line at a given concentration. Thermodynamically the phase separation in these systems can be easily explained in terms of Gibbs free energy of mixing (Equation 1).

$$\Delta G_m = \Delta H_m - T \Delta S_m > 0 \qquad (1)$$

When the gain in entropy of mixing is not large enough to compensate for the repulsive polymer–polymer interaction enthalpy, the mixing of the two polymers is thermodynamically unfavorable and phase separation occurs.
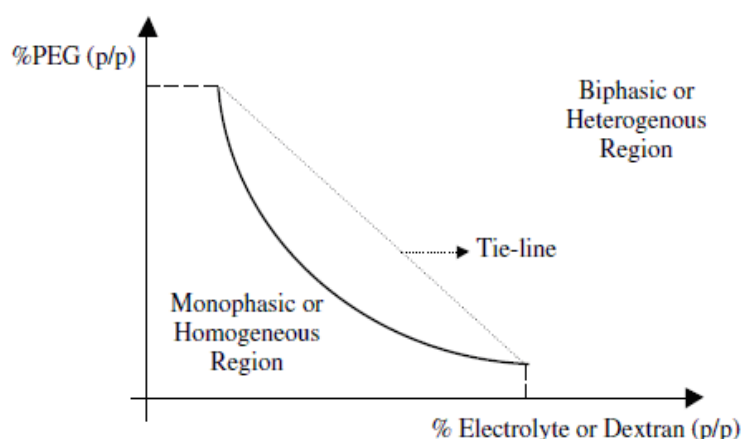
Figure 2.2: Schematic phase diagram for a general aqueous two-phase system (PEG/electrolyte or PEG/Dextran). The coexistence curve is represented by the full curve, the dashed line represents the tie-line. Reproduced from [8].

The main idea around which Chapter 3 was developed was inspired by the first category of systems, the phase separation of two non-ionic polymers in water, namely PEG/dextran systems. Several phase diagrams have been established for this system at different temperatures and with different molar masses and polydispersities. The general outcome of them is that phase separation of ternary mixtures can happen with relatively low molecular mass polymers but also at relatively low concentrations.[9] And although high molecular masses are often preferred because they sharpen the partition coefficient of the biomolecule to purify, ATPS remains a source of inspiration for some biological phenomena, such as

microcompartmentation in cells.

2.1.2 Microcompartmentation in cells
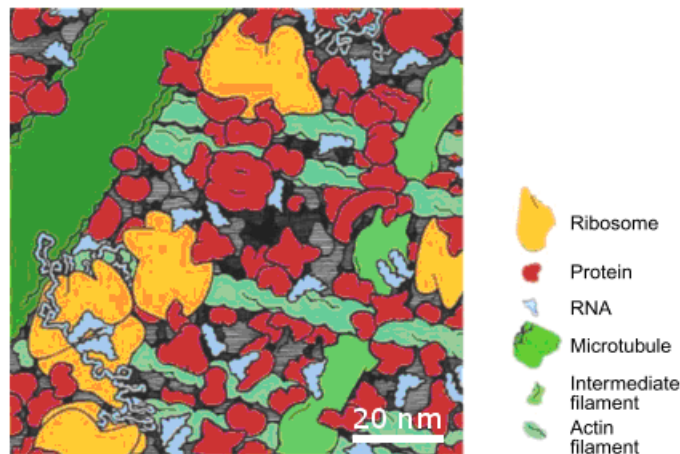
Figure 2.3: Figure 3: The crowded state of the cytoplasm in eukaryotic cells. The sizes, shapes and numbers of macromolecules are approximately correct. Small molecules are not shown. Reproduced from [13]. Originally published in [14].

The inside of living cells is a crowded space. The total concentration of macromolecules is extremely high (10 to 50 wt% depending on the cell type[10]) in both eukaryotic cytoplasm and prokaryotic cells (Figure 2.3). It is known for example that the concentration of proteins and RNA in *E. Coli* is around 300-400 g·L^{-1} [11] and that red blood cells contain about 350 g·L^{-1} of hemoglobin alone.[12] This has profound implications on diffusion, reaction rates and equilibria of interactions involving macromolecules.[10][13] All these implications have been traditionally attributed to the excluded volume effect by proving that first, diffusion of both small and macro- molecules are reduced in the cytoplasm by factors up to 10-fold[14][15] dropping the rate of any diffusion-limited process. Secondly, that it favors the protein's more compact conformation i.e. the native biological active one[16][17] enhancing thus the rates of biochemical reactions when they are not diffusion-limited. And last, that it also promotes collisions and electrostatic interactions in proteins, affecting the equilibrium of interactions by two or three orders of magnitude.[11][14]

But excluded volume cannot explain directly the fact that the solvent viscosity of the cytoplasm is not substantially different from the viscosity of water itself. Ovádi *et al.*[18]

suggested that this observation could only be explained if the intracellular medium was heterogeneous as reported previously by Clegg *et al.*[19] and Porter *et al.*[20]: the inside of the cell is divided into water-rich phases and protein-rich phases. Experimental evidence was later given[21] that virtually all cytoplasmic proteins have non-diffusive forms, and this could be explained by highly organized regions inside the cytoplasm. This heterogeneity has since been linked to a microcompartmentation phenomenon defined as the functional isolation of molecules to create local composition differences[22] or compartments. This compartmentation is indeed supposed to facilitate metabolic pathways.[23]

No particular protein is concentrated enough to phase separate with another protein but since a protein can only occupy the non-excluded volume in the crowded cytoplasm, its effective concentration is much higher than expected. This effective concentration is similar to the total polymer concentration used in ATPS and can lead to multiphase separation inside the cytoplasm.[24] This phase separation is today believed to be responsible for the microcompartmentation observed in cells.[25]
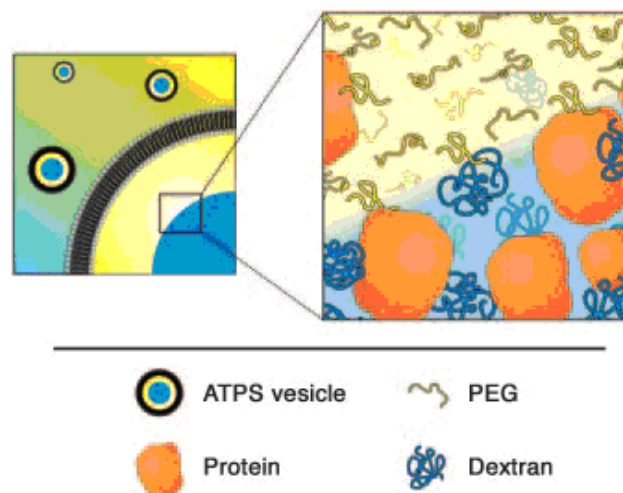
Figure 2.4: Synthetic cell model developped by Long *et al.* developed a dextran/polyethylene glycol ATPS inside a giant vesicles (GV) as a primitive cell model. Reproduced from .

ATPS has since been used to mimic the dynamic intracellular microcompartmentation. Long *et al.*[26] developed a dextran/polyethylene glycol ATPS inside a giant vesicles (GV) as a primitive cell model (Figure 2.4). It was shown that biological material such as DNA could indeed be compartmentalized inside these GVs.

It is not surprising that dextran systems are able to mimic microcompartmentation in biological media as polysaccharides also contribute to molecular crowding. Outside the cells, polysaccharides are found in high concentration in the extracellular matrix of tissues such as collagen[14] and in the glycocalyx on the outer membrane surface of cells.[27]

2.2   Phase behavior of block copolymers

2.2.1 Phase behavior of block copolymers in bulk

Most polymer pairs are incompatible. As a result upon mixing, the enthalpic contribution (usually positive and decreasing with temperature) to the free energy of mixing of the two components is greater than the magnitude of the entropic contribution (always negative and ideally temperature-independent), and the polymers phase separate to minimize the interaction.[28] In block copolymers of two incompatible blocks ((AB)$_n$ type, n=1 for diblocks, n=2 for triblocks…) linked by covalent bonds, a combination of long-range repulsive forces (physicochemical incompatibility) and short-range attractive forces (covalent bonding) manifests. As a consequence the block copolymer in bulk undergoes a microscopic phase separation to minimize the system's free energy as demixing is preluded by the covalent bond. This microscopic phase separation leads to a number of ordered phases in the nanometric length scale. Common morphologies include hexagonally packed cylinders, lamellar phases, and bicontinous phases among others (Figure 2.5, right).[29][30] The phase behavior of a given copolymer is determined by three experimentally controllable factors: the overall degree of polymerization N, the architectural constraints (n and the overall volume fraction f of the block A) and the A-B Flory-Huggins polymer-polymer interaction paramenter χ_{AB} (representing the strength of the repulsive interaction between A and B).[31]

Since the enthalpic and entropic contributions to the free energy are proportional to N^{-1} and χ, the product χN dictates the block copolymer phase state. This microphase separation can thus be represented by phase diagram of χN against f [32] (Figure 2.5, left). Two regimes of this diagram are usually identified, a weak segregation limit (WSL) for $\chi N \sim 10$ where both

blocks are miscible, a strong segregation limit (SSL) for $\chi N \sim$ 10-100 where the different ordered phases are stable. Rarely,[33][34] a super strong segregation limit (SSSL) for $\chi N \gg 100$ appears in will each domain of the phase contains purely one of the two blocks and the interface is strictly the covalent bond.
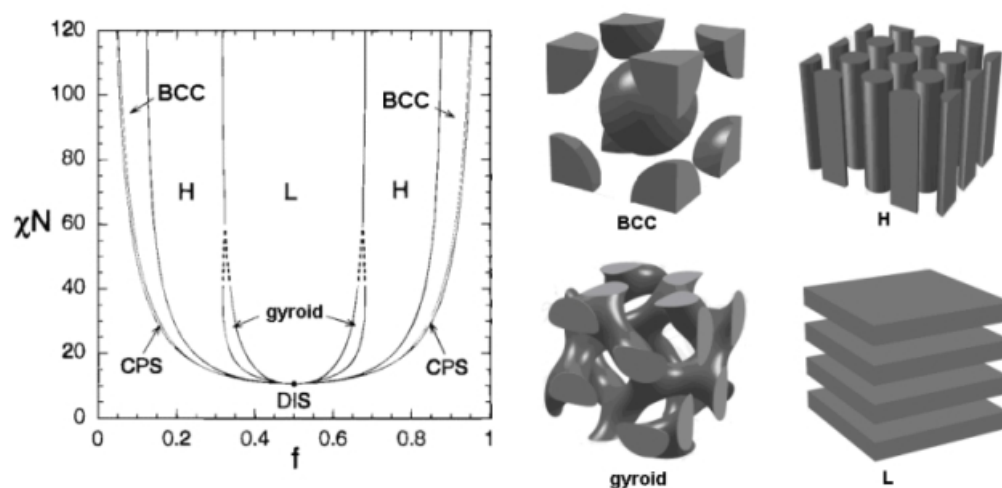
Figure 2.5: Left: Mean-field phase diagram for conformationally symmetric diblock melts. Right: representation of different ideal block copolymer phases in bulk. BCC (bcc spheres), H (hexagonally packed cylinder), L (lamellae), gyroid (bicontinous gyroid), CPS (closely packed spheres). DIS stands for disordered state. Reproduced from [29] and [30].

It should be noted that because χ varies with T^{-1}, it is possible to induce phase transitions (order-disorder transition ODT, order-order transition OOT) by cooling a polymer melt. In other words in the diagram, transition between phases for a given f can be achieved by varying the temperature. In dilute and semi-dilute regimes, i.e. in copolymer- solvent(s) systems, lyotropic phases can be formed.

2.2.2 Phase behavior of block copolymers in solution

The phase behavior of block copolymers in solution depends not only on the Flory-Huggins polymer-polymer interaction parameter χ_{AB} (considering the simplest AB type copolymer), but also on the polymer-solvent interaction parameters χ_{AS} and χ_{BS}[35] and even concentration.[36] An effective Flory-Huggins interaction parameter can be written from this

combination (Equation 2).

$$\chi_{eff} = \varphi(\chi_{AB} + \Delta\chi) = \varphi(\chi_{AB} + |\chi_{AS} - \chi_{BS}|) \qquad (2)$$

where φ is the volume concentration of the copolymer in the solvent. In the case of a neutral solvent (good solvent for both A and B), $\Delta\chi \to 0$ and the effective Flory-Huggins interaction parameter becomes $\chi_{eff} \approx \varphi\chi_{AB}$. Because then $\chi_{eff}N \approx \varphi\chi_{AB}N$, the addition of a neutral solvent ($\varphi<1$) can induce an ODT (Figure 2.6). In other words the addition of a non-selective solvent can increase compatibility. In practical terms a block copolymer in a non-selective solvent in the absence of specific interactions adopts a coil conformation where the monomer subunits are oriented randomly.
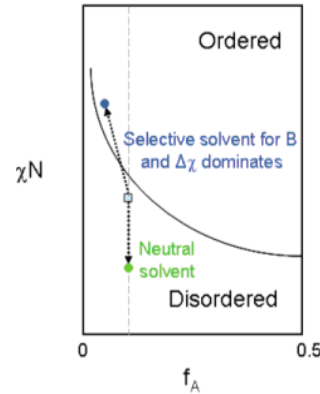
Figure 2.6: : Schematic phase diagrams for a typical diblock copolymer to show the effects of both neutral and selective solvents. Reproduced from [35].

By addition of a selective solvent the description is more complex due to the interplay between φ and $\Delta\chi$. The solvent swells preferentially a block (e.g. block B) and changes the volume fraction of the other block (block A) modifying thus the interaction parameter as follows in equations (3) and (4).

$$f \approx f_A\varphi \qquad (3)$$

$$\chi_{eff}N \approx \varphi(\chi_{AB} + \Delta\chi)N = \varphi(\chi_{AB} + |\chi_{AS} - \chi_{BS}|)N \qquad (4)$$

So generally, a large $\Delta\chi$ will raise $\chi_{eff}N$ from a disordered into an ordered state (Figure 2.6). Because the volume fraction of A can significantly decrease by addition of a selective solvent for B, the consequent decrease in f_A can cause an OOT as in Hanley's work[36] where a polystyrene-*block*-polyisoprene showed sequential phase changes from from lamella (L), to perforated layer (PL) to gyroid (G) to cylinder (C) by addition of selective solvent.

2.2.2.a Amphiphilic copolymers in water

In practice, in colloid chemistry the addition of a selective solvent for one block to a block copolymer produces aggregates in dilute solution. For example, amphiphilic block copolymers in water tend to self-assemble into well-defined structures. From the simplest case of the spherical micelles with a hydrophobic core and a hydrophilic corona to more complex geometries like vesicles or rod-like micelles (Figure 1.1) they all correspond to energy minima.

In water, the self-assembly of block copolymers is assumed to be driven by the hydrophobic effect.[37] In order to minimize the unfavorable interaction of water molecules with the hydrophobic block, this latter tends to segregate into a solvent-poor phase with the hydrophilic block forming a corona and promoting solubility.

The observed morphologies of these aggregates depend strongly on the geometry of the single blocks and can be predicted by the so-called critical packing parameter.[38] This dimensionless parameter first developed for low-molecular weight surfactants is now extensively applied for block copolymers (Equation (5)):

$$\rho = \frac{V}{a_0 \cdot l} \qquad (5)$$

where V is the volume occupied by the hydrophobic block, l its length and a_0 the area occupied by the hydrophilic block. $\rho < 0.5$ favors aggregates with high curvation radii such as micelles while $\rho > 0.5$ promotes the formation of less curved bilayer structures such as vesicles and lamellae. It is common for block copolymers to consider the relative size of the hydrophilic and hydrophobic blocks to predict the geometry of the aggregates. A decrease in the hydrophilic block length with respect to the hydrophobic promotes less-curved aggregates.[39]

Besides classic amphiphilic block copolymers, a rather new class of copolymers capable of forming phases following a stimulus have emerged. This aggregation exploits the properties of certain synthetic polymers to respond by abrupt changes in their chemical and physical properties to external stimuli. Outside stimuli these copolymers are formed by two water soluble blocks (double hydrophilic block copolymers: DHBCs) and adopt random coil conformation in water . When an adequate stimulus is applied, one of the blocks becomes hydrophobic turning the system into an amphiphilic copolymer in water that aggregates. Generally by stopping the stimulus the aggregation can be reversed.

In stimuli-controlled self-assembly of DHBC the main stimuli used are pH, ionic strength, and temperature.[40]-[44] In the next paragraph a theoretical and practical overview of thermo-controlled aggregation of DHBCs in water relevant to this work is presented.

2.2.2.b Thermo-responsive block copolymers

Similarly to the thermodynamic dependencies for block copolymers-solvent systems, for single polymer-solvent binary systems, the thermodynamics also depend on the polymer-solvent interaction. Solvent quality can be tuned for instance by temperature, co-solvent addition, pH... As the solvent quality is decreased it becomes energetically favorable for the system to minimize the contact with solvent molecules promoting thus the polymer chain-polymer chain interactions. In practical terms, by decreasing the solvent quality the random coil (that represents the conformational lowest energy in a good solvent) collapses into mesoglobules that, except in very dilute solution,[45] subsequently aggregate leading to a

macroscopic phase separation (precipitation). Inversely, increasing the solvent quality favors solvent-polymer chains interaction promoting the solubilization of the polymer.

Formally, the modified[46] Flory-Huggins expression for the Gibbs free energy[47] of mixing can be expressed as in Equation (6).

$$\Delta G_m = RT \left[\varphi_A \ln \varphi_A + \varphi_S \ln \varphi_S + g \, \varphi_A \varphi_S \right] \qquad (6)$$

where R is the ideal gas constant, and φ_A is the volume fraction of the polymer (A) or the solvent (S) and g an empirical dependence term introduced to improve agreement with experimental data that corresponds to an interaction energy term.

The expression for totally miscible system corresponds to $\Delta G_m < 0$ and the second derivative of the Gibbs free energy of mixing with respect to the volume fraction of polymer or solvent positive $\left(\dfrac{\partial^2 \Delta G_m}{\partial \varphi_A^2} \right)_{p,T} > 0$. When a solution exhibits a minimum or minima in the ΔG_m versus composition curve ($\left(\dfrac{\partial \Delta G_m}{\partial \varphi_A} \right)_{p,T} = 0$) it will separate at equilibrium into two phases at such point(s). In a phase diagram of temperature against composition, that transition is represented by the binodal (or coexistence) curve. The condition $\left(\dfrac{\partial^2 \Delta G_m}{\partial \varphi_A^2} \right)_{p,T} = 0$ represents the spinodal curve in such diagram. The region delimited by the binodal and the spinodal curve represents a metastable phase (in which phase-separation takes place *via* a nucleation-growth mechanism), whereas under the spinodal it is an unstable region (and phase separation takes place *via* spinodal decomposition). The point at which the spinodal touches the binodal is the critical point $\left(\dfrac{\partial^3 \Delta G_m}{\partial \varphi_A^3} \right)_{p,T} = 0$.

15
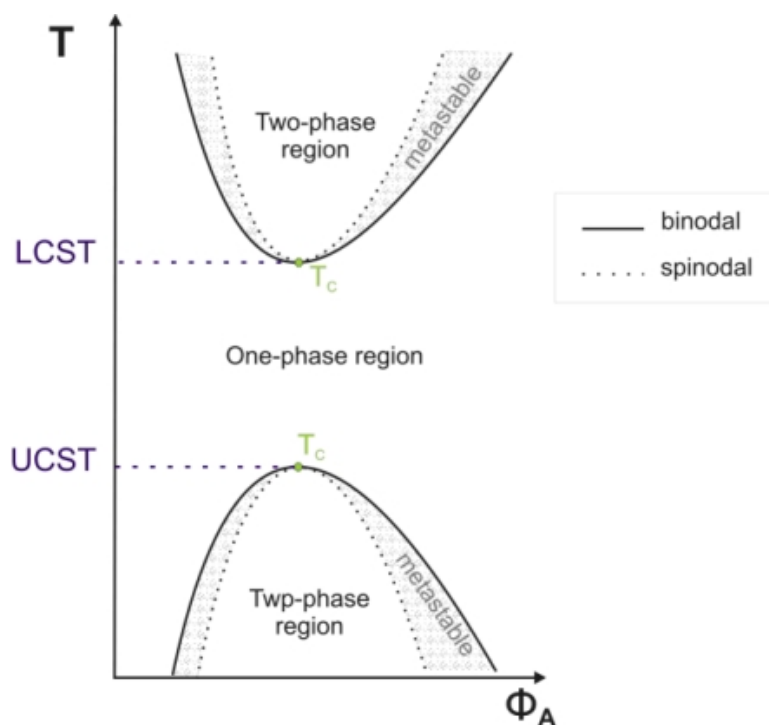
Figure 2.7: General phase diagram of a polymer in a solvent. The relative position of the LCST and UCST are arbitrary, inversing them would describe the situation of a polymer is not soluble in a solvent in the whole temperature range.

In practical terms, all polymers exhibit a minimum and a maximum point upon heating or cooling. This can be represented by a phase diagram (Figure 2.7). The upper critical solution temperature (UCST) represents the maximum and the lower critical solution temperature (LCST) the minimum. When the critical temperature UCST or LCST are in the range in which the solvent is liquid, the polymer is called thermoresponsive because by the application of a thermal stimulus (heating or cooling) a transition is induced. The most well-known example of polymer exhibiting a UCST near room temperature and a LCST at higher temperature is polystyrene in cyclohexane.[48] An exhaustive list of polymers exhibiting UCST and/or LCST behavior can be found in the literature.[49]

In water, LCST behavior arises from a balance between hydrophilic and hydrophobic moieties within a repeating unit.[50] The most studied example is poly(N-isopropyl acrylamide) (PNIPAM) that contains an hydrophobic isopropyl group and hydrophilic acrylamide backbone whose balance sets the LCST at ~ 32 °C. When this temperature does not correspond to the critical point but is rather the temperature of the coil-to-globule

transition at a given concentration, it is called the cloud point (CP). The CP slightly depends on the polymer molar mass and can be tuned either by copolymerization of PNIPAM with other monomers or addition of salts, surfactants…The transition can be monitored by turbidimetry[51] and shows a relatively large hysteresis upon cooling due to intramolecular interactions between PNIPAM chains in the collapsed state.

The synthesis of DHBCs (or graft copolymers) with a thermoresponsive block presenting a LCST allows the access to a new class of "smart" nanomaterials. Upon temperature-induced collapse of the responsive block, the mesoglobule is stabilized by the other block forming micelle-like structures. Because this transition is reversible, the micellization is switchable and presents itself with a great potential for drug delivery and sensing applications.

One of the first and more widely studies examples of thermo-responsive micellization is with poly(ethylene glycol)-*block*-poly(propylene glycol) (PEG-*b*-PPG or PEO-*b*-PPO) and poly(ethylene glycol)-*block*-poly(propylene glycol)-*block*- poly(ethylene glycol) (PEG-*b*-PPG-*b*-PEG or PEO-*b*-PPO-*b*-PEO) commercially known as Pluronics™.[52][53] These polymers cover critical temperatures from 20 °C to 50 °C depending on the composition. Other polymers exhibiting a LCST behavior such as PNIPAM,[54] poly(N-vinylcaprolactam (PNVCL)[55] and poly(2-isopropyl oxazoline) (PIPOX) have been associated to hydrophilic blocks such as PEO to obtain biocompatible smart materials.

2.3 Block copolymer synthesis & other tools of polymer chemistry

2.3.1 Block copolymers synthesis

The properties of block copolymers in bulk and solution are dramatically dependent on various parameters such as composition but also architecture, compositional homogeneity, functionality and molecular polydispersity.[56] The strategies to obtain polymers with such precision have been regrouped under the label "living/controlled". "Living" refers to chain polymerizations from which chain transfer and chain termination are absent (although this

restriction has since been relaxed), in other terms polymerizations that allow block copolymer synthesis by sequential monomer addition. "Controlled" refers to preparations methods to afford polymers that are well-defined in terms of topology, terminal functionality, composition, arrangement of comonomers, with predictable molecular weight as well as designed polydispersity. Nevertheless "living" polymerizations are not always "controlled". Slow initiation and slow exchanges in "living" processes can lead to polymers with unpredictable molecular weight and high polydispersity index.[57]
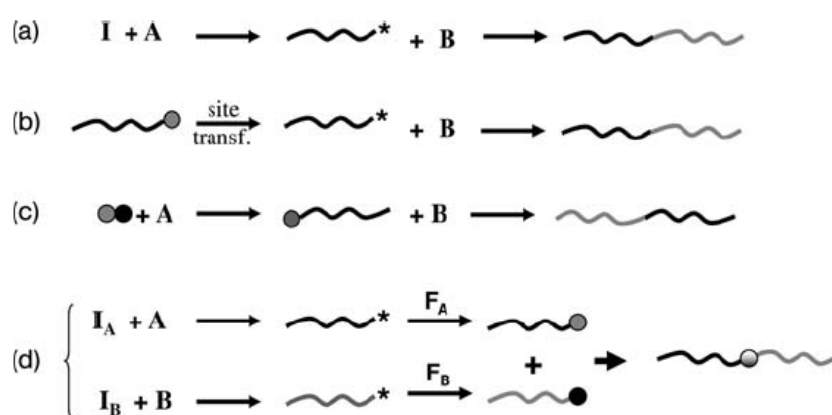
Figure 2.8: Synthetic strategies towards AB diblock copolymers. (a) sequential monomer addition, (b) site-transformation technique, (c) by dual initiator and (d) by coupling ω-functional polymers. * refers to active site. Reproduced from [57].

Strategies to obtain block copolymers by "controlled/living" polymerization in the simplest AB copolymers case include sequential monomer addition (Figure 2.8 (a)) provided that termination and transfer reactions are negligible, site-transformation technique (Figure 2.8 (b)) that requires the transformation of the propagation site into an initiating site for the second monomer, dual bifunctional initiation (Figure 2.8 (c)), and polymer-polymer coupling (Figure 2.8 (d)).

The "controlled/living" methods adapted to those strategies include anionic polymerization in which the propagating species are anions, cationic polymerization in which the propagating species are cations, several radical polymerizations (atom transfer radical polymerization ATRP, Nitroxide-mediated polymerization NMP and Reversible Addition Fragmentation chain Transfer RAFT) and some ring opening processes. In the next two paragraphs an overview of the controlled or potentially controlled polymerization techniques used in this

work, namely NCA polymerization and RAFT polymerization, will be presented.

2.3.1.a NCA polymerization

Polymerization of N-carboxyanhydrides (NCA) is the prefered synthetic pathway for the obtention of high molecular-weight polypeptides with engineered architecture.[58] These N-carboxyanhydrides of amino acids can be prepared by cyclisation of N-alkoxycarbonyl-amino acid halogenides as described by Leuchs,[59] or more commonly by phosgenation of the aminoacid by phosgene or preferentially triphosgene (Figure 2.9).[60]
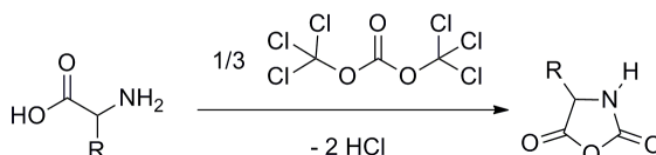
Figure 2.9: General NCA synthesis by phosgenation of an aminoacid using triphosgene

Purification of the N-carboxyanhydride from its byproducts and most notably the aminoacid·HCl salt is a challenge in this synthesis and numerous techniques have been developed for it.[61][62]

Subsequent polymerization of the monomer has been traditionally achieved by initiation by primary amines. Under these conditions the polymerization takes place *via* two different pathways, the primary amine mechanism (Figure 2.10 (a)) and the activated monomer mechanism (Figure 2.10.(b)).

The primary amine mechanism is the nucleophilic ring opening chain growth mechanism. When the polymerization proceeds uniquely *via* this mechanism, it has "living" characteristics,[58] but normally this mechanism coexists with the activated monomer one where the deprotonated NCA can act as an initiator and the polymerization proceeds *via* step growth or condensation. Schlaad *et al.*[63] introduced an ammonium mediated synthesis of monodisperse polystyrene-polypeptide block copolymers. In this study the use of the amine ammonium salt as initiator suppressed the activated monomer mechanism by suppressing the

deprotonation of the NCA (Figure 2.11) and seemed to have "living" characteristics.
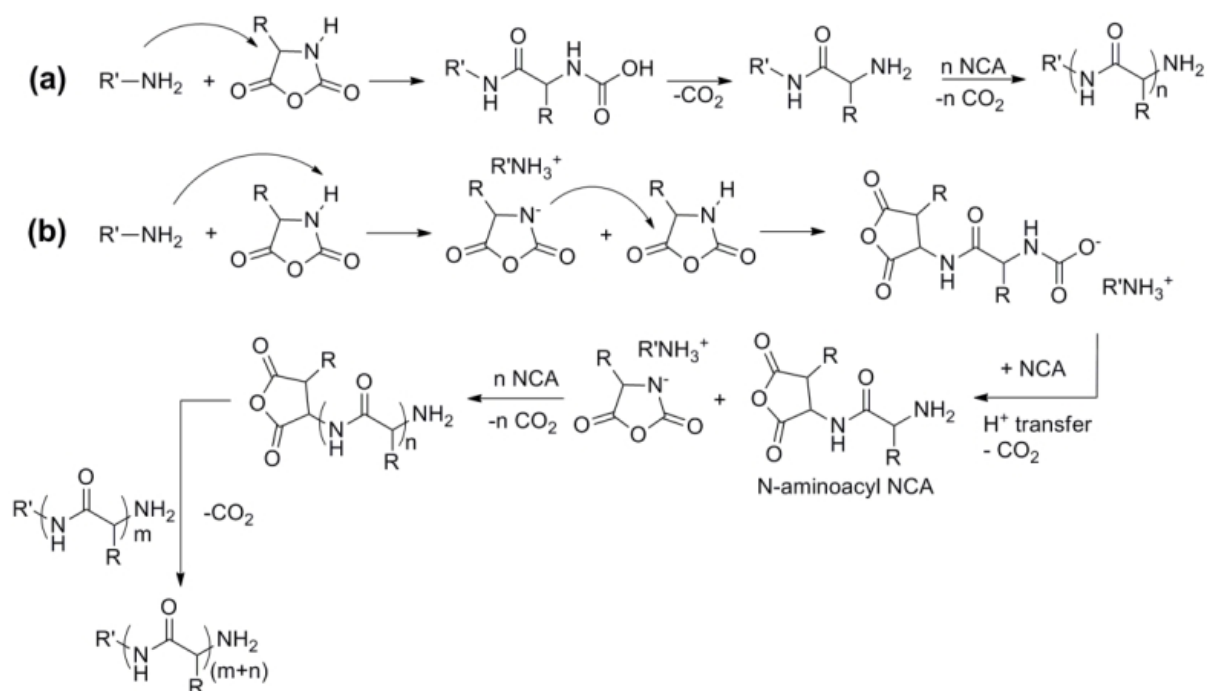
Figure 2.10: (a) Primary amine mechanism and (b) activated monomer mechanism in N-carboxyanhydride polymerization.

Deming *et al.*[64] reported the use of organonickel initiators in the NCA polymerization that resulted in a side-reaction free process. This polymerization was totally controlled and allowed the preparation of well-defined homo and block copolymers. Other groups reported the used of high-vacuum techniques that also resulted in living systems.[65]
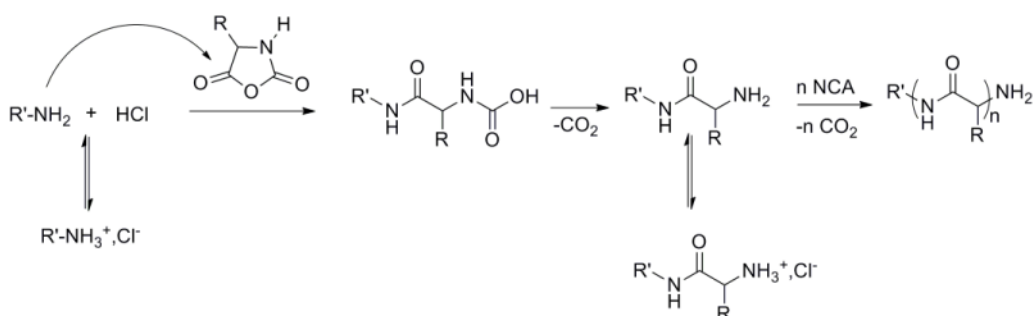
Figure 2.11: Proposed mechanism for the "ammonium-mediated" ring opening polymerization of NCAs.

2.3.1.b RAFT polymerization

Approximately 50 % of all synthetic polymers are currently obtained *via* radical polymerization,[66] because of the large variety of monomers available and the mild polymerization conditions needed (low temperatures, compatible with some impurities, water...). In macromolecular science, free radical polymerization is very often unsuitable because of the unavoidable terminations that lead to ill-defined polymers. A lot of effort has been put into developing "living/controlled" radical polymerizations techniques. These techniques, ATRP,[67][68] NMP[69] and RAFT[70][71] are all based on the dynamic equilibrium between propagating radicals and various dormant species.

In RAFT, reversible chain transfer agents (CTAs) are used (Figure 2.12).
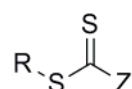
Figure 2.12: General structure of the chain transfer agents used in RAFT polymerizations.

In these polymerizations, the propagating oligomers react with the C=S bond leading to a transient radical that subsequently undergoes a β-scission (Figure 2.13) generating a R· radical capable of reinitiating the polymerization. The equilibrium is established by these successive chain transfer-fragmentation reactions.
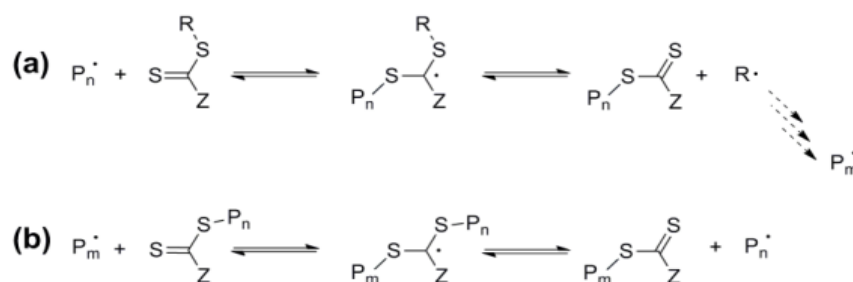
Figure 2.13: Chain transfer processes in reversible-addition fragmentation polymerization (a) Transfer to CTA (b) Chain to chain transfer. Reproduced from [40].

The choice of the CTA for a given monomer is very important and determines the degree of control in the polymerization. The activating substituent Z and the leaving group R have to be carefully chosen. For example, an increase in the radical intermediate may inhibit the polymerization. A fast equilibrium relative to the propagation rate must be sought after when

polymers with narrow polydispersity indexes are targeted.

2.3.2 Other tools of polymer chemistry: efficient linking

The design and preparation of more complex and highly functional macromolecular and polymeric structures have always been a challenge in macromolecular chemistry. With the quest of better well-defined and complex structure, modular approaches have appeared as the solution to overcome incompatible chemistries and other synthetic limitations. For instance, modification of easily accessible and well-defined "polymer precursors" exhibit several advantages as less synthetic steps, overcoming the use of protecting groups and allowing the easy tuning of certain properties. These modifications need to respect the "polymer precursor" architecture and thus classical organic reactions cannot always be used: byproducts translate into ill-defined polymer structures difficult to characterize and separate,[72] high temperatures may cause polymer degradation,… In that context, the organic reactions that Sharpless *et al.*[73] named "click" have become extremely popular. Pure "click" reactions are rare. "Click" refers to versatile (orthogonal to other chemistries), efficient (in high yields), specific (selective) and simple (simple experimental setups, mild reaction conditions…) reactions. Only a few reactions have gained the "click" label such as Diels-Alder cycloaddition, copper(I)-catalyzed alkyne-azide cycloaddition,[74] ring-opening reactions on strained heterocyclic electrophiles such as epoxides,[73]…and more recently thiol-ene[75]-[77] and thiol-yne[76][78][79] chemistry.
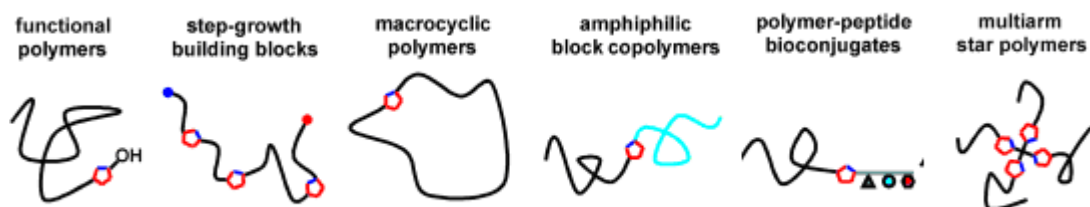
Figure 2.14: Variations on a simple theme: examples of macromolecular architectures recently obtained by click modification of well-defined polystyrene prepared by ATRP. Adapted from [74].

Macromolecular engineering has found in click reactions a versatile tool[72] not only to build functional structures in one step in a chain- or step-growth polymerization but also to

complement major synthetic polymerization techniques by allowing the chain-end, side-chain or site specific modification of preformed structures, or even by allowing the linkage of two separately formed segments[80] (Figure 2.14). Several excellent reviews summarize and present the use of "click" reactions[72][81][82] and particularly CuAAC[83] and thiol-ene[77] reactions in materials and polymer science.

 Although rarely in the literature these reactions fulfill all the click requirements, they remain a tool for efficient linking.[84] Two of these reactions were used in this work, Copper(I)-catalyzed alkyne-azide cycloaddition and thiol-ene radical addition. The next paragraphs aim at highlighting their principle and their use in polymer chemistry.

2.3.2.a Copper(I)-catalyzed alkyne-azide cycloaddition (CuAAC)

The Azide-Alkyne Huisgen Cycloaddition is a 1,3-dipolar cycloaddition between an azide and a terminal alkyne to give a 1,2,3-triazole (Scheme 2.1.(a)). First discovered by Michael[85] in the 19th century, it was later studied in detail by Huisgen[86][87] in the 1960s. Although orthogonal to other functionalities, the reaction was not regioselective (producing 1,4- and 1,5-substituted triazoles), was slow and required relative high temperatures until in 2002, Meldal et al.[88] reported that the use of catalytic amounts of copper(I) lead to a fast, efficient and regioselective (1,4-substituted triazole) cycloaddition at room temperature (Scheme 2.1.(b)).
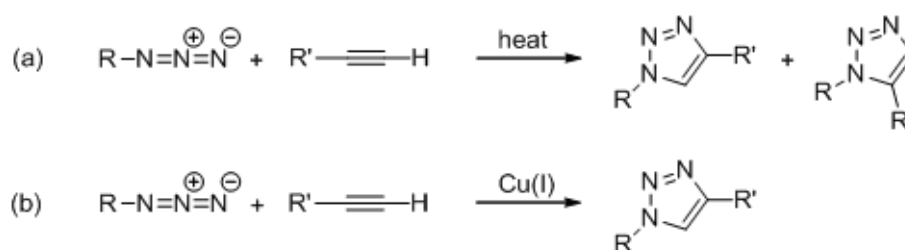
Scheme 2.1: (a) standart Huisgen thermal [3+2] cycloaddition and (b) copper-catalized alkyne-azide cycloaddition (CuAAC).

The complexity of ligand interaction with Cu(I) and particularly that of the alkyne complexation makes difficult the determination of the detailed structural secrets of the

transition state responsible for the extreme rate enhancement and selectivity in the copper(I) catalyzed reaction. Thus the mechanism is still controversial and remains unclear, although two different intermediates manage to explain most kinetic observations (Scheme 2.2).[89]
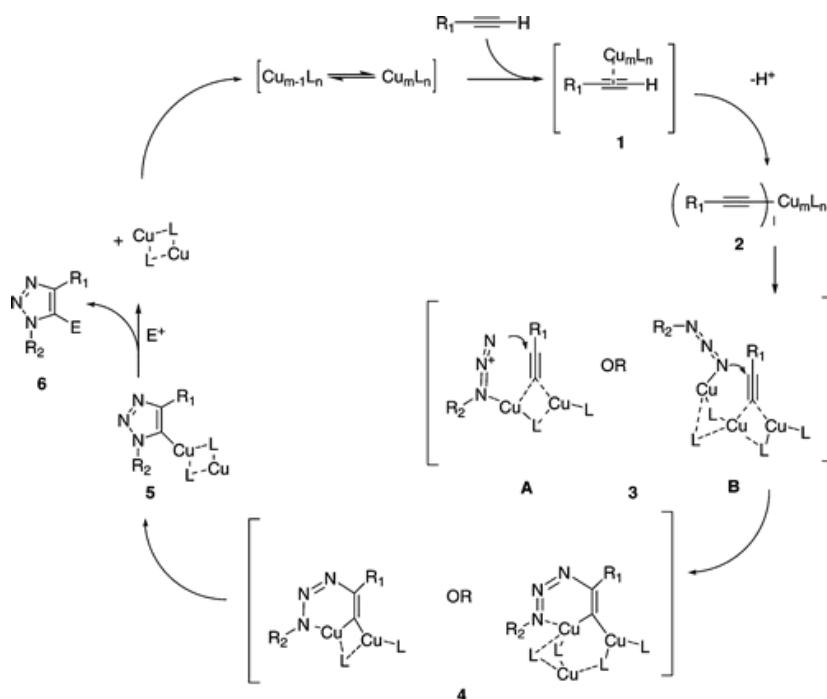
Scheme 2.2: Outline of Plausible Mechanisms for the Cu(1) Catalyzed Reaction between Organic Azides and Terminal Alkynes. Intermediate A is generally assumed to be the intermediate; however, it fails to explain much of the observed behavioral data of the reaction, Reproduced from [89].

The same year of Meldal *et al.*'s publication, Sharpless *et al.*[90] reported the same reaction in pure water, becoming "an ideal addition to the family of click reactions" that the same group had described and framed a year before.[73] Although not always fulfilling all the "click" requirements, the copper(I)-catalyzed formation of 1,2,3-triazoles has successfully been used in organic chemistry, biochemistry, macromolecular and polymer chemistry.[89] Its success is not only due to the fact that is a virtually quantitative, very robust, general and orthogonal ligation. The 1,2,3-triazole ring is essentially chemically inert to reactive conditions (oxidative, reductive or hydrolytic) and has intermediate polarity (dipolar moment of ~5 D). All these characteristics make the CuAAC a perfect candidate for macromolecular chemistry in its quest to well-defined structures, and especially well-defined bioinspired and biomimetic macromolecules by a modular approach.

The choice in this thesis of mainly using the triazole link to build up block copolymer had many reasons. The first one being the previously cited characteristics of the "click" reaction: universal, orthogonal to most functionalities and robust. The second one concerns the similarities with the peptidic bond. In a bioinspired approach, the conjugation of naturally recurrent polymers such as dextran for potential later biogical applications can be favoured by the use of biocompatible functionalities that mimic native natural bonds such as the peptidic bond. The 1,2,3-triazole ring has been shown to be a peptide bond isostere[1] [91] and the functional groups are similar in terms of distance and planarity (Figure 2.15).[92] This chemistry has been widely applied now in peptidomimetics,[92][93] nucleoside and nucleotide chemistry,[94] polymer chimeras,[95] and has also led its way into multivalent carbohydrate and polysaccharide chemistry.[93][96]
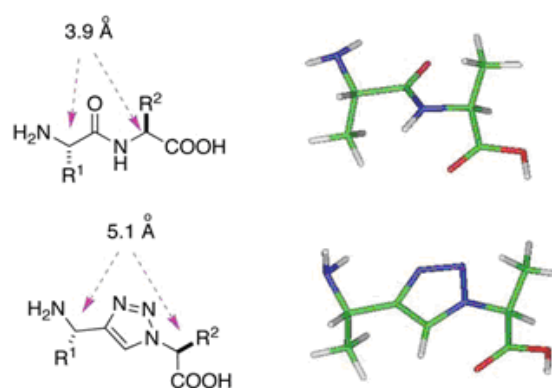
Figure 2.15: Molecular dimensions of the 1,4-disubstituted 1,2,3-triazoles are somewhat similar to amide bonds in terms of distance and planarity. Reproduced from reference [92]

CuAAC ligation has been found especially uselful in the ligation of preformed segments. Naturally recurrent saccharides polymers such as chitin/chitosan, dextran,.. cannot be made synthetically and are usually obtained from natural sources such as crab shells or in bacteria. The classic approach for the synthesis of well-defined polymers obtained by controlled methods such as step-growth polymerization is thus impossible. Selective chemical modification of functionalities in those polysaccharides allow though to access well-defined structures[97] constituted of for example, two blocks for which the copolymerization is impossible such as chitosan and poly(ethylene glycol). In a work by Makuška *et al.*,[98] the

---

1   Isosteres are molecules or ions with the same number of atoms and the same number of valence electrons. As a result, they can exhibit similar pharmacokinetic and pharmacodynamic properties.

anomeric end of chitosan was modified by reductive amination with amino propargyl. Azido terminated poly(ethylene glycol) was then "clicked" onto the polysaccharide to afford a polysaccharide-*block*-polyether hybrid with well-defined structure and architecture. Similarly in a work by Lecommandoux *et al.*,[99] dextran was modified by reductive amination with amino propargyl and coupled by CuAAC to a synthetical azido-modified polypeptide, poly(L-benzyl glutamate) obtained by NCA polymerization (see paragraph 2.3.1.a).

An implement to the CuAAC reaction as well as other polymer chemistry strategies [100] in the last years has been the use of the microwave (μW) irradiation. The reaction times can be decreased from hours to minutes.[101] In polymer chemistry, μW-assisted CuAAC has been successfully used in the coupling of azido-peptides to dendritic-alkynes[102] with a 96% yield, far above the 43-56% obtained with normal heating. Similarly, Morvan *et al.*[103] demonstrated that μW activation significantly improved the reaction kinetics compared to the standard conditions.

2.3.2.b Radical thiol-ene addition
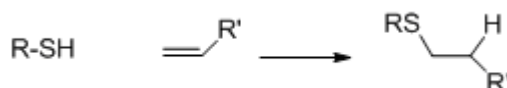
Scheme 2.3: General reaction of hydrothiolation of an ene with anti-Markovnikov product.

A thiol-ene reaction is simply the hydrothiolation of a C=C bond (Scheme 2.3) that has been known for over 100 years.[104] This reaction can proceed under a vide variety of conditions: radical pathway, catalyzed (nucleophile, base, acid, supramolecular) processes or nucleophilic in high polar solvents. As a consequence virtually any thiol and ene can be used but the reactivity in a given process will depend on the S-H bond characteristics for the thiol and the substitutives for the enes. These reactions are near-quantitative and extremely regioselective producing exclusively the anti-Markovnikov product. They are also usually fast and relatively tolerant to air and moisture.[105]

The radical addition pathway follows a chain process in which the thiyl radical adds to the

ene double bond, this radical intermediate reacts with another thiol generating a new thiyl radical and propagating thus the radical chain (Scheme 2.4). Side reactions include telomerization, that happens when the chain propagation is slow when compared to a new addition onto an ene molecule. Possible termination reactions are radical-radical recombination.
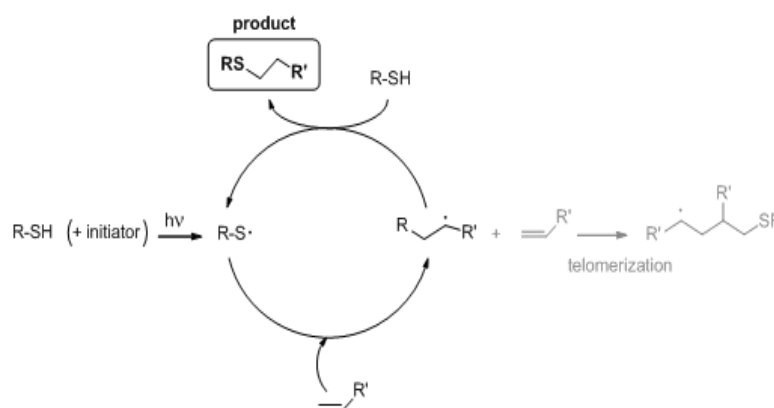
Scheme 2.4: Radical mechanism of thiol-ene addition. Adapted from [105].

Early on radical thiol-ene addition was exploited in polymer science for the derivatization of natural polymers such as rubbers.[106][107] Later it has principally been used for the post-functionalization of well-defined synthetic polymer precursors and even in the construction of well defined macromolecular structures. In that direction, Hawker *et al.*[108] synthesized a [G4]-ene dendrimer via sequential esterification/radical thiol-ene additions and post-functionalized the structure with a library of biological and labeling relevant thiols. In the same group,[109] double simultaneous end-functionalization of telechelic polymer with a combination of radical thiol-ene addition and CuAAC showed the high advantages of this modular approach to access a big library of functional polymers.

Post-functionalization of well-defined synthetic polymers has been applied to polysiloxanes[110] and more widely to poly-1,2-butadienes homo- and copolymers.[110]-[116] The variety of thiols used cover a wide range of chemical functions where the addition is performed under mild conditions. By avoiding heating for instance[117] it is possible to use biomolecule-derived thiols such as peptides[116] and sugars.[2][118][119] This strategy allows the easy access to well-defined biopolymers such as glycopolymers and pseudo polypeptides.

27
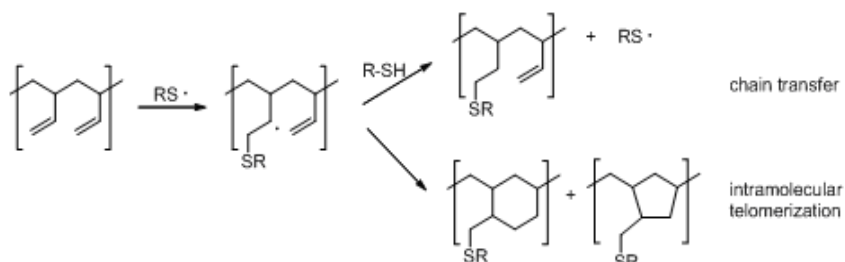
Scheme 2.5: Side reaction consisting on intramolecular cyclisation. The nature of the cyclic product of this side reaction is not exactly known. However the 6 member ring structure result of the anti-Markownikoff addition is formed by the most stable radical and should thus be preferred. Adapted from [121].

This 1,2-polybutadiene homo- and copolymers always showed a functionalization lower than 100% but no unreacted C=C. This was shown by Schlaad *et al.*[120] to be due to a cyclisation side reaction as shown in Scheme 2.5. As the degree of cyclisation was found to be dependent on the size of the thiol with the bulkier ones leading to a higher degree of cyclisation, it was concluded that the addition of the first thiol hinders the chain transfer and promotes this intramolecular telomerization.

A first approach to reduce this side reaction was the use of a high excess of thiol.[117] Another one was to change the system, engineering a polymer with a spacer between the double bond and the backbone. This system was poly(2-(3-butenyl)-2-oxazoline). Its modification *via* radical thiol-ene addition afforded a highly functional polymer without cyclisation products over a wide range of thiols (Scheme 2.6).[121] Beyond an effective linking, these reactions were formally "click" additions.
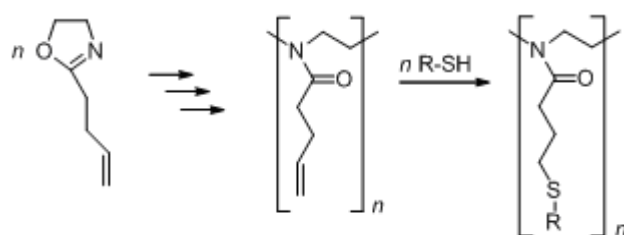
Scheme 2.6: poly(2-(3-butenyl)-2-oxazoline) synthesis and subsequent thiolation via radical thiol-ene additon. Reproduced from [121].

Chapter 3:   Self-assembly of double hydrophilic block copolymers:
The hydrophilic effect

Since the 1980s ATPS has been used in the biological sciences as a routine extraction technique. Some attention has been brought to the theory backing such phenomenon[122][123] but mainly to predict the composition of the phases and the partition coefficients of proteins.

The simplest description states that when the gain in entropy of mixing is not large enough to compensate for the repulsive polymer–polymer interaction enthalpy, the mixing of the two polymers is thermodynamically not favorable and phase separation occurs.[124] Just from a qualitative point of view it seems that phase separation in ATP systems could not purely be explained by the incompatibility of the polymers (high χ_{AB}) as it fails to explain why

relatively low molecular weight polymers mixtures[9] still phase-separate, and experimental evidence of the magnitude of the incompatibility of the dextran/PEG pair shows that it is not total.[125]

Two qualitative thermodynamic considerations can be evaluated to explain the phase separation in ATP systems outside polymer-polymer incompatibility, an enthalpic and an entropic one, and this discussion can be translated into the feasibility of transposing this phase separation to the microscale with block copolymers.

Scott[126] and Tompa[127] applied Flory-Huggins solution thermodynamics to the study of polymer-polymer-solvent (A-B-S) systems assuming that the phase equilibrium only depends on the polymer-polymer interaction parameter χ_{AB} and thus $\chi_{AS}=\chi_{BS}$. This approximation has found numerous limitations including the direct consequence that the phase separation does not depend on the nature of the solvent.[128] This limitation can be overcome by relaxing this restriction and introducing the dependence on $|\Delta\chi|$ as defined by Equation (7).

$$|\Delta\chi|=|\chi_{AS}-\chi_{BS}| \tag{7}$$

This so called "$|\Delta\chi|$ effect" even allows to predict phase separation in compatible polymer pairs-solvent ternary systems provided that $|\Delta\chi|$ is big enough.[129]

In block copolymers, the incompatibility of the two segments is at least partially compensated by the compatibility introduced by the covalent bond between them. Solubility difference in the Flory Huggins interaction parameter (see paragraph 2.2.2 and Equation (8))

$$\chi_{eff}\, N \approx \varphi\left(\chi_{AB}+\Delta\chi\right) N \approx \varphi\left(\chi_{AB}+|\chi_{AS}+\chi_{BS}|\right) N \tag{8}$$

is often read in terms of "selective solvent $|\Delta\chi| \neq 0$" and "common solvent $|\Delta\chi| = 0$" although

this is only an extreme solubility case. If $|\Delta\chi|$ is big enough without one of the polymers being insoluble provided that χ_{AB} remains high enough, then a block copolymer made of two water-soluble incompatible blocks could phase separate in water i.e. self-assemble in dilute solution.

In addition, entropic effects should be considered especially when working in water. The "hydrophobic effect"[37][130] is now widely acknowledged to be the main driving force for self-assembly of amphiphiles in water. A simple definition of this effect states that over a certain concentration of amphiphiles (critical aggregate concentration) in water, the non-soluble segments of the molecule and water segregate to overcome the loss of conformational entropy of water molecules next to these segments. From that point of view this effect could be generic and regroup all entropy-driven segregation phenomena, and could in principle not only be restricted to hydrophobic/amphiphilic molecules. Qualitatively, a block copolymer made of two water-soluble blocks should possess low free-energy in the random coil conformational state. But if the polymer is made of blocks presenting high solubility difference, a segregation could lower even more the system's free energy by freeing the conformation entropy of the water molecules that were trying to solubilize the "less soluble" block. This theory supports that to have an entropy-driven segregation, a big solubility difference is enough provided that the enthalpic contribution to the free energy does not compensate it.

In this work, a series of block copolymers designed to present incompatibility and high solubility difference were synthesized and their behavior in water studied. Perfect candidates were block copolymers based on the ATP systems as they seem to show both high incompatibility and high solubility difference, and they phase separate under mild conditions of concentration and temperature. Systems based on biomacromolecules (polysaccharides, polypeptides) were preferred as there phase separation has been proved in microcompartimentation in cells and they constitute biologically-relevant systems.

In the first part of this chapter polysaccharide-based polymers are studied. PEG-*b*-dextran block copolymers are synthesized and their behavior in aqueous solution is studied. Some

attention is paid to the influence of parameters such as concentration and temperature as well as some structural parameters on the self-assembly behavior. Other dextran-based copolymers were briefly studied to test the validity of ATPS as source of inspiration to engineer DHBCs with self-assembling capabilities.

In a second part, first a polypeptide-based copolymer system is studied to extend the principle to the main group of biomacromolecules. Secondly, a thermoresponsive polysaccharide-poly(N-isopropylacrylamide) system is studied and evaluated to increase complexity in the system and as a hybrid model.

3.1 Spontaneous self-assembly of polysaccharide-based block copolymers in water

3.1.1 Designing DHBCs for self-assembly: incompatibility and solubility difference

PEG/dextran is the most frequently used ATP system certainly due to the low cost of both polymers. Dextran is a glucan, for instance expressed by bacteria of the species *Leuconostoc spp.*. The most common dextran consists of D-glucose units, 95% linked by α(1→6) bonds with branching formed by α(1→3) and occasionally α(1→4) bonds. Many aspects of the fine structure of dextran (branching, molecular weight and molecular weight distribution) depend on the conditions and strain of the bacteria used for expression.[131] Poly(ethylene glycol) is a synthetic polymer widely used in biological and medical applications for its non-immunogenicity and biocompatibility. Although often reported as highly soluble in water,[123] its wide solubility in both water and organic media makes it often being referred as "amphiphile". Its solubility in water being complex,[132] PEG also shows a molar mass dependent LCST behavior.[133]

In our hypothesis of block copolymers microphase separation, both incompatibility of the polymers and their relative solubility in water are taken into account. To compare the solubility of both polymers in water, we made a comparison of the hydration of both

polymers as reported in literature.

In average, dextran was found to bind 7 water molecules per glycosidic residue for a low molecular weight polymer but can bind up to 10 water molecules per residue in high polymers.[134] This is in accordance with the water bounding capabilities of D-glucose that have been found to be 0.682 g of water per gram.[135] This also reflects the superior hydration capabilities of dextran compared to other polysaccharides (especially the ones with linking other than (1→6)) previously reported.[136] In the literature, for the hydration of PEG several values have been given ranging from 1 to 5,[137]-[140] although 2[141] water molecules per residue is the commonly acknowledged value. Despite the differences in the values, it seems clear that PEG binds a substantial lower quantity of water than dextran in solution. So from a qualitative point of view, these hydration values translate thus into a rather high solubility difference of the two polymers, and suggests thus that dextran-*b*-PEG could be a good candidate for our work.
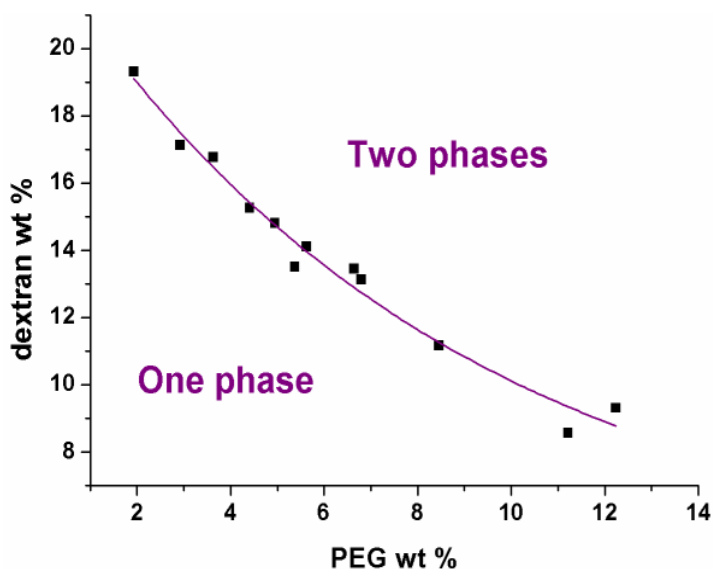
Figure 3.1: Binodal of dextran (M_w 6500 g·mol^{-1}) and PEG (M_w 5500 g·mol^{-1}) in aqueous solution at room. The line is just a guide for the eyes.

Incompatibility of two polymers can be evaluated from the thermodynamic parameters as previously reported[142] but also directly observing a phase separation diagram. A mixture of the polymers in water undergoes a phase separation when their concentration is above several weight percent. These phase diagrams can be established by cloud point titration. In these

experiments known amounts of a dextran stock solution is titrated with a PEG stock solution until the solution becomes turbid. By measuring the change in mass after the addition of the titrant, the quantity of PEG added can be calculated.

In Figure 3.1 the phase diagram of the PEG/dextran polymers used in this study obtained by cloud point titration at room temperature is shown. When the polymer solution is located below the binodal the solution is stable and homogeneous and when the solution mixture is above the binodal it becomes turbid and subsequently separates into two phases (Figure 3.2). Both homopolymers used in this experiments are characterized by a low-molecular weight (for dextran M_w ~6500 g·mol^{-1}and for PEG M_w ~5500 g·mol^{-1}). This choice will be discussed later, but the binodal curve shows phase separation for relatively low weight percentages (eg. ~10/10 wt% dextran/PEG) indicating a negative free energy of mixing above the binodal.

Typical ATP systems are usually performed with at least one of the polymers having a high molecular weight for several reasons including the fact that higher polymers result in a sharper separation of biomolecules between the two phases. This is related certainly to the composition of both phases that varies with temperature and concentration. What seems surprising is that the binodal in our case seems comparable to a certain extend with binodals of dextran 500 kDa/PEG 8 kDa,[27] dextran 40 kDa/PEG 3.4 kDa, dextran 70 kDa/ PEG 20 kDa[9]…in terms of position of the curves, so the phase-separation is less molecular-weight dependent than Scott's[126] and Tompa's[127] model could suggest.
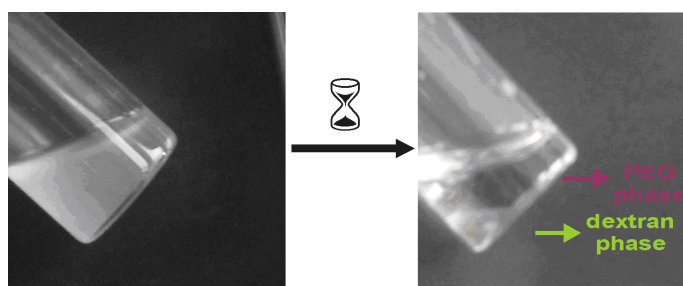

Figure 3.2: Cloud point and subsequent macrophase separation.

Qualitatively, PEG/dextran seems to be a good candidate for our work. Whether the macro

phase separation in the polymer mixtures can be translated into a microphase separation in the block copolymer cannot be evaluated directly from the polymer mixture thermodynamic parameters.

3.1.2 Polymers syntheses

The synthesis of dextran-*block*-poly(ethylene glycol) cannot be done by sequential polymerization or other elegant techniques.[143] Dextran being of bacterial origin, it is (at least currently) impossible to start its polymerization with a poly(ethylene glycol) macroinitiator. Viceversa dextran being a polyglucan, it is difficult to use it as a macroinitiator in anionic polymerization to afford a block copolymer. The adopted strategy was therefore polymer-polymer coupling. This approach has been used before to afford dextran-[99] and other natural polysaccharide-based [98] block copolymers. Dextran's anomeric end can be functionalized by either oxidizing it to a lactone or reducing it by reductive amination.

For getting a high coupling yield, relatively low molecular mass polymers were used, and the chosen coupling reaction was a well-known one belonging to the "click" family, which is the microwave-assisted copper(I)-catalyzed alkyne-azide cycloaddition (see paragraph 2.3.2.a). The same approach was used to synthesize a triblock dextran-*b*-PEG-*b*-dextran. For comparison, an additional dextran-*b*-PEG block copolymer with an amide link was prepared by lactone ring opening.

3.1.2.a Dextran-block-poly(ethylene glycol) by CuAAC

Dextran was derivatized in this study by reductive amination with propargyl amine to afford α-alkyne dextran (Scheme 3.1). This reaction exploits the ability of sodium cyanoborohydride to selectively reduce double bonds in Schiff bases.[144] At pH values of 5-6 this reaction reaches yields of 90-95%. Commercial dextran was reacted in acetate buffer (pH 5.6) with a large excess of propargyl amine in the presence of a large excess of sodium

cyanoborohydride (NaCNBH$_3$). Additional excess amounts of NaCNBH$_3$ were added daily as this compound is water sensitive. The success of the reaction was assessed by the complete disappearance of the protons of the anomeric end in the ^{1}H NMR spectrum (See Supporting experimental data).
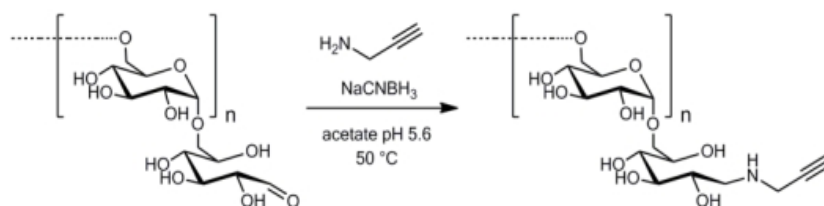
Scheme 3.1: Reaction scheme of the reductive amination of dextran with propargyl amine.

Commercial methoxy-poly(ethylene glycol) was functionalized in a two step synthesis (Scheme 3.2). First the ω-hydroxyl was activated by tosylation in dichloromethane with p-toluenesulfonyl chloride (TsCl), high functionalization (close to quantitative) was assessed by the disappearance of the OH signal in ^{1}H NMR at 4.57 ppm as well as a ratio close to 1 of the integrals of the peaks corresponding to the methoxy group and the methyl of the tosyl. This last ratio also shows the effectiveness of recrystallization from ethanol as a purification method as an excess of TsCl and triethylamine (TEA) is usually difficult to remove by reprecipitation with diethyl ether. Secondly the azido group was introduced by nucleophilic substitution of this α-methoxy-ω-p-toluenesulfonyl-poly(ethylene glycol) with an excess of sodium azide to afford α-methoxy-ω-azido-poly(ethylene glycol). The completion of the reaction was assessed by the disappearance of the tosyl group peaks in ^{1}H NMR.
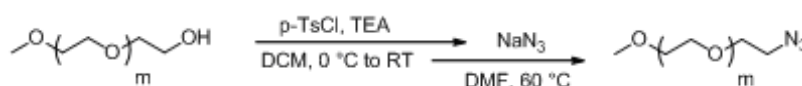
Scheme 3.2: Reaction scheme of the two step azidation of methoxypolyethylene glycol.

Ultimately, both blocks were coupled under microwave irradiation (~900 W) with CuI/1,8-Diazabicyclo[5.4.0]undec-7-ene (DBU) as catalyst/ligand system (Scheme 3.3). CuI/DBU as been shown to induced high yields in 1,2,3-triazole formation not only in organic chemistry[145] but also in polymer science.[146] For simultaneous solubilization of both blocks and the catalyst/ligand, a mixture of water and tetrahydrofuran (THF) was used. This

approach also allowed the easy removal of the copper catalyst: as a large excess of ligand was used, all the copper ions were complexed, so after the reaction the simple removal of the THF precipitated the Cu(I)/DBU complex and the free DBU. Although no control of the Cu(I) content of the sample was performed after the THF removal, the polymer was additionally purified with activated charcoal.
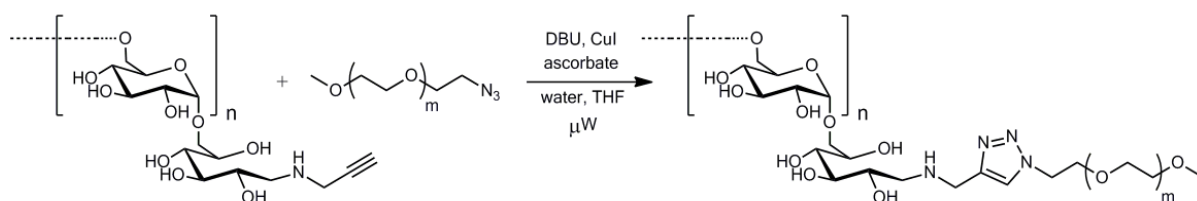
Scheme 3.3: Reaction scheme of the coupling of ω-alkyne dextran and α-methoxy-ω-azido-PEG by CuAAC under microwave irradiation.

Four dextran-*block*-poly(ethylene glycol) were prepared this way with varying block lengths (Table 3.1).

Table 3.1: List of the synthesized polymers (first column). The second and third column correspond to the commercial starting blocks used. The fourth column corresponds to the block copolymers.

Polymer	*Dextran M_w (PDI)* [1]	*PEG M_w (PDI)* [2]	*$M_{w, app}$ (PDI)* [3]
dex$_{6500}$-*b*-PEG$_{5500}$	6500 (1.81)	5500 (1.03)	13000 (1.71)
dex$_{6500}$-*b*-PEG$_{1900}$	6500 (1.81)	1900 (1.05)	11400 (1.61)
dex$_{6500}$-*b*-PEG$_{13200}$	6500 (1.81)	13200 (1.08)	20000 (1.85) [*]
dex$_{11000}$-*b*-PEG$_{5500}$	11000 (1.85)	5500 (1.03)	11000 (1.44)

[1] as determined by GPC in DMSO with dextran standard [2] as determined by GPC in NMP with PEG standard
[3] as determined by GPC in DMSO with dextran standard [*] contains residual homopolymer

With this reaction the polymers were recovered with yields ranging from 72 to 93%.
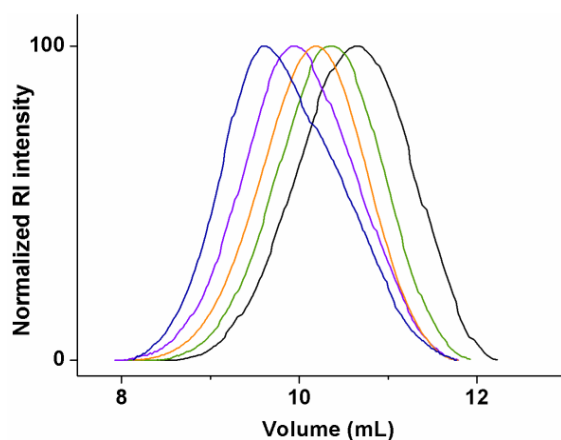
Figure 3.3: GPC (DMSO) traces of starting dextran polymer M_w 6500 g·mol^{-1} (black), α-alkyne dextran$_{6500}$ (green), dex$_{6500}$-*b*-PEG$_{1900}$ (orange), dex$_{6500}$-*b*-PEG$_{5500}$ copolymer (violet) and dex$_{6500}$-*b*-PEG$_{13200}$ (blue).

Although this reaction was not performed under "click" conditions, the control of three parameters assured the efficient linking of the blocks: the good performance of the CuI/DBU catalytic complex, the use of microwave irradiation and excess of PEG precursor. The success of the reaction and effective removal of excess of PEG precursor was assessed by GPC (Figure 3.3) and NMR (Figure 3.4) in every case except for dex$_{6500}$-*b*-PEG$_{13200}$ for which GPC showed residual homopolymer. Attempts to purify by extraction with chloroform yielded an emulsion that was stable over weeks.
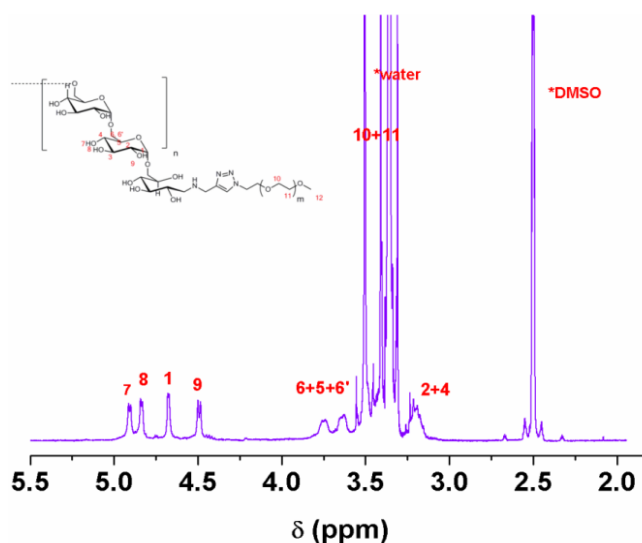
Figure 3.4: ^{1}H NMR of dex_{6500}-b-PEG_{5500} in DMSO-d_6

3.1.2.b Dextran-block-poly(ethylene glycol)-block-dextran

In order to investigate the architecture influence on the self-assembly behavior of the dex-*block*-PEG copolymer, a triblock dex-*b*-PEG-*b*-dex was synthesized. The approach was the same as for the diblock copolymer, but the polyethylene(glycol) starting polymer was α-ω-diol and thus the copolymer was synthesized with α,ω-bisazido-poly(ethylene glycol).

The GPC traces (Figure 3.5) show the successful coupling of the copolymer. The low apparent molecular weight (Table 3.2) could suggest incomplete coupling but the elemental analysis (EA) of the powder (and compared to the carbon content for the diblock) together with the single peak in GPC confirm its triblock structure.

Table 3.2: Characteristic of the synthesized dextran-*block*-poly(ethylene glycol)-*block*-dextran triblock copolymer and its constituting building blocks.

Polymer	Dextran M_w (PDI) [1]	PEG M_w (PDI) [2]	$M_{w, app}$ (PDI) [3]
dex_{6500}-b-PEG_{5100}-b-dex_{6500}	6500 (1.81)	5100 (1.03)	12000 (1.62)

[1] as determined by GPC in DMSO with dextran standard [2] as determined by GPC in NMP with PEG standard
[3] as determined by GPC in DMSO with dextran standard

Figure 3.5: GPC traces in DMSO of α-alkyne dextran$_{6500}$ (black) and dex$_{6500}$-*b*-PEG$_{5100}$-*block*-dex$_{6500}$ (violet).

3.1.2.c Dextran-block-poly(ethylene glycol) by lactone ring opening
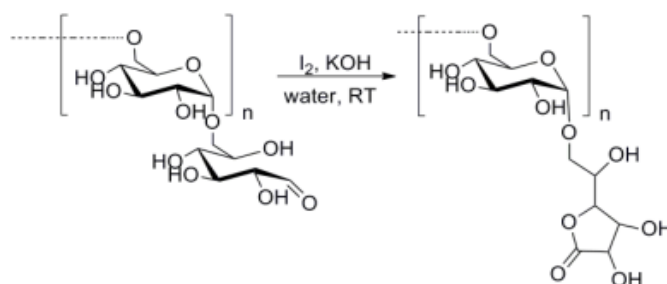
Scheme 3.4: Reaction scheme of the oxidation of dextran by potassium hydroxide/iodine.

To study the influence of the 1,2,3-triazole ring on the eventual self-assembly behavior of the block copolymer, a sample with an amide link was prepared. A starting commercial dextran was oxidized[147][148] with iodine in the presence of potassium hydroxide (KOH) to produce α-lactone-dextran (Scheme 3.4). The complete oxidation was assessed by the disappearance of the anomeric protons in ^{1}H NMR.

The block copolymer was then prepared by the ring opening of the α-lactone-dextran by a 5-fold excess of commercial α-methoxy-ω-amino-poly(ethylene glycol) (Scheme 3.5). After purification, dextran-*block*-PEG with an amide link was afforded in good yield (75%). Purity was assessed by GPC (Figure 3.6). The polymer characteristics are summarized in Table 3.3.
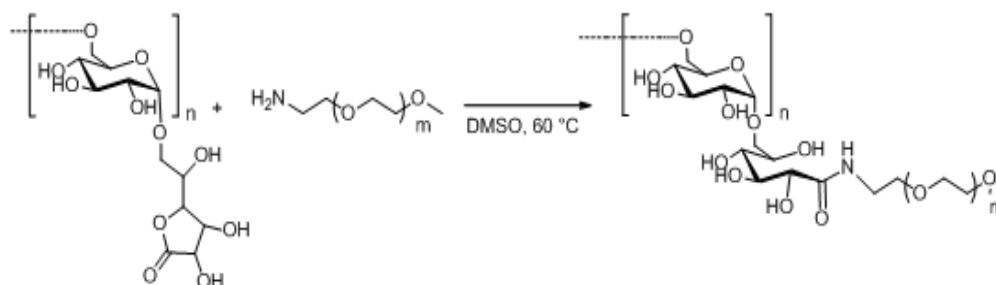
Scheme 3.5: Reaction scheme of the synthesis dextran-*block(amide)*-poly(ethylene glycol) by coupling.

Table 3.3: Characteristic of the synthesized dextran-*block*-poly(ethylene glycol) with amide link and its constituting building blocks.

Polymer	*Dextran M_w (PDI)* [1]	*PEG M_w (PDI)* [2]	*$M_{w, app}$ (PDI)* [3]
dex$_{6500}$-*b(amide)*-PEG$_{5700}$	6500 (1.81)	5700 (1.13)	14700 (1.67)

[1] as determined by GPC in DMSO with dextran standard [2] as determined by GPC in NMP with PEG standard [3] as determined by GPC in DMSO with dextran standard.
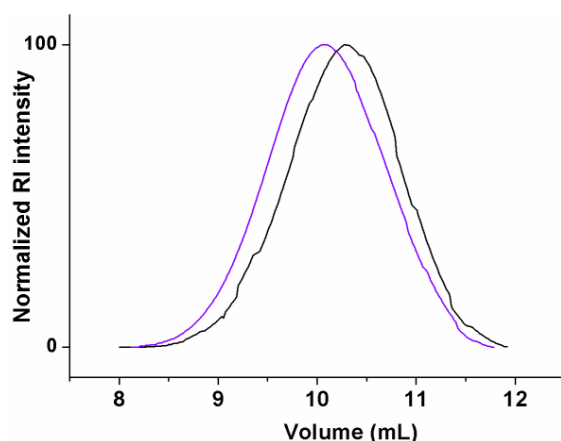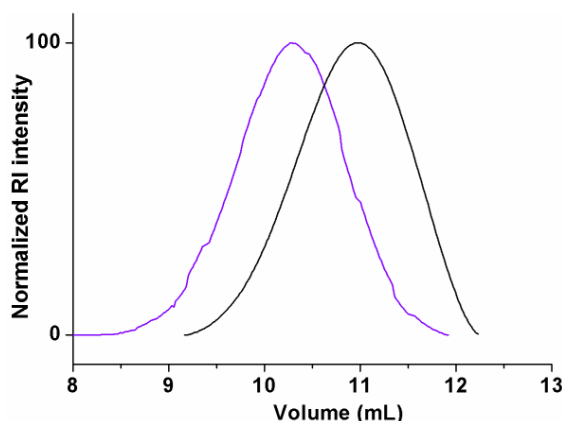

Figure 3.6: GPC traces in DMSO of dextran$_{6500}$-lactone (black) and dex$_{6500}$-*b(amide)*-PEG$_{5700}$ (violet).

3.1.3 Aggregation behavior in water

Block copolymers with short block lengths were used to make sure that the light scattering measurements would not deliver information on kinetically trapped structures, undissolved polymers clusters or easily reach the overlap concentration c* that could lead to a misinterpretation of the slow modes. A solution of dex$_{6500}$-*b*-PEG$_{5500}$ in milliQ water was stirred overnight and filtered (glass filter 0.7 μm). The correlation curve by dynamic light scattering was recorded. The data was treated with the REPES algorithm[149] that delivers the

intensity weighted distribution of hydrodynamic radii similarly to the widely used CONTIN.[150] The following distribution was obtained (Figure 3.7):
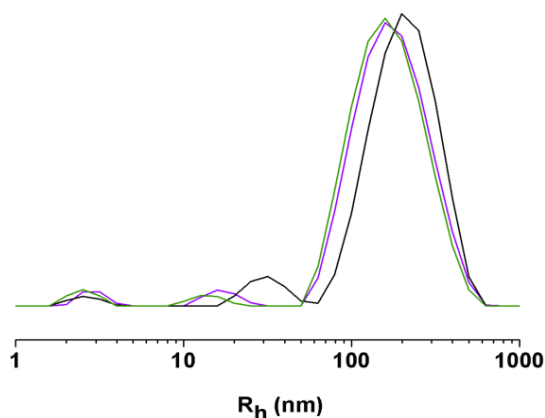
Figure 3.7: Intensity-weighted distribution of R_h (nm) obtained from a dex$_{6500}$-*b*-PEG$_{5500}$ solution at 10 mg·mL^{-1} after 3 days stirring (black), 10 days (violet) and 20 days (green) by DLS at 90°.

This distribution presents three modes. A fast mode of hydrodynamic radius 2 nm that can only correspond to the single polymer random coil. An intermediate mode of 30 nm that can correspond to micellar objects and a slow mode corresponding to a hydrodynamic radius of 226 ±41 nm was also present. This same solution was measured over time after 10 and 20 days and only showed a slight variation on the size of the slower and intermediate mode towards 180 ±16 nm and 16 nm respectively. The solution appeared clear and exhibited thus prolonged colloidal stability.

In static light scattering experiments, the intesity was acquired for a short time (typically 10 s) to make sure the scattering was mainly due to the slowest mode. A Berry plot was used to evaluate the static parameters overcoming the angular dependence (Figure 3.8).

$M_w = 1.21 \cdot 10^7 \ g \cdot mol^{-1}$

$R_g = 221 \ nm \pm 12\%$
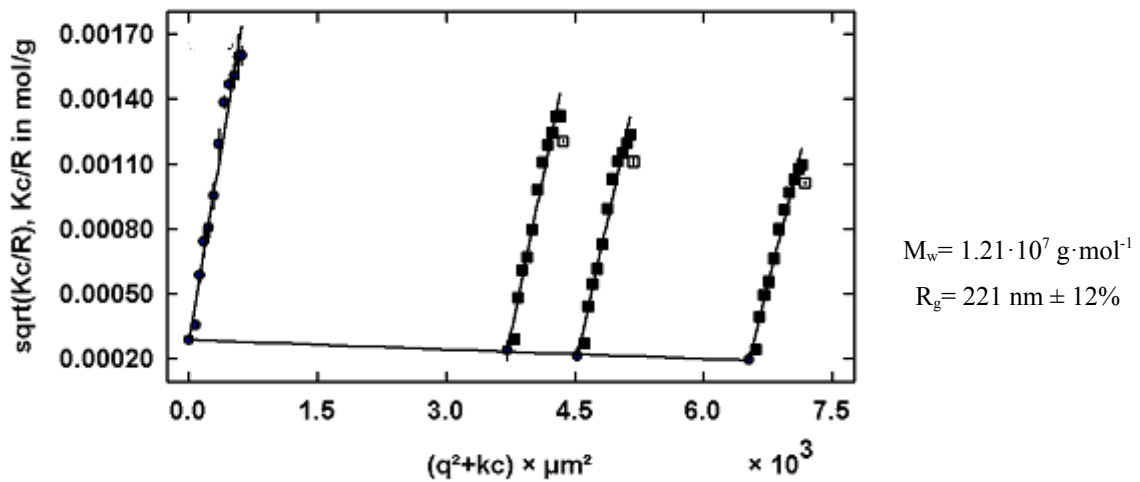
Figure 3.8: Berry plot of the SLS data obtained between 40° and 150° at room temperature for dex_{6500}-b-PEG_{5500} polymer solutions.

The gyration radius obtained and the subsequent calculated ρ-ratio of 0.98 suggest a vesicular structure that could further be confirmed by additional dynamic light scattering experiments and TEM.

	Value	Standard Error
Dz	0.5563	0.09559
Dz*C*Rg	9.16926E-4	5.87457E-4
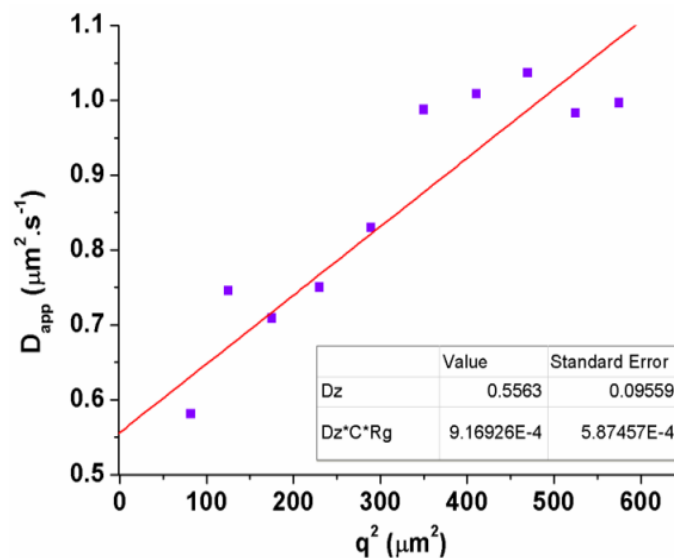
Figure 3.9: q^2-dependence of the apparent diffusion extrapolated at 0 concentration. The red line is the linear fitting at the lowest angles.

The diffusion extrapolated to 0 concentration against the square wave vector over a wide angle range was plotted to study the angular dependence (Figure 3.9) of the aggregates. The plot shows important angular dependence arising from the contribution of the form factor for

larger particles to the scattering intensity. This dependence is consistent with big spherical aggregates presenting polydispersity such as vesicles. The polydispersity was already revealed by the standard deviation from the average hydrodynamic radius 226 ±41 nm. The functional form of the apparent diffusion coefficient in equation (9) allows to extract the C coefficient that is calculated from the initial slope of the q^2-dependence curve. This C coefficient characterizes the contribution of the shape fluctuations (softness/polydispersity) to the relaxation of the correlation function measured in DLS.[151]

$$D_{app} = D_z \left(1 + C q^2 R_g^2 \right) \tag{9}$$

Typical values for C[152] include C=0 for hard spheres and C=2 for Gaussian coils. By considering the gyration radius extracted from static light scattering, the C coefficient could be evaluated to 0.18. This value characterizes very soft objects and is well above the values found in other vesicular objects (0.04-0.07).[2] The higher softness in this system compared to other classical vesicular values seems to translate an additional contribution to the shape fluctuations that in our case correlates with a highly hydrated membrane composed of hydrophilic polymers.

The TEM image was acquired from air-dried sample (Figure 3.10). The vesicles appear thus collapsed but their size seems to be roughly in agreement (R~100 nm) with the gyration radius of 221 nm. The interactions inside the barrier not being of hydrophobic nature, it is not surprising that the collapse induces such deformation. In a first approximation, PEG being less hydrophilic than dextran, we can think of this block copolymer as an amphiphile. It could then be predicted that the short dextran (M_n 3000 g·mol^{-1}, M_w 6500 g·mol^{-1}) would prefer low curved structures such as vesicles. Although the membrane thickness could not be measured from such a micrograph, its structure was elucidated as presented in the next section.
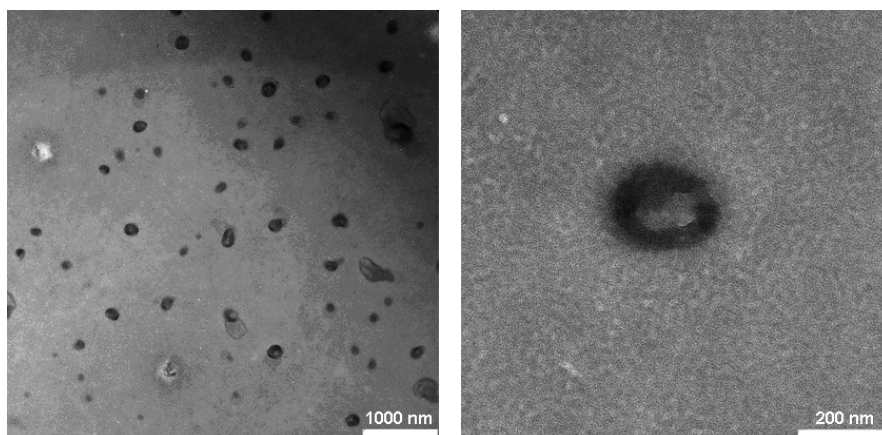
Figure 3.10: Negatively-stained transmission electron micrographs of a dex$_{6500}$-*b*-PEG$_{5500}$ 2 mg·mL^{-1} solution.

3.1.4 Membrane structure

Regular membranes of polymersomes of amphiphilic diblock copolymers have in a first approximation a structure analogous to the lipidic bilayer of cells walls and liposomes (Figure 3.11). In special cases the membrane can also have an asymmetric geometry.[2][153][154]
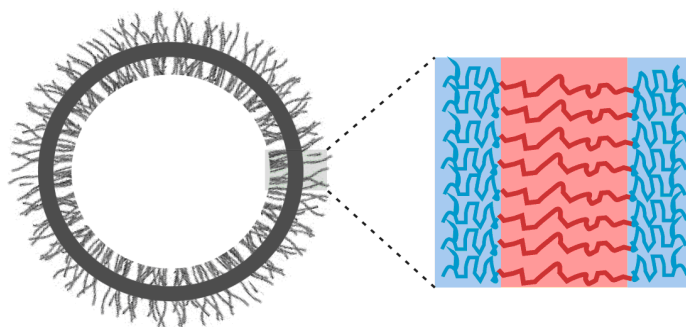
Figure 3.11: Typical membrane structure in polymersomes from amphiphilic block copolymers. In red the hydrophobic barrier formed by hydrophobic segments of the block copolymer, in blue the solubilizing hydrophilic segments.

In our study of the membranes of vesicles formed by DHBC a direct assumption of its structure is not possible although it could be reasoned that the PEG block being "less hydrophilic" segregates to form a "less hydrophilic" barrier just as hydrophobic blocks segregate into hydrophobic barriers in regular amphiphilic polymersomes. To prove the membranes structure Surface Enhanced Raman Spectroscopy (SERS) experiments were carried out in polymer solutions of dex$_{6500}$-b-PEG$_{5500}$.

45

3.1.4.a Preparation of the samples

The spontaneous formation of the vesicles by simple dissolution of the polymer in pure water allowed the development of a preparation method that could elucidate the membrane structure.

Figure 3.12: Preparation of the sample for the "visualization" of the external block by SERS. Step 1) is the dissolution of the polymer followed 2) by addition of colloidal gold.

SERS is a technique that results in the enhancement of Raman scattering by molecules adsorbed on rough metal surfaces.[155] In liquid samples, colloidal metal nanoparticles (typically Au or Ag) are used as metal surfaces.

The visualization of the external block was carried out as a typical SERS experiment. To a high concentration solution of dex_{6500}-*b*-PEG_{5500} polymer vesicles, a solution of gold nanoparticles was added. As the membrane has been shown to be little permeable (see paragraph 3.1.7.b), it is reasonable that 5-20 nm gold nanoparticles would not diffuse inside the vesicles (Figure 3.12).

Selective encapsulation of metal nanoparticles inside the vesicles would lead to a selective adsorption of the internal polymer block to the surface of the nanoparticle, resulting in an enhancement of the vibration modes of the bonds of that block. This encapsulation could be achieved by dissolution of the polymer directly in a colloidal gold solution followed by removal of the non-encapsulated gold by reaction with mercapto-functionalized silica particles. The strong covalent character of the S-Au bond (bond enthalpy of $418 \pm 25 \, kJ \cdot mol^{-1}$[156]) and the excess of sulfur sites[157] could lead first to the complete removal of external gold. The big size (10 μm) of the silica particles allowed the easy subsequent removal of the silica-Au particles by simple filtration (Figure 3.13).

46
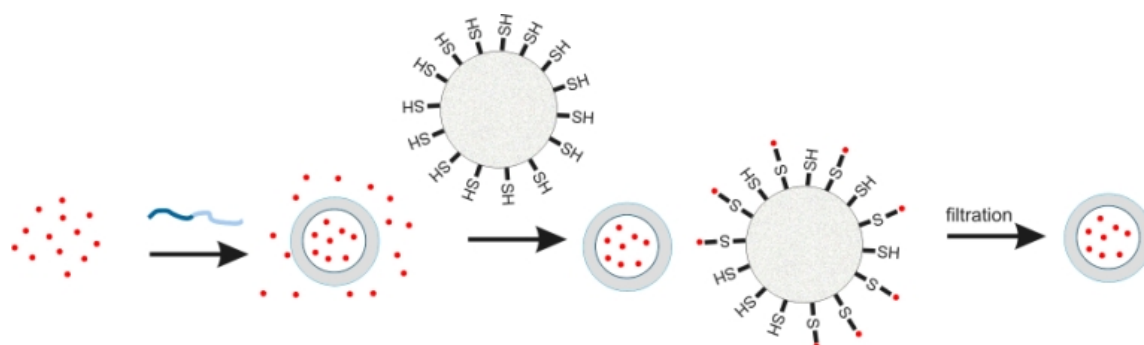
Figure 3.13: Encapsulation of gold nanoparticles for SERS experiments by 1) dissolution of the polymer in a colloidal gold solution, 2) addition of 3-mercaptopropyl-functionalized silica and 3) filtration of the SiO$_2$-Au composite.

The efficiency of the encapsulation and the removal of the gold were assessed by TEM (Figure 3.14). In this TEM image it can be appreciated that the metal nanoparticles (as black dots) are trapped inside a collapsed polymer structure. No metal nanoparticles were observed outside.
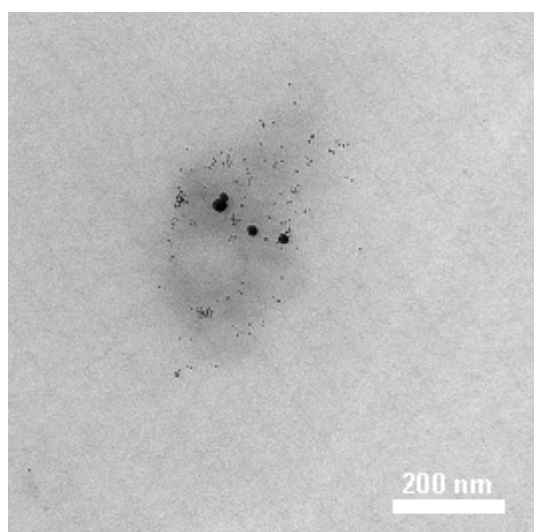
Figure 3.14: Non-stained TEM image of gold nanoparticles trapped inside a collapsed vesicle of dex$_{6500}$-*b*-PEG$_{5500}$.

3.1.4.b Structure of the membrane by Surface Enhanced Raman Spectroscopy

Conventional Raman spectroscopy experiments performed on 5 wt% solutions of dex$_{6500}$-*b*-PEG$_{5500}$ assess the chemical structure of the macromolecule. The main bands were attributed from the literature[158]-[161] and from the Raman spectra of single blocks solutions (Figure 3.15).

First, the Raman spectrum of the dex$_6$-*b*-PEG$_{5000}$ appears as the superposition of the spectra of both homopolymers assessing its chemical structure. An unexpected band arises at 1722 cm^{-1} that could only be attributed to a carbonyl C=O function. This is in contradiction with the formal structure of the polymer and could only be attributed to an impurity. For the PEG signals, the CH$_2$ rocking shows up at 843 cm^{-1}, the endo and exo C-O stretching appear at 1042 cm^{-1} and 1131 cm^{-1} respectively, the CH$_2$ twist at 1281 cm^{-1} and the symmetric plane bending of CH$_2$ at 1467 cm^{-1} as well as the symmetric and asymmetric stretching of CH$_2$ at around 2917 cm^{-1}. For the dextran signals, the low and medium intensity bands between 395 cm^{-1} and around 700 cm^{-1} are characteristic of the low frequency ring vibration in saccharides. The band at 510 cm^{-1} corresponds to the OH related stretching signal. The overlapped bands at around 1100 cm^{-1} correspond to the C-O-H bending (typically 1081 cm^{-1}) and the C-C stretching (typically 1130 cm^{-1}). Bands at 1335 and 1459 cm^{-1} arise from the C-O-H twisting and the CH$_2$ in plane bending respectively.
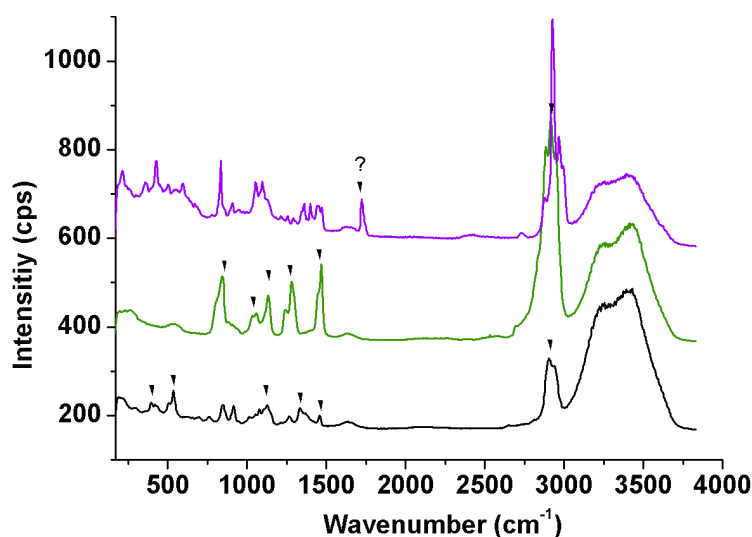
Figure 3.15: Raman spectra of dex$_{6500}$-*b*-PEG$_{5500}$ (violet), PEG homopolymer (green) and dextran homopolymer (black).

The Raman spectrum (Figure 3.16) of the polymer vesicles in the presence of gold nanoparticles of 20 nm was prepared as schematized in Figure 3.12. As explained before, this preparation could allow the "visualization" of the outer polymer if a surface-enhanced signal is obtained. The confocal Raman setup allows to optically visualize the sample *via* a CDD camera. The vesicles could be discerned as small dots (see paragraph 3.1.7.b), and were in

big quantity adsorbed on the glass surface. A careful manipulation could thus allow the recording of the Raman signal on the vesicle. A surface-enhanced Raman signal was recorded showing the exaggeration of three bands in the low frequency region and the suppression of all other bands (except the solvent) especially the ones characteristic of the PEG block. The three exaggerated bands correspond to wavenumbers 391 cm^{-1}, 511 cm^{-1} and 630 cm^{-1}. The bands at 391 cm^{-1} and 630 cm^{-1} are characteristic of the low frequency ring vibration in dextran and 511 cm^{-1} corresponds to the OH stretching signals. The exaggerated bands in the SERS correspond thus to vibration modes of the dextran block while the signals belonging to the PEG block are completely suppressed. This indicates that the dextran block is in contact with the Au nanoparticles and thus that it is this block that constitutes the vesicles' outer layer.
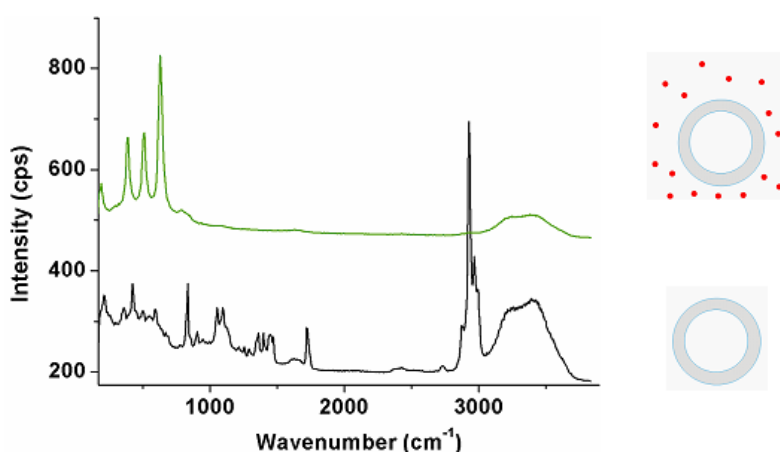
Figure 3.16: (*Left*) Raman (black) and SERS (green) spectrum of of dex$_{6500}$-*b*-PEG$_{5500}$ in water at 5 wt%. The solution for SERS was prepared as explained in Figure 3.12. (*Right*) Representation of the corresponding vesicles and vesicles/Au to the spectra on the left.

Bilayers are the most common membrane structures in polymer vesicles. An outer dextran layer in a bilayer structure could be rationalized if we consider that PEG is "less hydrophilic" than dextran, so in a self-assembly process into vesicular structures it would take the place of the hydrophobic block of a classic amphiphile to form a "less hydrophilic" barrier. A less common membrane structure is the asymmetric one (see Chapter 4). This structure could only be attainable if the triazole ring would pack to form a barrier but this option is geometrically improbable. To confirm the bilayer structure of the membrane, vesicles were

prepared according to Figure 3.13. A SERS spectrum could be recorded on a vesicle (Figure 3.17). The spectrum shows as in Figure 3.16 the enhancement of three bands corresponding to vibrations at 391 cm^{-1}, 508 cm^{-1}, 629 cm^{-1} very similarly to the one with the Au nanoparticles outside the vesicle. These vibration modes correspond also similarly to the ones of dextran. Equally, PEG bands are suppressed in the SERS spectrum thus proving that in the inner compartment of the vesicle the polymer adsorbed to the metal nanoparticle is dextran.
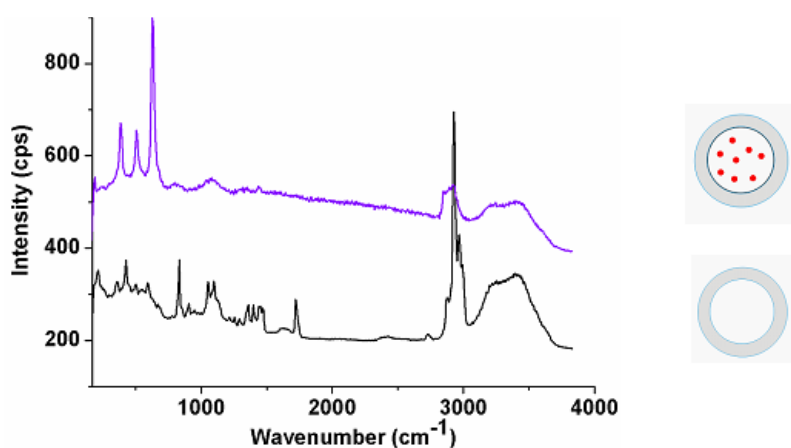
Figure 3.17: (*Left*) Raman (black) and SER (violet) spectrum of of dex$_{6500}$-*b*-PEG$_{5500}$ in water at 5 wt%. The solution for SERS was prepared as explained in Figure 3.13. (*Right*) Representation of the corresponding vesicles and vesicles/Au to the spectra on the left

This confirms the bilayer structure of the membrane that can be schematized as shown in Figure 3.18. Dex-*b*-PEG is thus capable of self-assembly in a similar way to amphiphilic block copolymers in water. The phase separation in the nanoscale is found in the membrane structure where dextran is preferentially solubilized. Some information concerning the membrane is missing such as its thickness. Calculations using a hollow sphere model (Equation (10)) and the bulk polymer density (ρ=1.321 g·cm^{-1}) give d=0.025 nm which is too small. Possible reasons for the impossibility to apply this model are the deviation from the perfect spherical geometry for fluctuating objects and the possible high water content in the membrane that makes the use of the bulk polymer density not adequate.

$$d = R - \sqrt[3]{R^3 - \frac{3M}{4\pi\rho N_A}} \tag{10}$$

In TEM, although the vesicles are visible they appear collapsed and an evaluation of d seems too inaccurate. Low contrast in small-angle X-ray scattering (SAXS) and cryo-TEM could not deliver either such information (data not shown). For SANS, in D_2O no aggregates seem to form (data not shown). This could be explained by the solubility difference of some poly(saccharides) in water and deuterium oxide[162]-[164] often attributed to the different H-bonding capabilities of the solvents. This also proves the importance of the solvent-polymer interaction parameters in this process.

Classic AB amphiphilic block copolymers usually present interdigitated membranes and are far from the idealized bilayer structure of liposomes. The robust entanglement within the hydrophobic layer is usually considered as a "physical cross-linking" able to enhance the mechanical properties when compared to liposomes.[153][165][166] In our case, although there is a barrier, it is rational to think that the PEG phase is hydrated and thus our vesicles are expected to show low-performance mechanical properties and high sensitivity to environment perturbations affecting the relative solubility balance (salts, additives...).
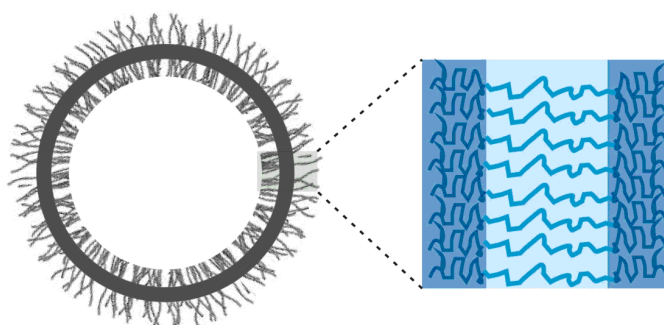
Figure 3.18: Idealized membrane structure in polymersomes from dex$_{6500}$-*b*-PEG$_{5500}$ DHBC. In light blue the "less hydrophilic" barrier formed by PEG segments of the block copolymer, in dark blue the "more hydrophilic" dextran segments.

3.1.5 Concentration and temperature influence

It is generally believed that concentration and temperature are two major parameters affecting the aggregation of block copolymers in selective solvent even beyond the possible phase transitions that they can induce (see paragraphs 2.2.2.a and 2.2.2.b). For example,

elevating the temperature can change the packing parameter of amphiphiles by partial dehydration of the "hydrophilic head" reducing thus *a* in the packing parameter expression (Equation (5) p.13). Concentration itself has been shown to have a great influence on several morphologies characteristic such as the aggregation number Z.[167] To establish a comparison with classic amphiphilic systems their influence on the self-assembly of dex$_{6500}$-*b*-PEG$_{5500}$ were studied.

3.1.5.a Concentration effect on the aggregate's size

The size of the aggregates turned out to be dependent in big measure on the preparation method and even stirring speed. The concentration dependence of the slower mode aggregates was studied when prepared *via* two different methods (Figure 3.19).
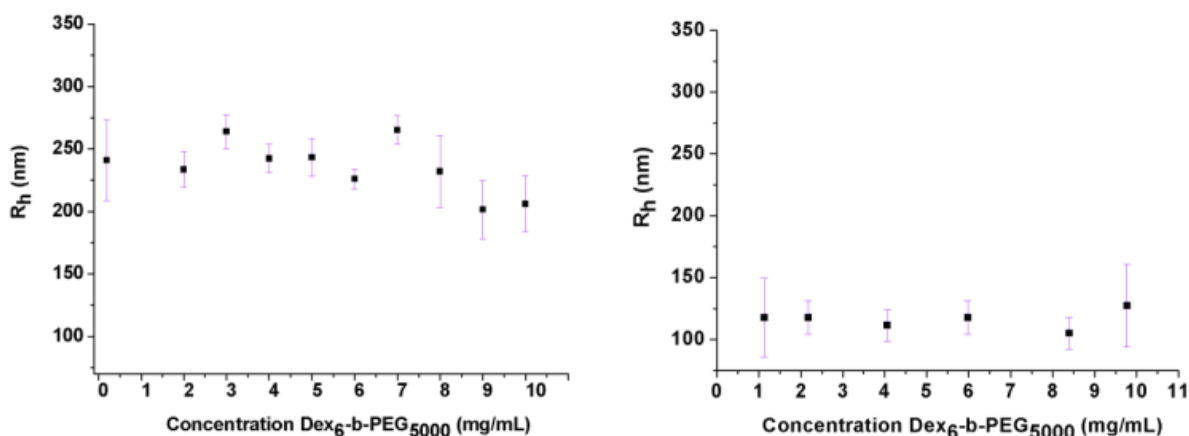
Figure 3.19: Hydrodynamic radii as a function of concentration obtained by a REPES analysis of DLS data at 90°. (*Left*) dex$_{6500}$-*b*-PEG$_{5500}$ solutions at different concentration obtained by dilution of a stock solution. (*Right*) dex$_{6500}$-*b*-PEG$_{5500}$ solutions obtained by direct dissolution of the polymer in milliQ water. In both graphs faster modes were omitted.

Polymer solutions prepared by dilution of a stock solution showed higher R$_h$ (200-250 nm) than the solutions obtained by direct dissolution of the polymer (110-130 nm). It is not uncommon to encounter method-dependent sizes in colloidal polymeric aggregates. For example, micelles and vesicles produced using the dialysis method have sizes strongly dependent on the organic solvent used.[168] It could be expected that the fast dynamics assured by relatively short block lengths and the simultaneous solubility of both blocks would produce a single aggregate size distribution corresponding to the energy minimum. This

difference confirms that the aggregates seen in DLS are non-equilibrium structures, as the multimodal distribution already suggested.

Whatever the sample preparation method might be, it seems clear that the aggregates sizes are not concentration dependent within each preparation. This confirms that the aggregates formed are not the result of an isodesmic process or specific supramolecular interactions but rather suggests a cooperative aggregation mechanism.

It should be noted that this concentration independence of the aggregate size is in accordance with the only other report by Liang *et al.* on the association of polymers in non-selective solvent.[169] In this study on the association of PEO_{44}-*b*-$PDMA_{173}$ in water, it was found that the slow mode was concentration independent in a 0.6 mg·mL^{-1}-2 mg·mL^{-1} range even though in their case the ρ-ratio of 1.4 indicated an extremely loose aggregate close to a random coil conformation.

3.1.5.b Temperature
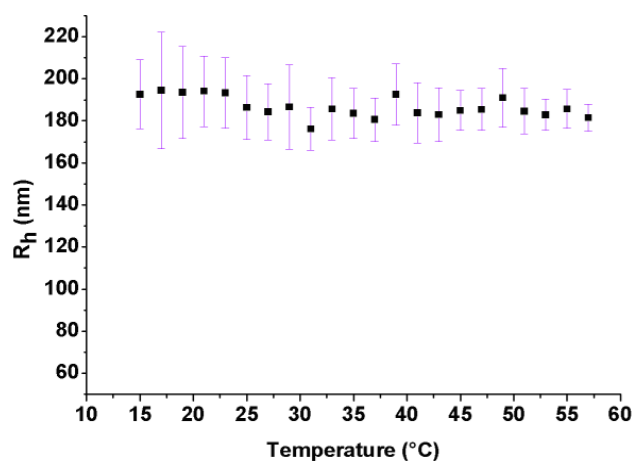
Figure 3.20: Hydrodynamic radius as a function of the temperature for the aggregates corresponding to the slow mode by DLS 90°.

A temperature gradient applied to a 1 mg·mL^{-1} solution of the polymer revealed that the aggregate's size is independent of the temperature within the studied range (Figure 3.20). PEG is a thermoresponsive polymer but its cloud point strongly depends on the molar mass. PEG of molar mass 5500 g·mol^{-1} exhibits a cloud point at around 105 °C, so in the studied

range no collapse was expected.

Towards higher temperatures the polydispersity of the aggregate's size decreases. That can be seen by plotting the standard deviation of the hydrodynamic radius against the temperature (Figure 3.21). For temperatures of around 17-19 °C the standard deviation is well over 20 nm, for the last temperatures around 57-59 °C this deviation is a little over 5 nm. Even outside phase transition this variation can be understood in terms of partial dehydration. PEG being "more hydrophobic" or rather "less hydrophilic" than dextran, it would preferentially partially loose hydration water molecules upon heating. Actually D-glucose only looses 0.05 g of water per gram of D-glucose from room temperature to 55 °C[135] remaining thus well hydrated. Its polymer dextran should thus follow the same tendency. So the decrease in the vesicle's polydispersity in size is mainly due to the partial dehydration of the PEG layer that rigidifies the vesicle's membrane minimizing the fluctuation of the size.
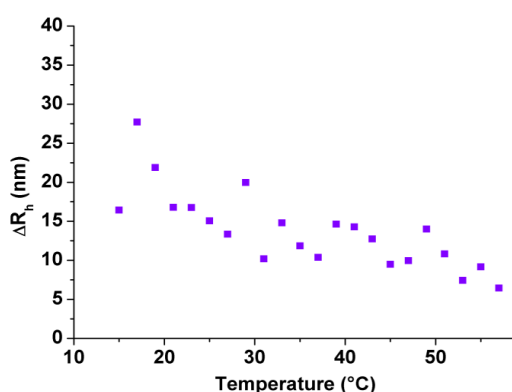
Figure 3.21: Standard deviation to the mean value of the hydrodynamic radius for each temperature point.

3.1.6 Structural parameters

3.1.6.a Chain length

Chain length influence on the topology of the aggregates was studied. Three additional dextran-*block*-poly(ethylene glycol) copolymers were synthesized (see paragraph 3.1.2.a), one with a shorter PEG block (dex$_{6500}$-*b*-PEG$_{1900}$), one with longer dextran block (dex$_{11000}$-*b*-PEG$_{5500}$) and one with longer PEG block (dex$_{6500}$-*b*-PEG$_{13200}$).

The dissolution of dex_{6500}-b-PEG_{5500} leads to a system off thermodynamic equilibrium and thus in this chain length study this fact should be considered. The sizes of the aggregates cannot be directly compared for example. But the topology of the aggregates can elucidate the role of each block especially in regards to a comparison with the influence of the different block in classic amphiphilic systems. Samples were prepared in the same way by dissolution of the polymer solids in water. All the samples show slow modes in light scattering. A simple comparison was made on the basis of the ρ-ratio of the aggregate in the systems. The light scattering plots used to determine the gyration and hydrodynamic mode can be found in the Supporting experimental data in appendix.

The influence of the PEG block on the ρ-ratio was first examined (Table 3.4). Although the ρ-ratio cannot unambiguously elucidate the geometry of an aggregate, its variation with the chain length is a proof of morphology change.

Table 3.4: Influence of the PEG block length on the ρ-ratio

	R_g *(nm)*[*1]	R_h *(nm)*[*2]	*ρ-ratio*
dex$_{6500}$-b-PEG$_{1900}$	144	117	1.23
dex$_{6500}$-b-PEG$_{5500}$	221	226	0.98
dex$_{6500}$-b-PEG$_{13200}$ [*3]	134	164	0.82

[*1] as determined by a Berry plot of the SLS data. [*2] as determined by the REPES analysis of a 1mg·mL^{-1} or dynamic Zimm plot. [*3] the polymer contains residual PEG homopolymer.

As previously discussed, the copolymer with intermediate block length (dex_{6500}-b-PEG_{5500}) see paragraph 3.1.3) presents vesicular structures in water with a ρ-ratio of 0.98. A shorter PEG block (dex_{6500}-b-PEG_{1900}) induces an increase of the radii ratio to 1.23. These values are characteristic of either rod-like (ρ-ratio >1.3) micelles or gaussian coils (ρ-ratio ~1.5). The good quality of the static scattering data allowed the fitting of the form factor with the coils and thin rod models using the gyration radius extracted from the Berry plot (see Supporting experimental data). The fitting seems to indicate that the polymer self-assembles into a loose conformation close to a Gaussian coil (Figure 3.22). If the analogy to a classic amphiphile is made, with the "less hydrophilic" PEG acting as the hydrophobic block, a transition from a loose conformation ("loose aggregates") to a more rigid one (vesicles) by varying the PEG

block length seems to be in accordance with the classic self-assembly processes for both enthalpic and entropic reasons.

Vice versa, by making the PEG block longer, a ρ-ratio of 0.82 is obtained. This value is intermediate for the values expected for a hard sphere (ρ-ratio =0.775) and vesicle (ρ-ratio=1) and probably corresponds to an poorly defined intermediate structure, such as "loose micelles" or "loose micelle clusters".[170] This transition from a vesicle to a more compact aggregate should be considered carefully as homopolymer PEG residues are known to affect the self-assembly even inducing phase transitions.[171]
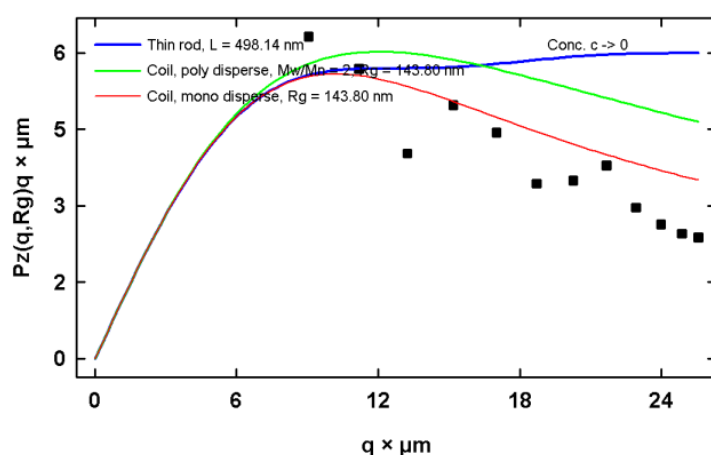
Figure 3.22: Holzer plot, z-averaged P(q,Rg)q as a function of the scattering angle.

When the PEG block is considered as the "less hydrophilic" block, the evolution of the packing parameter (Equation (5) p.13) with increasing PEG block length should predict transitions from curved structures such as micelles towards bilayered ones such as vesicles. In our case, the isothermal transition from coil to vesicles to "micellar" structures in dilute solution with increasing PEG block lengths follows the inverse trend.

Table 3.5: Influence of the dextran block length on the ρ-ratio

	R_g (nm)[*1]	R_h (nm)[*2]	ρ-ratio
dex_{6500}-b-PEG$_{5500}$	221	226	0.98
dex_{11000}-b-PEG$_{5500}$	96	119	0.81

[*1] as determined by a Berry plot of the SLS data. [*2]as determined by the REPES analysis of a 1mg·mL^{-1} or dynamic Zimm plot.

The variation of the "more hydrophilic" block length was also studied (Table 3.5). By introducing a longer dextran block with constant PEG block length the packing parameter evolved from a ρ-ratio of 0.98 to a ρ-ratio of 0.81. This ratio as previously discussed is intermediate from the ratios expected for micelles and vesicles, and sometimes translates "loose micelle-like" aggregates. It is commonly acknowledged that a shorter hydrophilic block tends to promote vesicular structures in amphiphilic block copolymers. This trend is confirmed in our system.

3.1.6.b Architecture

The influence of the polymer architecture on the self-assembly behavior was studied by means of a dextran$_{6500}$-*block*-poly(ethylene glycol)$_{5100}$-*block*-dextran$_{6500}$ triblock copolymer. This copolymer would be expected to form also vesicles in dilute aqueous solution with a membrane structure analogous to previously observed for the diblock copolymer.

REPES treatment of the dynamic light scattering 90° (Figure 3.23) shows a distribution analogous to the one observed in the case of the diblock copolymer. Two fast modes of low intensity corresponding to structures of a few nanometers were observed. A slower mode of 101 ±9 nm was responsible for 84 % of the scattered intensity. This size is smaller than the size observed in the diblock copolymers by direct dissolution of the polymer (116 ±30) nm but comparable.

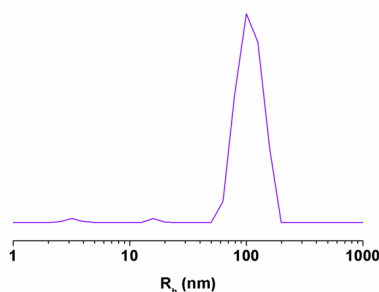Figure 3.23: Intensity-weighted distribution of the hydrodynamic radius of the dynamic light scattering at 90 ° for a dex$_{6500}$-*b*-PEG$_{5100}$-*b*-dex$_{6500}$.

Because of the low angular dependence of the aggregate's diffusion on the scattered intensity,

the static parameters could be fitted using a Zimm plot (Figure 3.24). The resulting ρ-ratio of 1.08 suggests a vesicular structure. Attempts to visualize any kind of colloidal object by TEM was unsuccessful.

$$M(c)= 2{,}77 \cdot 10^5 \text{ g·mol}^{-1} \pm 10\%$$
$$R_g= 109 \text{ nm} \pm 4\%$$
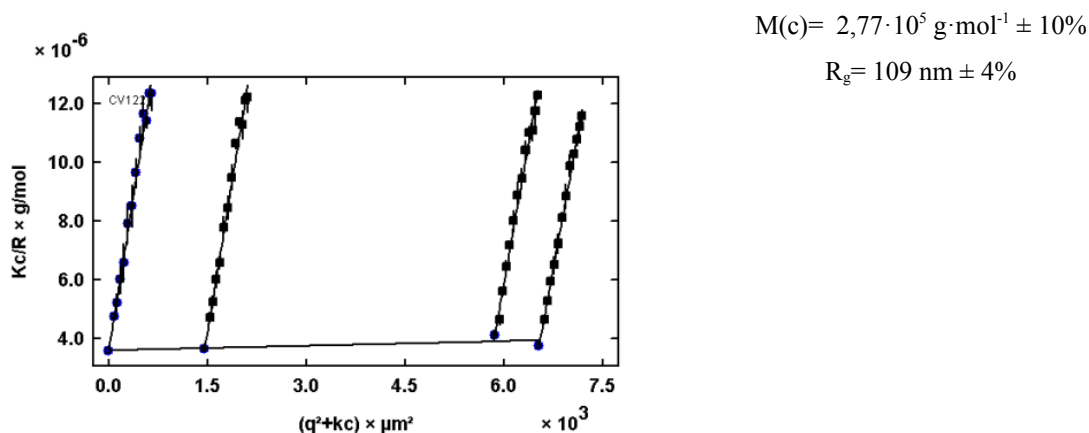
Figure 3.24: Zimm plot of the static light scattered data of the triblock copolymer

It seems though that the vesicular structure is maintained in the triblock copolymer dex_{6500}-*b*-PEG_{5100}-*b*-dex_{6500}. Because poly(ethylene glycol) is the middle block, that would confirm that this blocks acts as the barrier in the vesicles with dextran as solubilizing block.

3.1.6.c Linking

Another structural parameter studied was the linking function. To reject the possibility that the aggregates observed in dex-*b*-PEG copolymers synthesized *via* CuAAC could result from specific interactions involving the 1,2,3-triazole group or even from the residual Copper(II) impurities,[172] the aggregation behavior of a dex_{6500}-*b*-PEG_{5700} polymer with amide linking (see paragraph 3.1.2.c) was studied.

The REPES analysis of the dynamic light scattering of a 1 mg·mL^{-1} (prepared by direct dissolution of the solid) of this polymer (Figure 3.25) reveals an aggregation behavior in which a very slow mode at around 1000 nm is observed. Taking into account its intensity with respect to its size, it is clear that it involves a minimal fraction of polymer (if it is not dust particles) and should not be further considered.

A slow mode responsible for over 85% of the scattered intensity appears at 120 ±22 nm. Although this aggregate's size was found to correspond to the aggregates size of 116 ±30 nm found in this same polymer prepared by CuAAC by direct dissolution of the solid in water, its size was extremely dependent on the stirring speed.
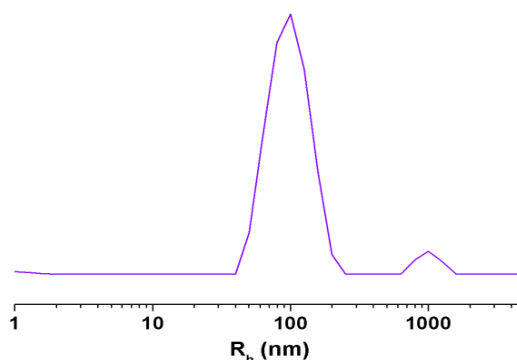
Figure 3.25: REPES algorithm treatment of the dynamic light scattering at 90 ° of a 1 mg·mL^{-1} solution in water of dex$_{6500}$-*b(amide)*-PEG$_{5500}$

Interestingly no fast mode was detected, which could mean that fastest modes in the dex-*b(triazole)*-PEG were maybe due to unreacted homopolymers, the product of copper(II)/homopolymer or copper(II)/copolymer interactions, or other product of triazole interaction.
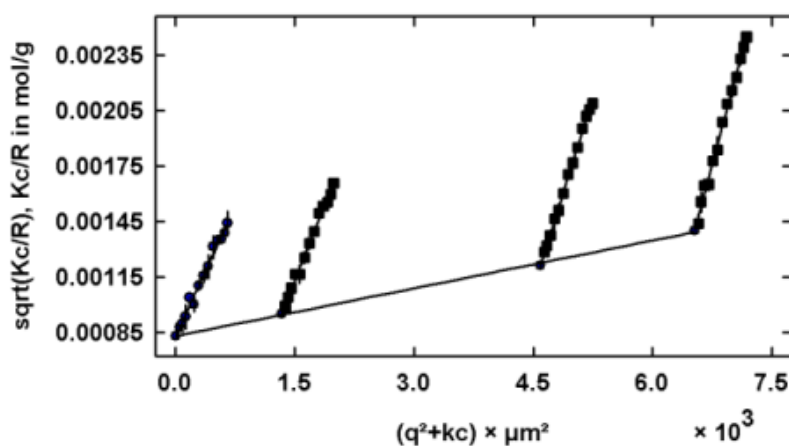
M_w= 1.45·10^6 g.mol^{-1}

R_g= 82 nm

A_2= 1.20·10^{-7} dm^3·g^{-2}

Figure 3.26: Berry plot of the SLS data obtained between 40° and 150° at room temperature for dex$_{6500}$-b(amide)-PEG$_{5500}$ polymer solutions.

Because as previously mentioned, the diffusion mode of the aggregate was found to be extremely dependent on the stirring speed during the dissolution of the polymer powder, a simultaneous angular dependent dynamic light scattering and static light scattering experiment was performed to evaluate the hydrodynamic and the gyration radii respectively. The Berry plot (Figure 3.26) of the SLS data delivered a gyration radius of 82 nm and the dynamic Zimm plot of the DLS (Figure 3.27) a hydrodynamic radius of 98 nm. The resulting ρ-ratio of 0.837 does not correspond unambiguously to either a homogeneous sphere (ρ-ratio= 0.775) or a hollow sphere model (ρ-ratio=1) and more likely translates a vesicle with very thick shell or rather a core-shell type of aggregate with low density core.

$D_{z,0} = 2{,}51 \ \mu m^2.s^{-1} \pm 2\%$

$R_h = 98 \ mn$
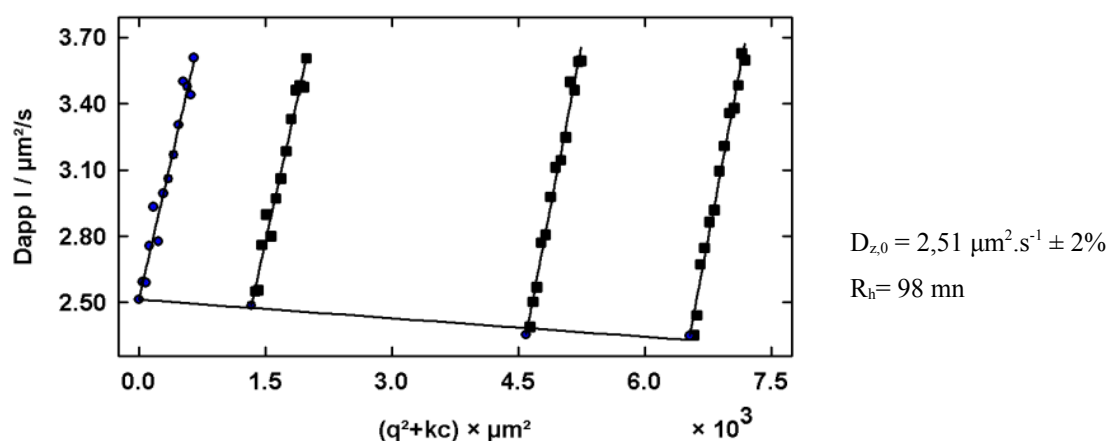
Figure 3.27: Dynamic Zimm plot of the DLS recorded between 30 ° and 150 °.

A possible explanation for the difference in the morphology of the aggregate for this dex-*b*(amide)-PEG when compared to dex-*b*(triazole)-PEG could be given in terms of packing parameters. Because the block lengths are equal in both polymers, the origin could reside in the unimer's curvature. If the triazole ring can induce a higher packing parameter, then the vesicular shape should be preferred. In this case the origin of this difference can be double: either the triazole ring induces conformational changes in the blocks or the copper used for the coupling complexes with one or both of the blocks and induces these changes. Which seems nevertheless confirmed is the fact that the self-assembly in itself is not the result of complexation or any other specific interaction involving the copper ions or the triazole. This was further confirmed by other control experiments involving the addition of

copper and other cations (calcium(II)...) to the block copolymer and the single block and studying the systems by light scattering (data not shown).

3.1.7 Towards biologicals applications

3.1.7.a Lectin-carbohydrate interaction

A colloidal structure with an external layer of saccharides/polysaccharides is a privileged system on which to study lectin-carbohydrate interaction (see chapter 4.4.1). The evolution of the hydrodynamic radius of the dex_{6500}-*b*-PEG_{5500} vesicles in HBS buffer after addition of a ConA solution was monitored over time at 25 °C (Figure 3.28). The graph shows the slow evolution of the hydrodynamic radius over time and big particles over a micron where only detected after a day. Interestingly, even after a week no precipitation was visually observed although after two days clusters of over 2 μm were detected by DLS.
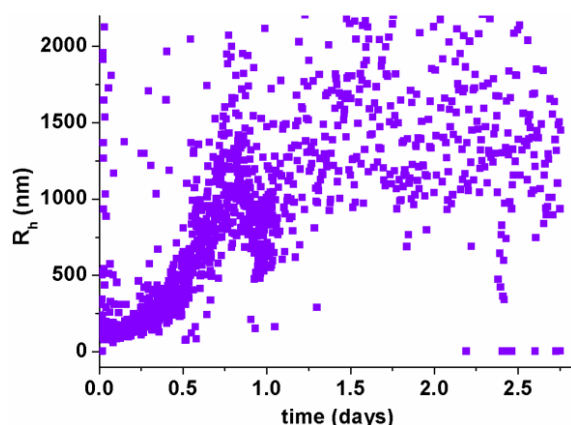
Figure 3.28: Monitoring of the evolution of the hydrodynamic radius after addition of ConA
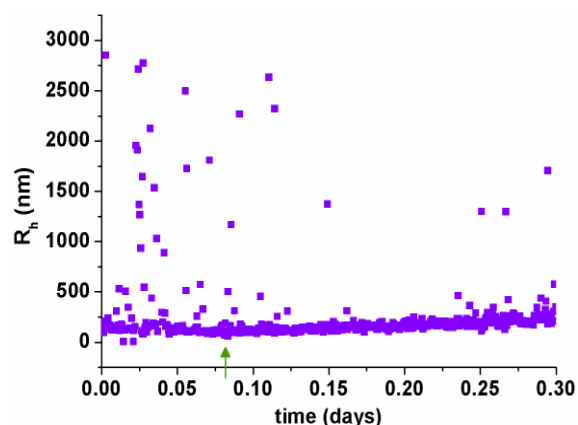
Figure 3.29: Detail of the evolution of the hydrodynamic radius on the first hours after addition of ConA. The green arrow marks the time at which the FCS measurement was carried out.

In the first hours after addition of the ConA solution (Figure 3.29) no apparent evolution of the hydrodynamic radius is observed. This could be due to the absence of specific interactions between the vesicles and the proteins. But if there was a ligand-receptor interaction between glycosydic groups and Con A, it could be that the geometrical arrangements of the carbohydrate epitopes and the CDRs of the lectins do not allow a

multivalent interaction. This was previously reported for vesicles of big size[173] and in paragraph 4.4.1 .

In order to investigate the interaction in the first hours after the addition of ConA, fluorescence correlation spectroscopy (FCS) was performed on liquid samples of the vesicles after addition of fluorescein isothiocyanate (FITC)-labeled ConA (Figure 3.30).
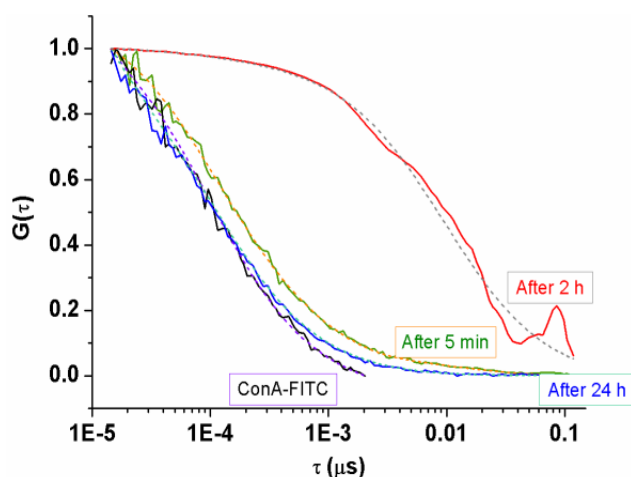
Figure 3.30: Normalized autocorrelation of fluctuation of the fluorescence intensity and its fittings: in black (violet fitting) FITC-ConA in HBS solution; in green (orange fitting) dex$_{6500}$-b-PEG$_{5500}$ with FITC-ConA in HBS solution after 5 min; in red (gray fitting) dex$_{6500}$-b-PEG$_{5500}$ with FITC-ConA in HBS solution after 2 h. and in blue (turquoise fitting) dex$_{6500}$-b-PEG$_{5500}$ with FITC-ConA in HBS solution after 24 h.

Table 3.6: Data extracted from the analysis in the FCS experiments.

Sample	CR (kHz)	CPM (kHz)	N	Fraction 1		Fraction 2	
				%	$\tau_D(\mu s)$	%	$\tau_D(\mu s)$
FITC-ConA	17.3	13,3	1.3	96	110	-	-
Dex$_{6500}$-b-PEG$_{5500}$ +FITC-ConA after 5 min	37.5	0,49	76	80	110	20	10200
Dex$_{6500}$-b-PEG$_{5500}$ +FITC-ConA after 2 h	34.2	49,1	0.7	4	110	96	3500
Dex$_{6500}$-b-PEG$_{5500}$ +FITC-ConA after 24 h	29.7	1,6	20.5	95	110	5	2700

The normalized autocorrelation curve of the FITC-ConA protein (in black) shows a fast diffusion that could be fitted to a single population of objects with diffusion time of 110 μs as previously described (see paragraph 4.4.1). By addition of this same quantity of FITC-ConA

to a solution of dex$_{6500}$-*b*-PEG$_{5500}$ in HBS buffer at room temperature, after 5 minutes that autocorrelation curve (in green) shows only a slightly slower relaxation that could be fitted to a mixed population of 80% of objects corresponding to FITC-ConA and 20 % corresponds to slower diffusing objects. After 2 h the fitting of this curve revealed an almost unique (96%, Table 3.6) population of objects with a diffusion time of around 3500 µs and barely any free FITC-ConA. This corresponds to particles of around 230 nm in diameter with corresponds exactly to the size found by DLS in HBS for the vesicles (R$_h$=115 ±30 nm). This point is represented by the green arrow in Figure 3.29 and it proves that indeed ConA binds to the vesicles' surface at room temperature but does not induce agglutination in the first hours. This is certainly related to the vesicles' size that hinders the intermolecular interaction of the ConA with dextran.

After 22 hours, a fast diffusing mode fitted at 95% to the diffusion of FITC-ConA was recorded. This is in contradiction with the DLS monitoring of the hydrodynamic radius, that reveals at that time a polydisperse population but comprised of objects of big size (R$_h$>500 nm). This observation is difficult to explain unless some sedimentation had excluded clusters from the confocal volume. Later clustering can be explained if the interaction of ConA with the dextran locally disrupts the vesicles to fullfill the multivalent interaction. Seeing as the forces holding the vesicles can only be weak, the monovalent interaction of the lectin with the dextran could be sufficient for its disruption over time.

Evidently the lectin-carbohydrate interaction is fast but clustering is slow and no precipitation is visible for several days. This interesting kinetics could potentially be used in a biological context.

3.1.7.b Encapsulation of molecules

To achieve effective encapsulation of organic molecules inside the polymer vesicles, a dex$_{6500}$-*b*-PEG$_{5500}$ was functionalized with maleic anhydride (dex$_{6500}$(MA)-*b*-PEG$_{5500}$) in order to make the system crosslinkable (see Appendix I.A.I.2.c)). Briefly, previously synthesized dextran$_{6500}$-*b(triazole)*-PEG$_{5500}$ (~9·10^{-4} mol of OH when approximating dextran to a linear α-

1,6-polyglucan) was dissolved in 0.1 M LiCl/DMF at 60 °C. Triethylamine and 0.2 eq (to OH) of maleic anhydride were added and the mixture was stirred at 60 °C for 24 h and subsequently dialyzed against milliQ water. The functionalization could be assessed by ^{1}H NMR (Figure 3.31) and evaluated at ~ 8% (of the OH functions) by integration of the peaks at δ ~6.0 ppm and δ =4.7 ppm
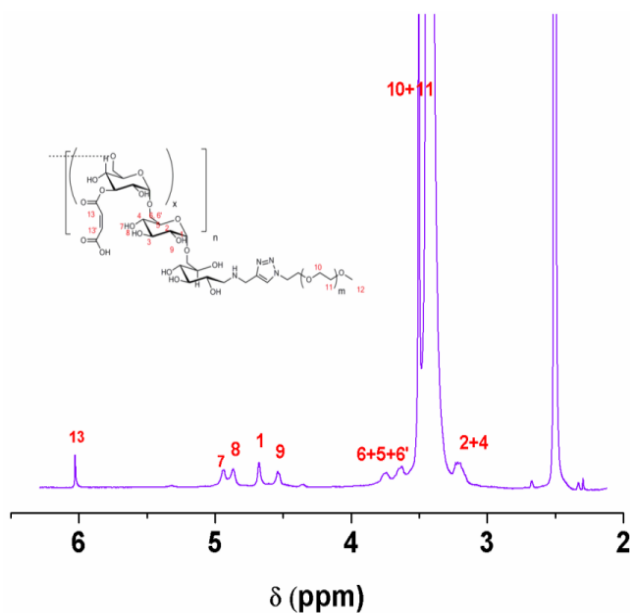
Figure 3.31: ^{1}H NMR dex$_{6500}$(MA)-b-PEG$_{5500}$ in DMSO-d$_6$

The polymer powder could be directly dissolved in milliQ water. Crosslinking was achieved by exposure of a 1 mg·mL^{-1} solution to an intense UV irradiation for 10 minutes. The crosslinking was assessed by comparison on the integral of peaks at δ ~6.0 ppm and δ =4.7 ppm before and after exposure to UV. 33% of the double bonds were found to have reacted.

Dynamic light scattering before (Figure 3.32.a)) and after (Figure 3.32.b)) crosslinking shows first that the introduction of maleic acid modifies the system only slightly and does not prevent the self-assembly process, the size increases from 116 ±30 nm to 139±7 nm. The crosslinking does not significantly affect the size that remains equal within the given error. The system is thus adapted for the encapsulation of organic molecules.

$R_h= 139 \pm 7$ nm $R_h= 146 \pm 7$ nm
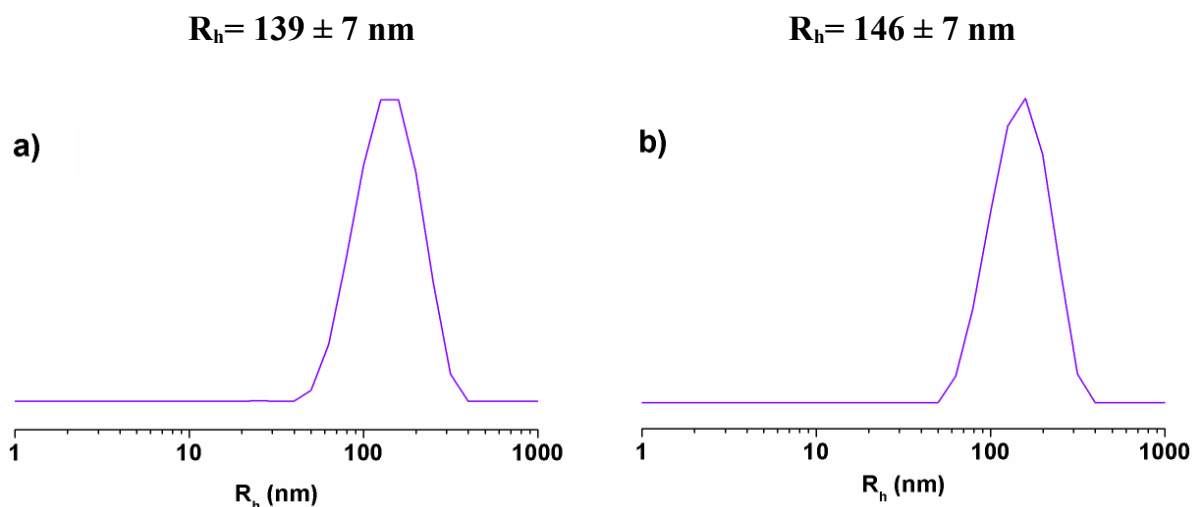
Figure 3.32: Maleic anhydride modified dex_{6500}-b-PEG_{5500} solution at 1 mg·mL^{-1} a) before crosslinking and b) after crosslinking.

For the encapsulation experiments, the modified polymer was directly dissolved in a 0.5 M Rhodamine B solution and subsequently exposed to UV irradiation. After dialysis the solution as well as a non-crosslinked solution of the $dex_{6500}(MA)$-*b*-PEG_{5500} and the non-modified dex_{6500}-*b*-PEG_{5500} as controls were tested for encapsulation properties under the confocal fluorescent microscope. Taking advantage of the slight polydispersity of non filtered samples, vesicles could be individually visualized with the optical transmission and fluorescent microscope as dots (Figure 3.33).

The micrograph in Figure 3.33 b) shows bright red dots corresponding to higher Rhodamine B concentration zones. The encapsulation of Rhodamine B inside the crosslinked vesicles is thus effective. Surprisingly native dex_{6500}-*b*-PEG_{5500} (Figure 3.33 a)) is also able to encapsulate the dye. In both cases the transmission intensity profile translates the vesicle's boundaries into a higher intense level. From the comparison with the fluorescence channel, it can be observed that the increase in fluorescent intensity starts in the membrane boundary, showing that some of the dye is located in the membrane.
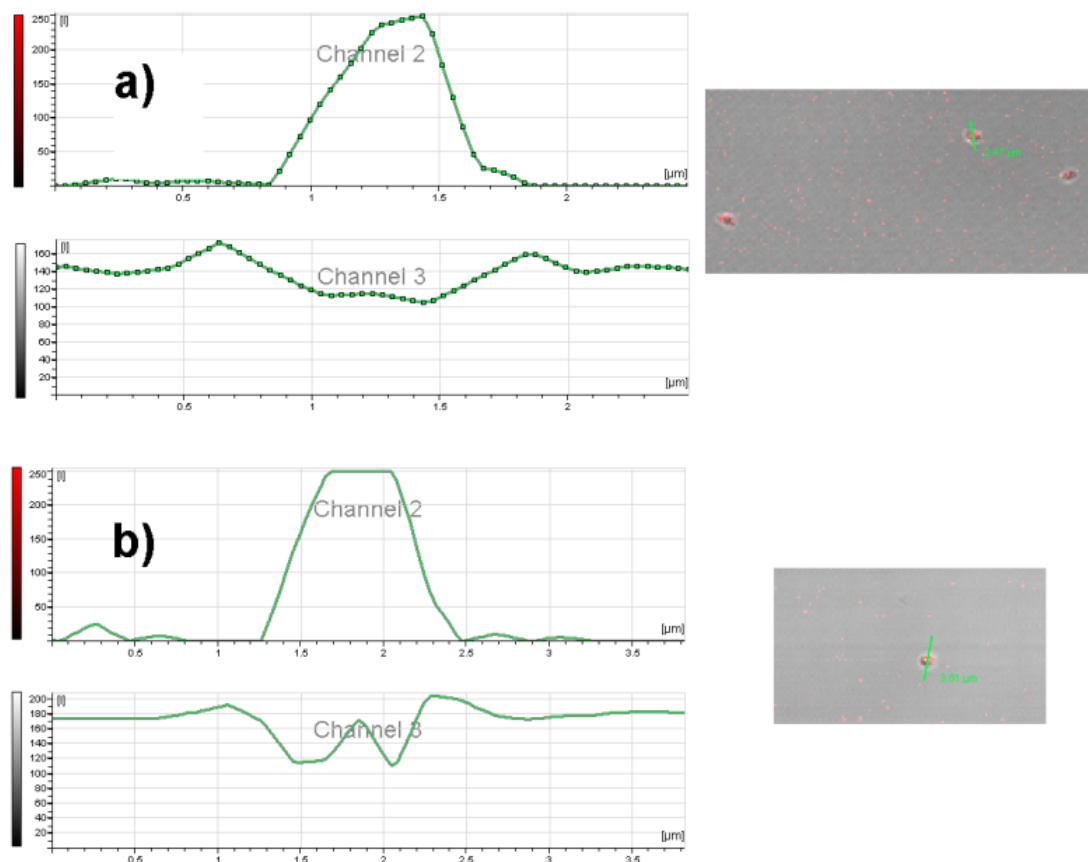
Figure 3.33: Overlay micrographs (right), fluorescence intensity profile (left red scale) and transmission intensity profile (left grey scale) of a)Vesicles based on native dex$_{6500}$-*b*-PEG$_{5500}$. b)vesicles based on crosslinked dex$_{6500}$(MA)-*b*-PEG$_{5500}$

In order to confirm that at least some of the dye was encapsulated and not systematically localized in the membrane and the "fluorescent dots" were due to encapsulation, control experiments were performed by addition of Rhodamine B solution to a solution of vesicles. Micrographs (Figure 3.34) show a continuous fluorescent phase with the vesicles as white dots. The fluorescent intensity of the vesicle's membrane does appear slightly more intense but does not concentrate all the fluorescence; confirming that in our previous experiment the fluorescent dots were due to the effective encapsulation of Rhodamine B. This has profound implications concerning the membrane characteristics. Because vesicle formed in dye solution were subjected to dialysis for two days first, it firstly means that the membrane is impermeable to some extend. This impermeability can only come from at least the partial exclusion of water from the "less hydrophilic" barrier. It also means that there must be some

chain-chain interaction between the PEG segments and that the membrane constitutes a real "barrier". The double hydrophilic membrane effectively separates two distinct aqueous phases.
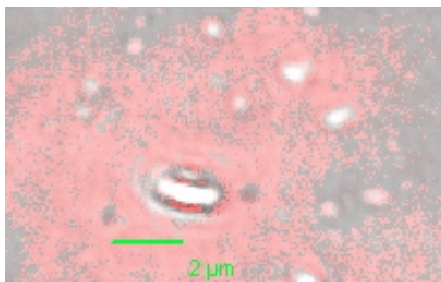
Figure 3.34: Overlay micrographs of the control experiment performed on preformed vesicles.

3.1.8 Other polysaccharide-based copolymers

Albertsson[174] published a list of polymer systems capable of phase separation in aqueous media. Two easily accessible synthetic polymers of the vinyl family appear as capable of phase separation with dextran, poly(vinyl alcohol) and poly(vinyl pyrrolidone). Poly(vinyl alcohol) is a polymer of great industrial relevance and is applied in a wide range of fields such as paper coating, water-soluble packaging, biomedical agents... Poly(vinyl pyrrolidone) is another synthetic highly hygroscopic polymer with industrial applications as adhesive, additive, membrane, thickening agent. In order to test our working hypothesis concerning the validity of ATPS as source of polymer pairs for block copolymer microphase separation, dextran-*block*-poly(vinyl alcohol) and dextran-*block*-poly(vinyl pyrrolidone) were synthesized. The advantage of working with usual vinyl polymer is that they are easily accessible *via* radical controlled polymerizations and well-defined block copolymers should thus be accessible.

3.1.8.a Synthesis

The synthesis was realized via RAFT polymerization (see paragraph 2.3.1.b) using a macro-dextran CTA prepared by CuAAC chemistry (see paragraph 2.3.2.a). First, an azido functionalized xanthate CTA (2-azidoethyl-2-((ethoxycarbonothioyl)thio)propanoate) was

prepared in a three step synthesis (Scheme 3.6) adapting a procedure reported by Stenzel *et al.*[146] for the preparation of 3-azidopropyl-2-((ethoxycarbonothioyl)thio)acetate.
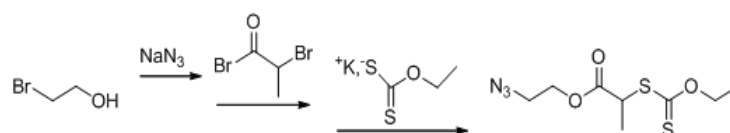
Scheme 3.6: Synthetic procedure adopted for the preparation on a azido-CTA

In a first step bromoethanol was derivatized to azidoethanol by nucleophilic subtitution using sodium azide. This azidoethanol was in a second step coupled to 2-bromopropionyl bromide in dry THF and purified by column chromatography to afford 2-azidoethyl-1-bromoethanoate. In a last step, 2-azidoethyl-1-bromoethanoate was reacted with O-ethylxantic acid potassium salt and purified by column chromatography to afford pure 2-azidoethyl 2-((ethoxycarbonothioyl)thio)propanoate (CTA-N$_3$) with an overall yield of 42% (Figure 3.35).
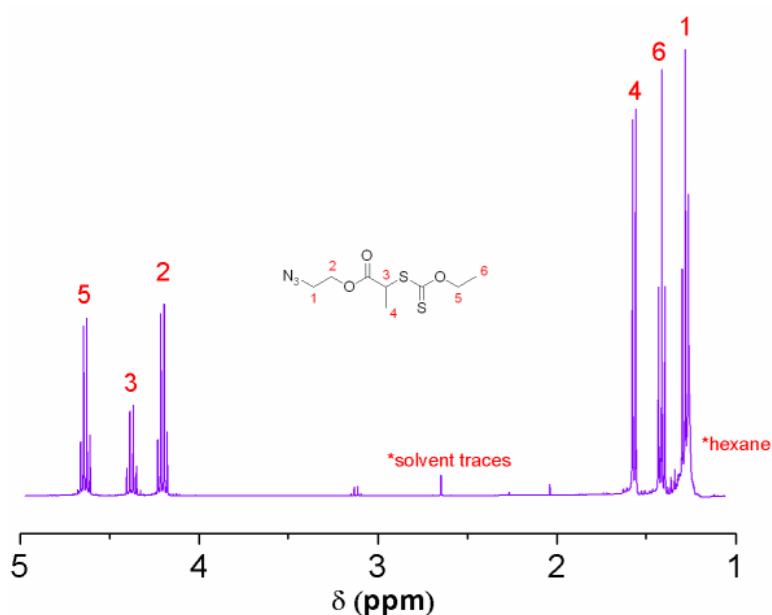
Figure 3.35: ^{1}H NMR of in CDCl$_3$

Coupling to dextran was performed by CuAAC using the dextran alkyne previously prepared for the polymer-polymer coupling. The same synthetical procedure was used including the microware irradiation (Scheme 3.7). The obtained dextran macro-CTA was purified by

dialysis. The yield of the coupling was difficult to evaluate by routine analytical methods. The only evidence was that in the first attempts to polymerize vinyl monomers using this macroinitiator, GPC traces of unreacted dextran homopolymer could be seen. After optimization of the coupling reaction conditions, polymerization yielded a single peak for the copolymer.
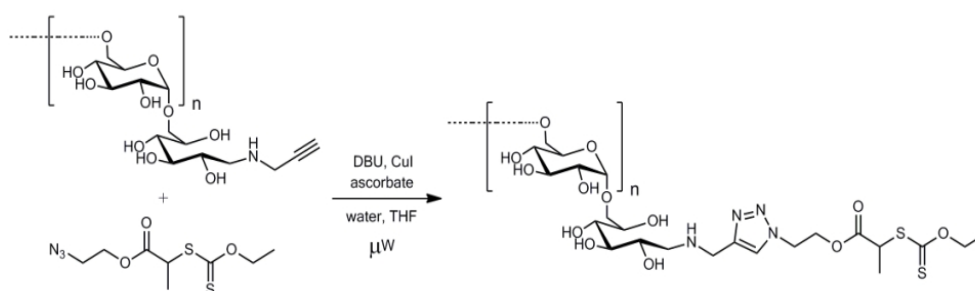
Scheme 3.7: Microwave assisted CuAAC for the coupling to the N$_3$-CTA to dextran alkyne

Although xanthate substituents are critical[175] for the control in a Macromolecular design *via* interchange of xanthanes (MADIX) polymerization, this dextran macro CTA was a good starting point as a generic tool for the polymerization of vinyl monomers *via* RAFT.

As very often when working with polysaccharides-based copolymers the challenge is to find a suitable solvent or solvent mixture. For dextran, the solubility is usually reduced to DMSO and water.
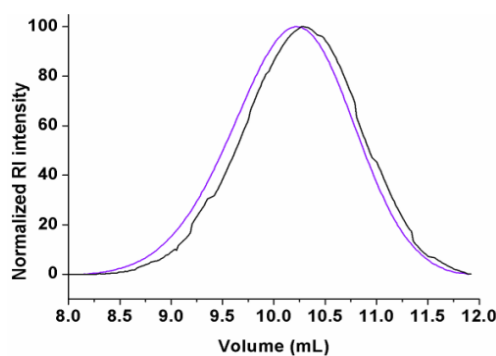
Figure 3.36: GPC traces of dextran-CTA (black) and dex-b-PVP$_6$ (violet).

With poly(N-vinyl-2-pyrrolidone), the synthesis was performed in DMSO. Although DMSO in a non-selective solvent for both blocks, the solution was turbid at the end of the reaction. A

short block could be thus expected for this copolymer. GPC (Figure 3.36) and ^{1}H NMR (Figure 3.37) confirmed the structure of the copolymer but by elemental analysis the length of the PVP block was determined to be only 6 repeating units.
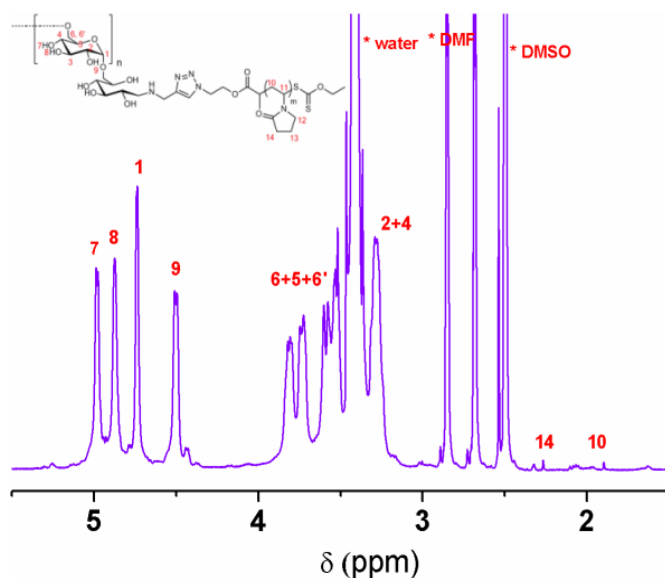
Figure 3.37: ^{1}H NMR of dex-*b*-PVP$_6$ in a DMF-d$_7$ and DMSO-d$_6$ mixture

With vinyl acetate monomer the solubility was achieved by a mixture of DMF and DMSO. Nevertheless at the of the reaction the mixtures were in all cases turbid indicating poor solubility of the copolymers. It could be thus expected an oligomeric poly(vinyl acetate) block that was confirmed by ^{1}H NMR (Figure 3.38). Attempts to perform GPC in DMSO delivered traces with apparent molecular mass lower than the dextran-CTA precursor. It seems like DMSO being a non-solvent for PVAc, it induces the partial collapse of the coil
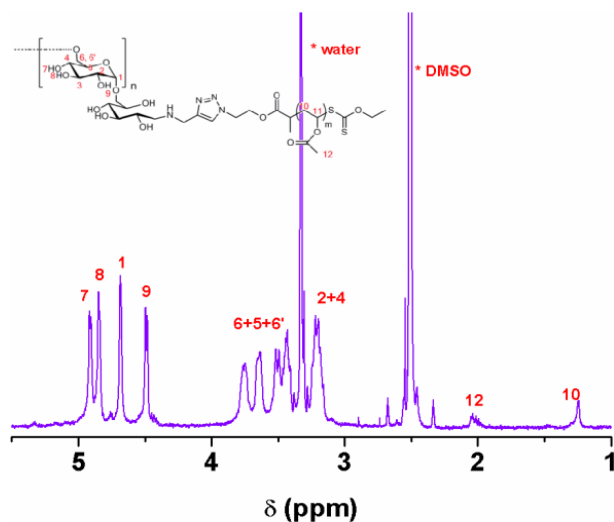
Figure 3.38: ^{1}H NMR of dex-b-PVAc in DMSO-d$_6$.

into a globule.
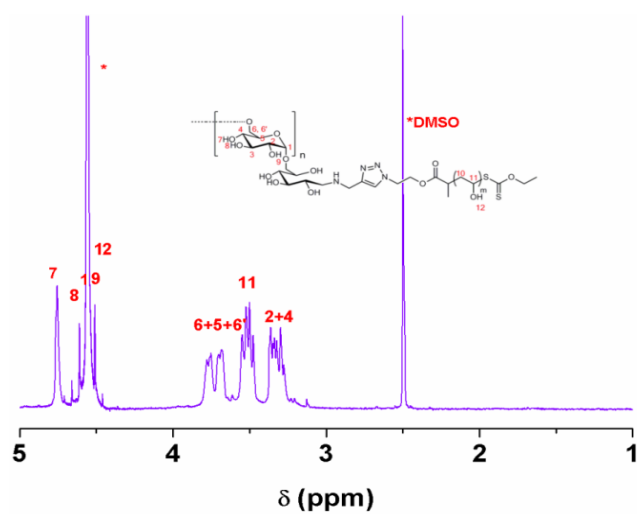
Figure 3.39: ^{1}H NMR of dex-b-PVOH in DMSO-d$_6$/D$_2$O mixture.

Hydrolysis to dextran-*b*-poly(vinyl alcohol) was performed in acidic conditions. Near quantitative hydrolysis was assesed by the disappearance of the acetate CH$_3$-COO- at $\delta \sim$ 2 ppm (Figure 3.39). The block length could not be calculated from EA for either PVAc or PVOH.

3.1.8.b Self-assembly behavior in water

3.1.8.b.1   dextran-block-poly(N-vinyl-2-pyrrolidone)
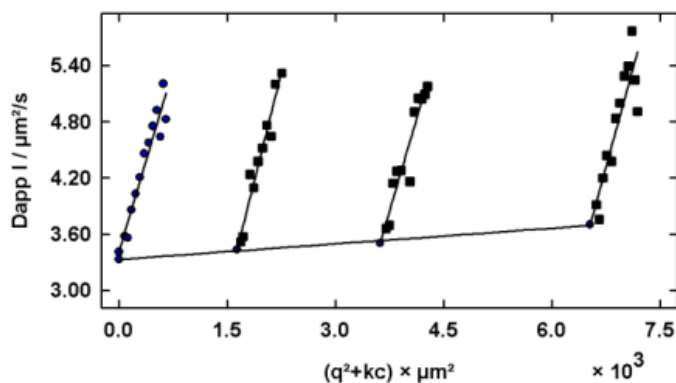
Figure 3.40: Dynamic Zimm plot of the DLS recorded between 30 ° and 150 °.
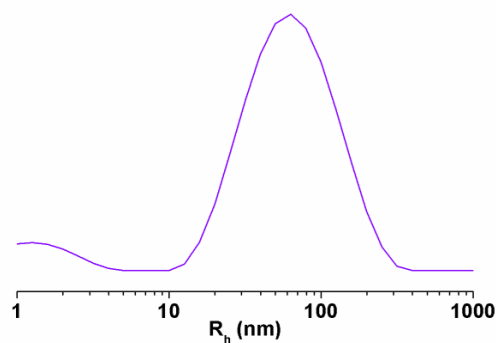
Figure 3.41: REPES analysis of the DLS data recorded at 90°

The dextran-*block*-poly(N-vinyl-2-pyrrolidone) (dex-*b*-PVP) synthesized readily dissolves in water. The DLS reveals the presence of aggregates as well as a fast mode (Figure 3.41). The size of the aggregates is R_h=79 ±9 nm as determined by the REPES analysis of the dynamic light scattering at 90° and R_h=74 nm as calculated from the diffusion coefficient extrapolated to concentration 0 in the dynamic Zimm plot (Figure 3.40).

The fitting of the static light scattering with a Berry plot (Figure 3.42) delivered a gyration radius of 74 nm. The subsequent ρ-ratio of 0.93 (for R_h=79) or 1.0 (for R_h=74) as well as the relatively low molecular weight of the aggregate suggests that the slow mode is due to vesicles.

$M_w = 4.42 \cdot 10^5 \text{ g} \cdot \text{mol}^{-1}$

$R_g = 74$ nm

$A_2 = 7.21 \cdot 10^{-7} \text{ dm}^3 \cdot \text{g}^{-2}$
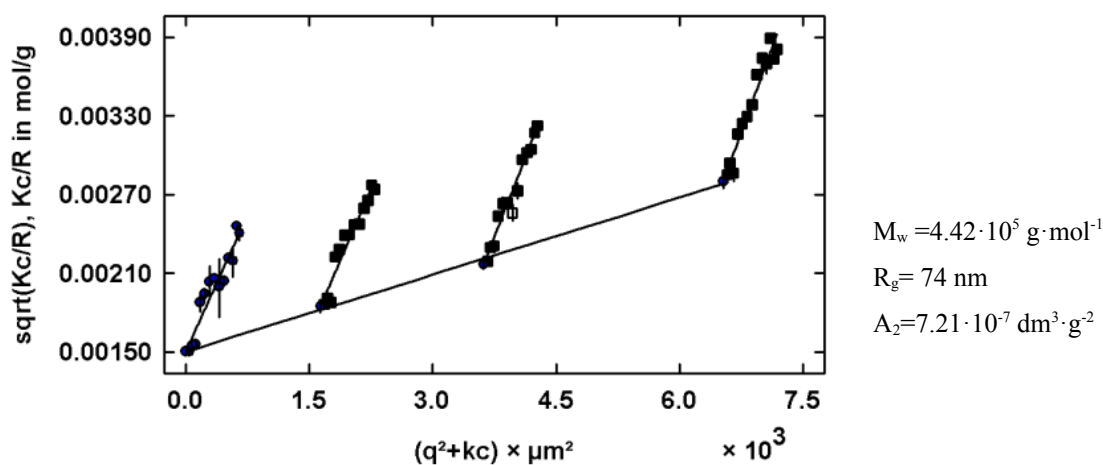
Figure 3.42: Berry plot of the SLS data obtained between 40° and 150° at room temperature for dex6-*b*-PVP polymer solutions.

3.1.8.b.2   *dextran-block-poly(vinylalcohol)*
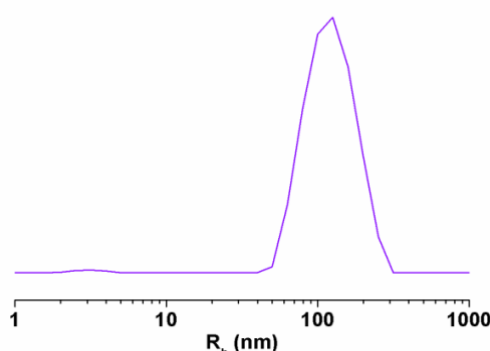
Figure 3.43: REPES analysis of the DLS data recorded at 90°.

The dextran-*block*-polyvinylalcohol (dex-*b*-PVOH) could also be readily dissolved in milliQ water. The REPES analysis of the dynamic light scattering at 90° shows a main mode at $R_{h,app} = 123 \pm 20$ nm (Figure 3.43).

In the Berry plot (Figure 3.44) of the static light scattering the $R_g = 193$ nm found give a ρ-ratio of 1.56. This value slightly over 1.50 suggests that the aggregate responsible for the slow mode is close to a coil (theoretical ρ= 1.50). As previously found in the only other report on self-assembly of non-responsive block copolymers in dilute solution in water,[169] this polymer self-assembles into a loose conformation close to a Gaussian coil

73
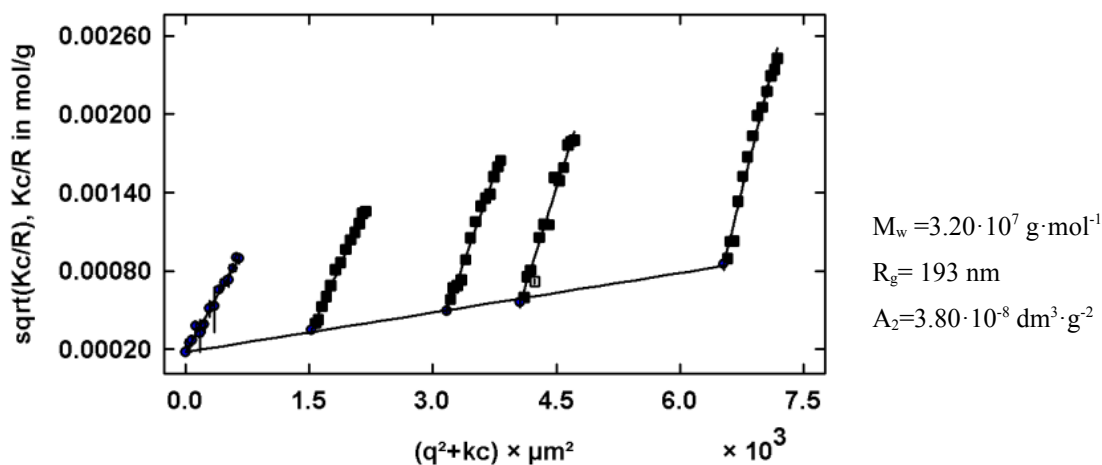
Figure 3.44: Berry plot of the SLS data obtained between 40° and 150° at room temperature for dex-*b*-PVOH polymer solutions.

$M_w = 3.20 \cdot 10^7$ g·mol^{-1}

$R_g = 193$ nm

$A_2 = 3.80 \cdot 10^{-8}$ dm^3·g^{-2}

Both polymers directly inspired from ATPS systems seem to form aggregates in dilute solution. This proves that ATPS systems are an excellent and valid source of inspiration to engineer such systems. It also strongly suggests that the study of the macrophase separation in the ATPS systems should be an excellent model for the deep understanding of the microphase separation in the block copolymers and the detail of their driving forces.

3.2 Spontaneous self-assembly of polypeptide-based and polysaccharide hybrid block copolymers

3.2.1 Spontaneous self-assembly of polypeptide-based block copolymers

De Schryver *et al.*[176] *r*eported in 1996 the "potential tensioactive properties" of poly(N-(2-hydroethyl)-L-glutamine)-*graft*-poly(ethylene glycol) after studying its emulsification properties with water/octanol mixtures and performing analytical GPC. They postulated simply that «Since dextran and PHEG are water soluble, but PEG is soluble in water and organic solvent, one can anticipate that, in aqueous solution, dextran-PEG and PEG-PHEG act as tensioactive and form aggregates with the "more" hydrophilic polymeric carrier as the outer shell and the "less" hydrophilic PEG as the core.» This statement was never

accompanied by a light scattering and never underlined the reasons behind such behavior. In our study, the development of a peptide-based DHBC capable of microphase separation seemed thus the perfect target to explore the scope of self-assembly in biological macromolecules.

3.2.1.a Synthesis
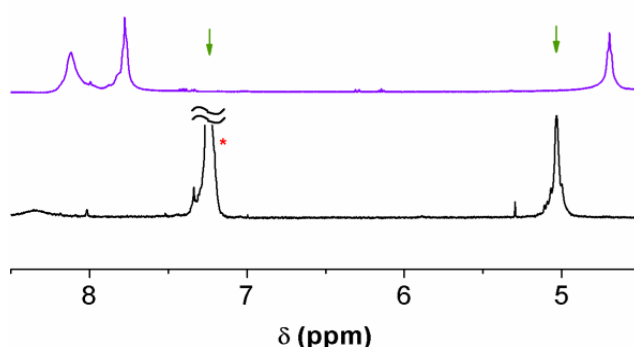
Figure 3.45: Detail of the ^{1}H NMR spectrum of Poly(ethylene glycol)-*block*-poly(benzyl-L-glutamate) in CDCl$_3$ (black) and Poly(ethylene glycol)-*block*-poly(N-(2-hydroethyl)-L-glutamine) in DMSO-d$_6$ (violet). The arrows point the shift of the -CH$_2$-C$_6$H$_5$ (~7.3 ppm) and CH$_2$-C$_6$H$_5$ (~5.1 ppm). The star points the solvent signal.

Poly(ethylene glycol)-*block*-poly(N-(2-hydroethyl)-L-glutamine) was synthesized in a two-step process. First, Poly(ethylene glycol)-*block*-poly(benzyl-L-glutamate) was obtained *via* NCA polymerization of γ-benzyl-L-glutamate N-carboxyanhydride by initiation with an α-amino-poly(ethylene glycol). Subsequently, the poly(ethylene glycol)-*block*-poly(N-(2-hydroethyl)-L-glutamine) (PEG-*b*-PHEG) was obtained by aminolysis of this polymer by aminoethanol in an optimized process published by De Marre.[177] The success of the aminolysis was confirmed by the total disappearance of the benzyl signals in ^{1}H NMR (Figure 3.45).

Integration of the peaks of the α-methoxy and the chiral center of the amino acids allows the determination of the polypeptide chain length *m*. These results are summarized in Table 3.7.
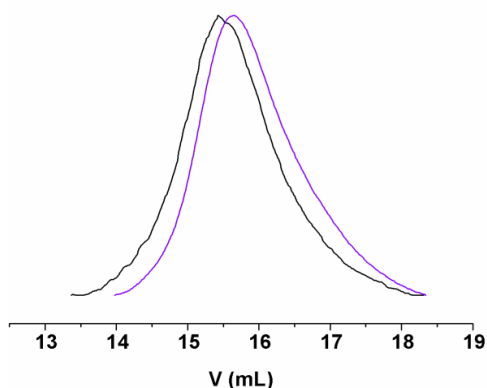
Figure 3.46: GPC traces of PEG-*b*-PLBG (black) and PEG-*b*-PHEG (violet) in NMP

Table 3.7: Polymer characteristics. $M_{n,app}$ as determined by GPC in NMP with PEG calibration. *m* was determined by ^{1}H NMR.

	$M_{n,\,app}$	*PDI*	*m*
mPEG-*b*-PBLG	20000	1.34	24
mPEG-*b*-PHEG	17000	1.31	24

The constant degree of polymerization confirms that the aminolysis proceeded without chain degradation. The GPC traces of the polymers in NMP (Figure 3.46) confirm this fact.

3.2.1.b   Self-assembly behavior in water

The PEG-*b*-PHEG block copolymer solid could be directly dissolved in milliQ water. The dynamic light scattering at an angle of 90° of the solution shows a polydisperse population (Figure 3.47).

Three modes can be discerned. Two low-intensity fast modes corresponding to 2.4 nm random coils and a 18.3 nm structure. This last medium fast mode was not present during all runs and its low intensity even when compared to its size suggests that its concentration in solution is extremely low. A final slow mode with very high intensity is detected at 115 nm.
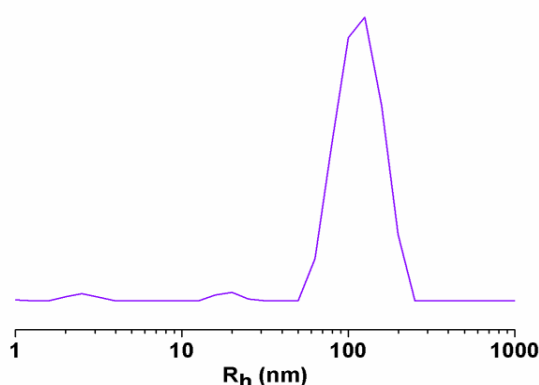
Figure 3.47: Dynamic light scattering at 90 ° of mPEG-*b*-PHEG block copolymer in water.

This slow mode was characterized by a relative small size distribution of ±8 nm for its 115 nm size which suggests a rather well-defined aggregate. The morphology of the aggregate was further investigated by a combination of static light scattering and negatively stained TEM. Static light scattering measurements on samples of different concentrations were performed. The fitting of the statical parameters was difficult and could only be acceptable with a Berry plot (Figure 3.48). The ρ-ratio calculated from DLS and SLS data is 1.0 suggesting vesicular type of aggregate with thin shell thickness. The molecular weight of the aggregates is relatively low regarding its size which would be compatible with a vesicular object.

$M_w(q)=1.07 \cdot 10^6 \, g \cdot mol^{-1}$
±12%

$R_g=117 \, nm \pm 4\%$
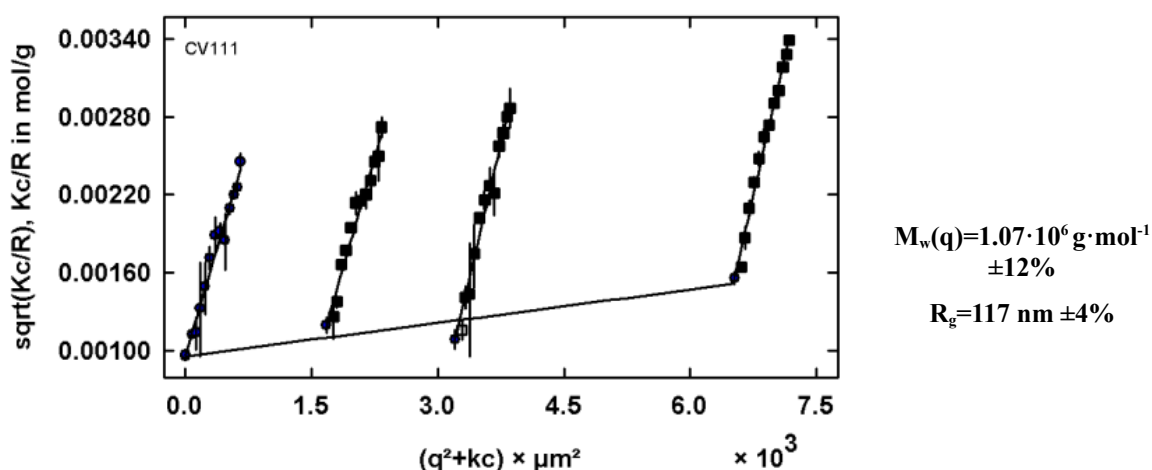
Figure 3.48: Berry plot of the static light scattering data on PEG-*b*-PHEG copolymer in water.

To confirm the nature of the aggregates, negatively stained TEM was performed on a

1 mg·mL^{-1} solution. The samples were air-dried on a copper grid. The micrographs show a polydisperse population of vesicles (Figure 3.49). The sharp boundaries of the vesicles are unexpected for aggregates formed by DHBC copolymer. It seems that the vesicles have a dual distribution, one of size ~250 nm in diameter that could be consistent with the slowest mode detected by DLS and a population of diameter ~ 1 μm. This mode could not be detected by DLS as the solutions for those measurements were filtered to avoid saturation of the detectors by the scattering of dust and big particles. These big aggregates were thus certainly extruded or filtered in the 0.7 μm glass filter.
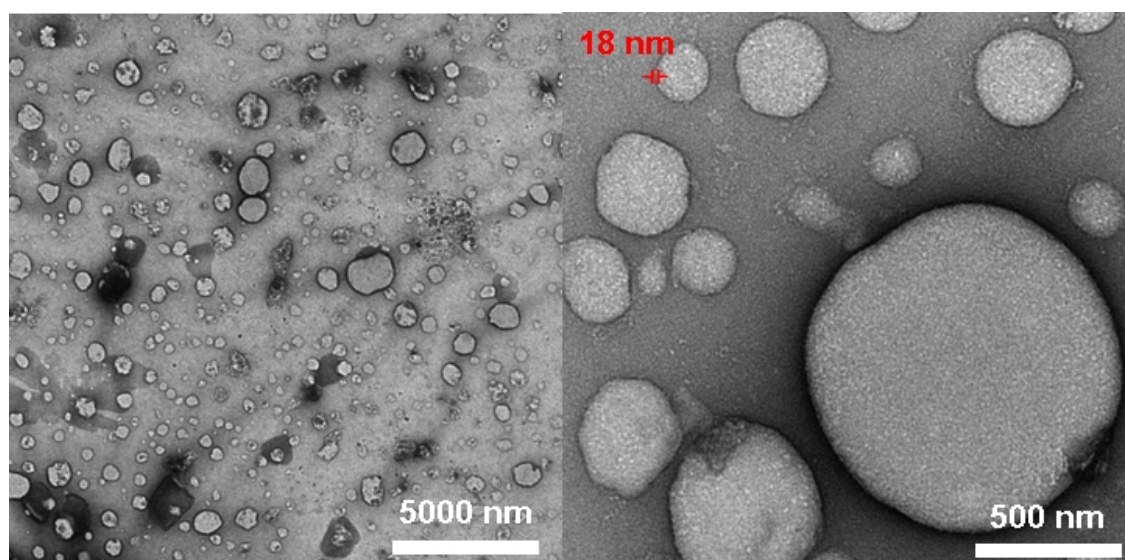
Figure 3.49: Negatively-stained transmission electron micrographs of a 1mg·mL^{-1} solution of PEG-*b*-PHEG

The membrane thickness could be measured from those micrographs and has a value of ~ 18 nm. This thickness is consistent with the membrane thickness of other usual polymer vesicles obtained with amphiphilic polymers.[99] The expected membrane structure is poly(N-(2-hydroethyl)-L-glutamine) on the outside promoting solubility with a "less hydrophilic" PEG barrier, similarly to the dex$_{6500}$-*b*-PEG$_{5500}$ vesicles.

The plot of the diffusion *vs* the scattering vector extrapolated to concentration 0 (Figure 3.50) shows an important angular dependence which is characteristic of big objects. The C value in the expression of the apparent diffusion (equation (9) p.44) as the initial slope characterizes the contribution of the shape fluctuations (softness/polydispersity) to the relaxation and was

calculated to 0.47 in this case. Because the filtered solution presented a rather monodisperse population (and the contribution to the diffusion coefficient must be mainly from the slowest species), this C value was characteristic of extremely soft aggregates.

	Value	Standard Erro
Dz	1.2235	0.10825
Dz*C*Rg	0.0036	5.95251E-4
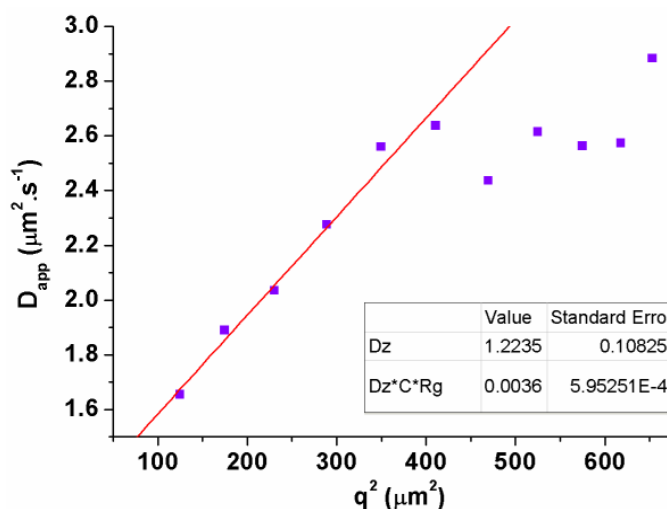
Figure 3.50: Angular dependence on the diffusion of the slow mode for a 1mg·mL^{-1} solution in milliQ water

Last, concentration influence on the slow mode was studied (Figure 3.51). First this sample preparation delivered aggregates with slightly higher hydrodynamic radius for the same concentration. The preparation method was the same except for the stirring speed but it delivered objects with $R_h \sim 143$ nm instead of 115 nm. This could be because in one or both cases the vesicles are not in the conformational lowest energy level. Anyway, for objects of weak curvature it could be imagined that the conformational energy is not so different over a wide range of sizes.
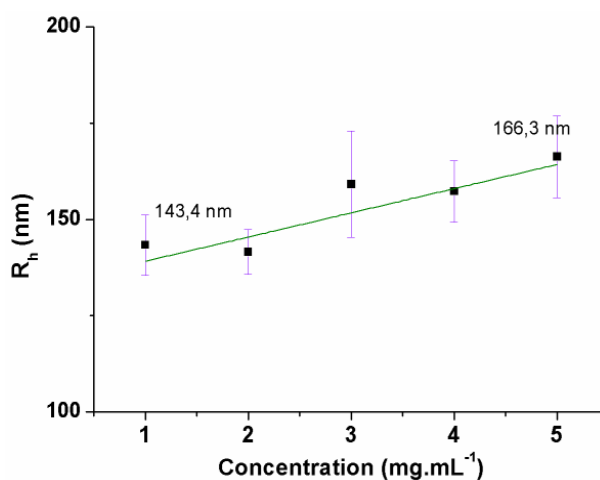
Figure 3.51: Concentration dependence on the aggregates size for PEG-*b*-PHEG in water.

Secondly, the size of the aggregate seems to change but generally increases with the concentration of polymer in solution. This behavior is different from the one observed for dextran-*block*-poly(ethylene glycol) copolymers and falls within experimental observations in self-assembly behavior of typical amphiphilic block copolymers in water.

3.2.2 Spontaneous self-assembly of polysaccharide thermoresponsive block copolymers

Poly(N-isopropylacrylamide) (PNIPAM) is a thermoresponsive polymer of LCST around 32 °C (see paragraph 2.2.2.b) resulting of the balance between the hydrophobicity of the isopropyl groups and the hydrophilicity of the acryl amide backbone. Because the LCST is so close to room temperature PNIPAM is considered to be "*mildly hydrophobic*".[178] PNIPAM is also an isomere of poly(leucine) and could be thus be a good canditate in the self-assembly of DHBC: it is analogous to a biomacromolecule so it could have phase-separation capacity and because its LCST is close to room temperature it could be "less hydrophilic" enough. With those qualitative considerations in mind, dextran-*block*-poly(N-isopropylacrylamide) copolymers were synthesized and their self-assembly behavior below and above the LCST of PNIPAM tested.

3.2.2.a Synthesis
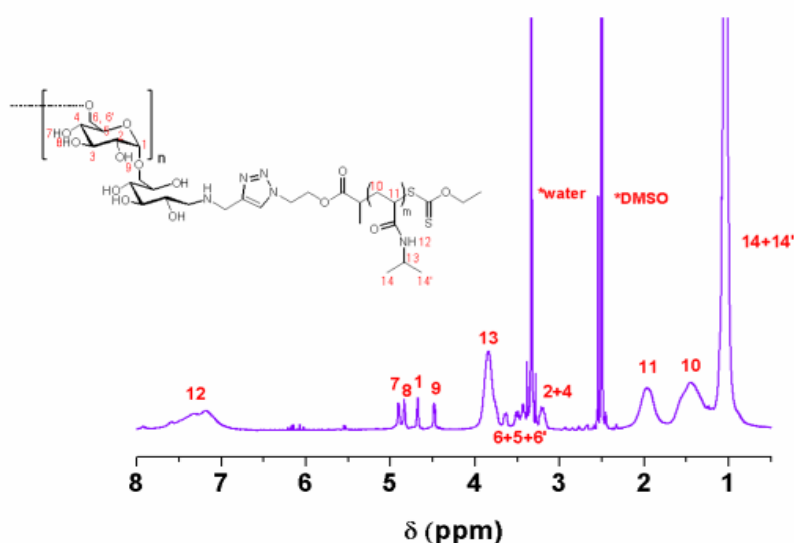
Figure 3.52: ^{1}H NMR of dex-*b*-PNIPAM$_{51}$ in DMSO-d$_6$

Dex-*b*-PNIPAM was synthesized by RAFT using the previously synthesized dextran macro-CTA (see the synthesis in paragraph 3.1.8.a and Scheme 3.7). Three different block lengths were targeted and the obtained block lengths were calculated from the elemental analysis of the dry polymers powder (Table 3.8). The ^{1}H assessed the chemical structures of the polymers (Error: Reference source not found).

Table 3.8: Polymers characteristics

Sample	$M_{n, app}$	*PDI*
dex-*b*-PNIPAM$_6$	3400	1,89
dex-*b*-PNIPAM$_{16}$	3700	1,90
dex-*b*-PNIPAM$_{51}$	4915	2,10
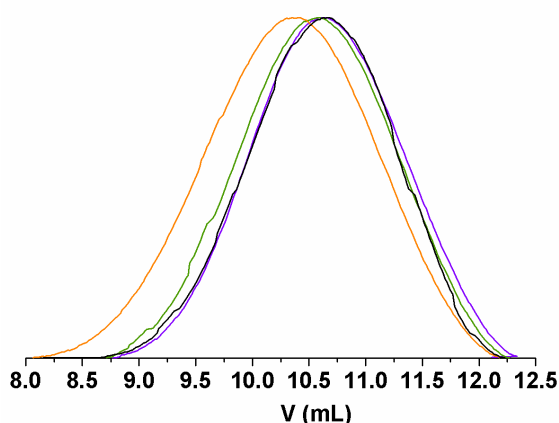
Figure 3.53: GPC traces in DMSO of dextran-CTA (black), dextran-PNIPAM$_6$ (violet), dextran-PNIPAM$_{16}$ (green) and dextran-PNIPAM$_{51}$ (orange)

GPC traces (Figure 3.53) show the limited growth of one of the polymers. Because it showed macroscopic thermoresponsive behavior it was nevertheless tested for its self-assembly behavior.

3.2.2.b Self-assembly behavior at room temperature

The direct dissolution of the polymer solids in water lead to clear solutions that were analyzed at 25 °C by dynamic light scattering at an angle of 90°. By treatment of the autocorrelation curve with the algorithm REPES, all three samples present slow modes indicating that dex-*b*-PNIPAM$_m$ self-assemble in water below LCST (Figure 3.54 and Table 3.9).

The two block copolymers with shorter PNIPAM block present monomodal distribution and in the block copolymer with longer PNIPAM chain length two modes are detected. As

attempt to elucidate the structure of the aggregates, SLS was performed on the samples as well as negatively-stained TEM.
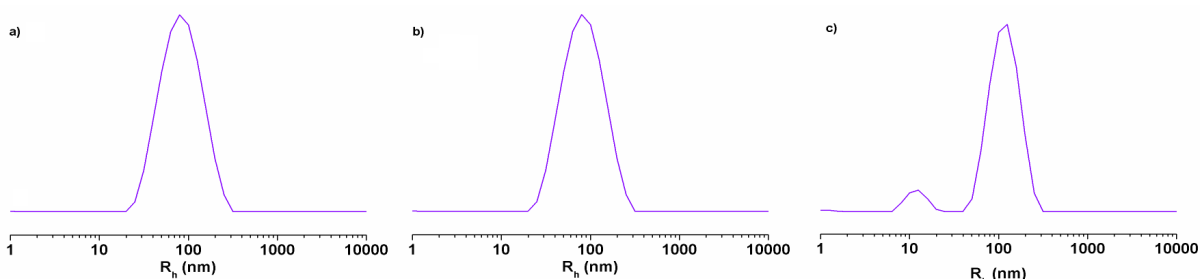
Figure 3.54: Dynamic light scattering at 90 ° of dextran-b-PNIPAM$_m$ block copolymer in water a)dex-*b*-PNIPAM$_6$ b)dex-*b*-PNIPAM$_{16}$ c)dex-*b*-PNIPAM$_{51}$

Table 3.9: Hydrodynamic radius corresponding of the slowest mode in dex-*b*-PNIPAM$_m$ solution in water at 25 °C

	$R_h \pm \Delta R_h$ *(nm)*	R_g *(nm)*	*ρ-ratio*
dex-b-PNIPAM$_6$	84 ± 9 nm	90	1,07
dex-b-PNIPAM$_{16}$	97 ± 12 nm	123	1,27
dex-b-PNIPAM$_{51}$	113 ± 10 nm	135	1,19

The Berry plot static light scattering data (see Supporting experimental data) delivered the gyration radius that allowed to determine the ρ-ratio (Table 3.9). Although none of the ρ-ratios correspond to the theoretical values for the well-established models (hard sphere, vesicle, coils, rods...) the values are close to the value expected for vesicles with infinite shell (ρ-ratio=1) or gaussian coils (ρ-ratio=1.5).
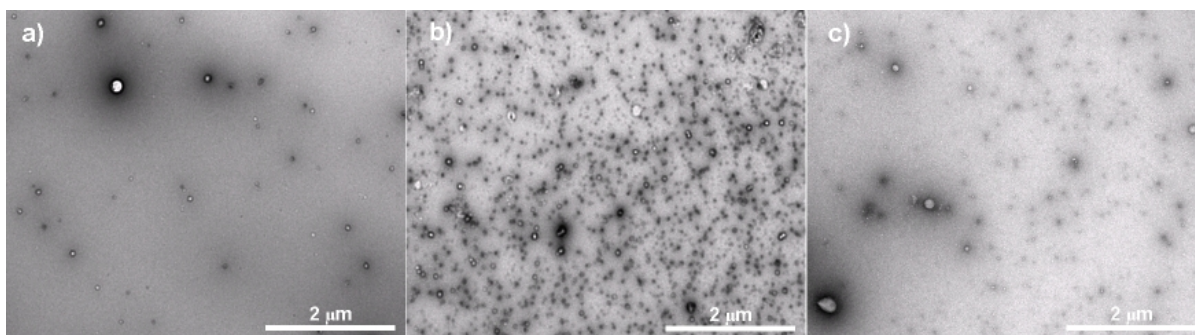
Figure 3.55: Negatively-stained transmission electron micrographs of air-dried samples of dextran-*b*-PNIPAM$_m$ block copolymer in water a)dex-*b*-PNIPAM$_6$ b)dex-*b*-PNIPAM$_{16}$ c)dex-*b*-PNIPAM$_{51}$

Negatively-stained TEM micrographs of air-dried samples (Figure 3.55), reveal for all of them spherical, supposedly vesicular structures. Because this technique is subjected to numerous artifacts and the ρ-ratio significantly deviate from the models,[179] an unambiguous attribution could not be made but strongly suggests vesicular structures.

3.2.2.c Thermoresponsive behavior

Typical thermoresponsive DHBC adopt a random coil conformation when no other specific interactions or responsiveness are present. Upon heating, the thermoresponsive block collapses (see paragraph 2.2.2.b) and when the solubilizing blocks manages to stabilize the structure, micelle-like objects are formed. In our case the temperature phase transition at the cloud point should be the result from the collapse of the PNIPAM block in the previously spontaneously formed colloidal aggregates. This transition was monitored by turbidimetry and DLS.
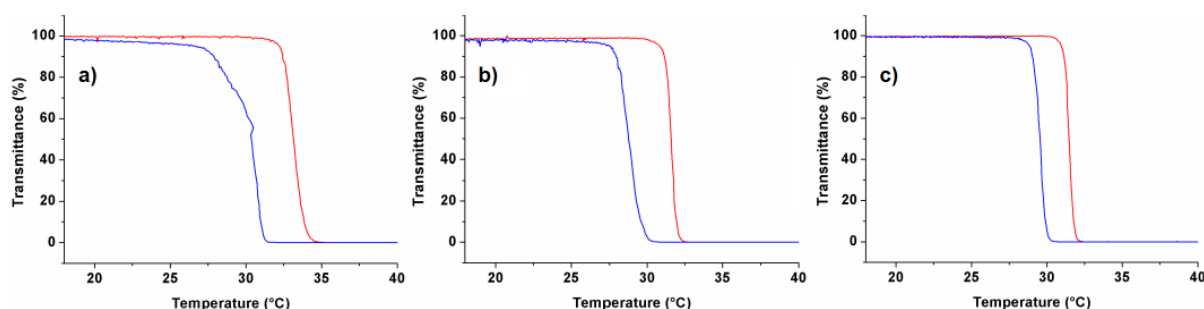
Figure 3.56: Turbidity profiles of 1 mg·mL^{-1} solution of polymers in water a) dex-b-PNIPAM$_6$, b) dex-b-PNIPAM$_{16}$ and c) dex-b-PNIPAM$_{51}$.

The turbidimetry profile (Figure 3.56) of 1 mg·mL^{-1} polymer solutions upon heating show a transition at 33.2 °C for dex-b-PNIPAM$_6$ and at around 31.7 °C for dex-b-PNIPAM$_{16}$ and dex-b-PNIPAM$_{51}$, close to the typical cloud point (CP) of PNIPAM in water. The shift in temperature the case of the shorter PNIPAM is common for oligomeric chains and is attributed to the decrease of entropy of mixing with decreasing molecular weight.[180] Visually a change from clear transparent solutions at room temperature to opaque white solutions at 40 °C (Figure 3.57) is observed. Importantly, no precipitation is observed even after several hours at 40 °C showing that the turbidity is not due to precipitation but rather to the probable

formation of stable objects of several hundreds of nanometers in diameter.
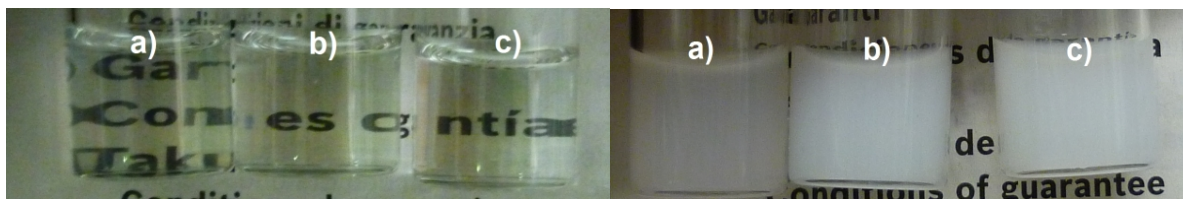
Figure 3.57: Visual appearance of 1 mg·mL^{-1} solutions of a) dex-b-PNIPAM$_6$, b) dex-b-PNIPAM$_{16}$ and c) dex-b-PNIPAM$_{51}$ at room temperature (left) and 40 °C (right).

By DLS the evolution of the hydrodynamic radius upon heating was followed. For the polymer with shorter PNIPAM (Figure 3.58 a)) an interesting behavior is observed. Below LCST as expected the object previously studied (see paragraph 3.2.2.b) of $R_h \sim 90$ nm was detected. At the CP determined by turbidimetry of 33.2 °C (Figure 3.56) no apparent change in the aggregate's size is detected although the transmittance drops to 0%. This suggests that the aggregate increases in mass without increasing in size for the 33-36 °C temperature range. By further increasing the temperature, the size rapidly increases but is relatively stable (low size deviation) for every temperature. For the copolymer with the intermediate PNIPAM size (Figure 3.57 b)) several size domains upon heating can be described. Below the CP, the aggregates previously studied are (see paragraph 3.2.2.b) stable in size. Sharply at the CP the size triplicates and increases almost linearly with the temperature until around 52 °C. Above this temperature the size seems to be stable and of about 2 μm which is certainly a precipipate. As visually seen, at 40 °C, monodisperse objects of R_h ~400 nm are present, which correlates with the turbidity observed. For the copolymer with the longer PNIPAM chain the transition appears even more complex (Figure 3.57 c)). As for the other polymers below the CP the size is stable and even slightly decreases. Upon heating the sizes increases and reaches a plateau at 38 °C until 46 °C. Upon further heating, the size increases again until it reaches a second plateau at $R_h \sim 300$ nm.

The collapse of the PNIPAM chains upon heating is more complex than the model of micellisation from thermoresponsive copolymers. Within moderate temperatures, the particles progressively grow reaching stable particle sizes within some temperature ranges.

Because the starting morphology of the aggregates below LCST is difficult to assess with certainty, the mechanism of collapse remains unclear. The fact that turbidity increases demonstrates that there is a mass increase. And for a given temperature over the CP the particles are stable showing that the systems behaves like classic amphiphilic systems with dextran as stabilizing block.

Figure 3.58: Evolution of the hydrodynamic radius with temperature monitored by DLS at 90 °C treated with REPES algorithm of 1 mg.mL^{-1} solutions of a) dex-b-PNIPAM$_6$, b) dex-b-PNIPAM$_{16}$ and c) dex-b-PNIPAM$_{51}$

Upon cooling, the association was found to be reversible (Figure 3.59). The process shows, in accordance with the reported temperature behavior of PNIPAM, hysteresis by both DLS and turbidimetry. This hysteresis is caused by the strong chain-chain interactions above the LCST. Importantly the relaxation of the PNIPAM chains upon cooling leads to an aggregate in the same order of size (R_h ~90 nm) as the initial system.
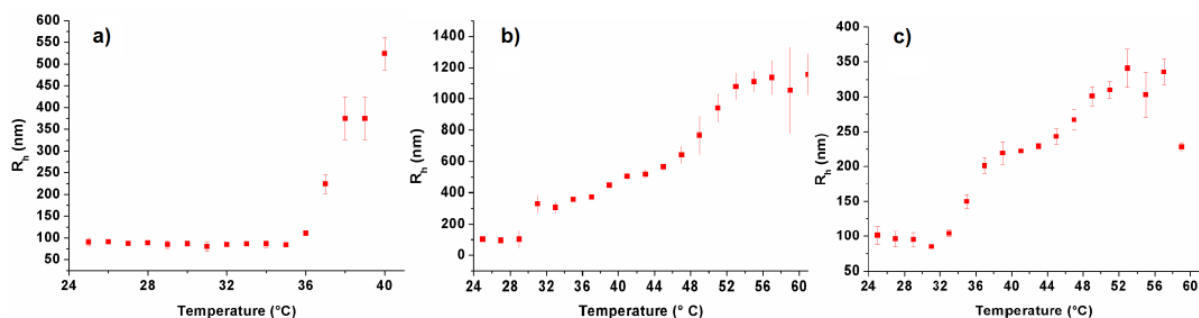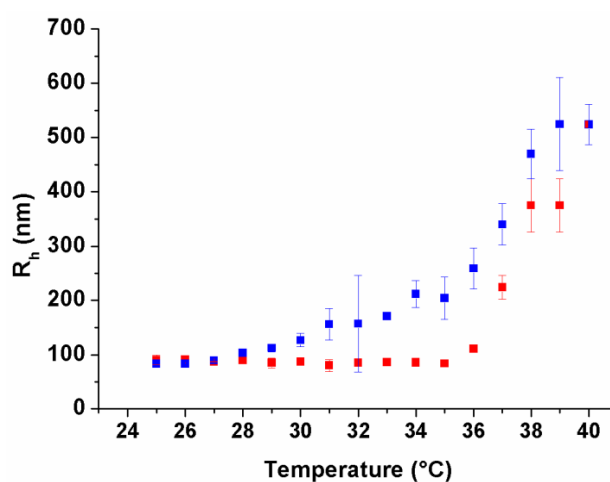

Figure 3.59: Evolution of the hydrodynamic radius with temperature monitored by DLS at 90 °C treated with REPES algorithm of 1 mg.mL^{-1} solutions of dex-b-PNIPAM$_6$. In red the heating and in blue the cooling process.

3.3   Summary

In this chapter a family of dextran-*block*-poly(ethylene glycol) block copolymers were synthesized. These block copolymers directly inspired from the widely used PEG/dextran ATPS system were able to form aggregates in water by simply dissolution of the solid. Dex_{6500}-*b*-PEG_{5500} copolymer spontaneously formed vesicles with PEG as the "less hydrophilic" barrier and dextran as the solubilizing block. The aggregates were found to be insensitive to the polymer architecture and to the concentration (in the dilute range) and only mildly sensitive to temperature. Variation of the block length, yielded different morphologies. A longer PEG chain seemed to promote more curved aggregates following the inverse trend usually observed in amphiphilic block copolymers. A shorter dextran promoted vesicular structures as usually observed for the amphiphilic counterparts. The linking function was shown to have an influence of the morphology but not on the self-assembly capability in itself. The vesicles formed by dex_{6500}-*b*-PEG_{5500} showed slow kinetics of clustering in the presence of ConA lectin. In addition both dex_{6500}-*b*-PEG_{5500} and its crosslinked derivative were able to encapsulate fluorescent dyes. Two additional dextran-based copolymers were synthesized, dextran-b-poly(vinyl alcohol) and poly(vinyl pyrrolidone). The study of their self-assembly allowed to conclude that ATPS is a valid source of inspiration to conceive DHBCs capable of self-assembling.

In the second part the principle was extended to polypeptide systems with the synthesis of a poly(N-hydroxyethylglutamine)-*block*-poly(ethylene glycol) copolymer. The copolymer that had been previously reported to have emulsifying properties was able to form vesicles by direct dissolution of the solid in water. Last, a series of thermoresponsive copolymers were prepared, dextran-*block*-poly(N-isopropylacrylamide)$_m$. These polymers formed aggregates below the LCST. Their structure could not be unambiguously elucidated but seemed to correspond to vesicles. Above the LCST, the collapse of the PNIPAM chains induced the formation of stable objects of several hundreds of nanometers in radius that evolved with increasing temperature. The cooling of these solution below LCST restored the initial aggregates.

Chapter 4:   Thermoresponsive vesicles with an asymmetric membrane

Biological membranes are highly heterogeneous (lateral heterogeneity) and asymmetric (transverse asymmetry) structures (Figure 4.1[181]). Lateral heterogeneity arises from clustering of particular types of proteins or lipids in the plane of the membrane. This heterogeneity has several potential functions such as the binding of charged macromolecules, rigidity control as well as lateral compressibility that facilitates membrane fusion, cytosis...[182] The transverse asymmetry arises from the different lipid and protein composition of the two monolayers. For example, amine-containing phospholipids (intracellular communication) are enriched in the inner cytofacial monolayer whereas choline-containing phospholipids (cell signaling, enzyme activation) and sphingolipids (transmission, cell recognition) are enriched in the exofacial monolayer. Carbohydrate groups of glycolipids and glycoproteins are also always found in the exofacial layer where they participate in cell

recognition phenomena.[183]
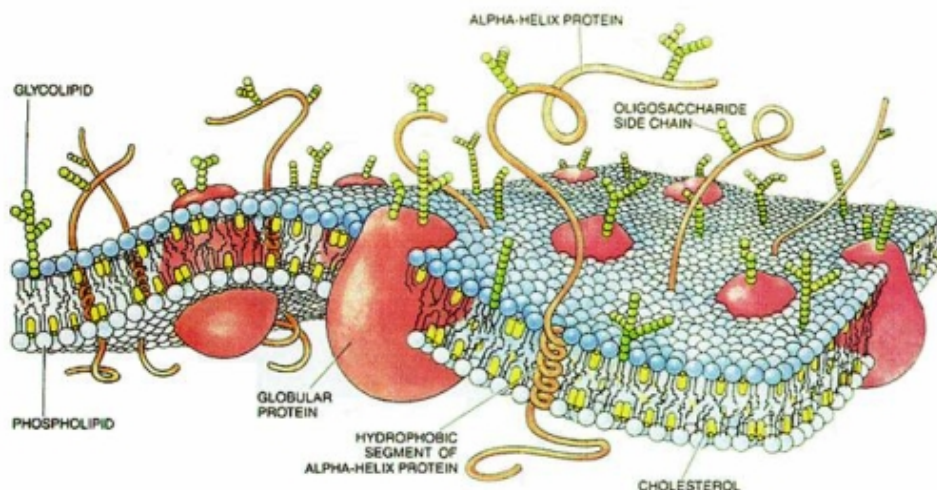
Figure 4.1: Schematic three dimensional cross section of a cell membrane. Reproduced from [181]

Lipid bilayers and vesicles (liposomes) as cell mimics have shown to be a good architectural model of cell membranes but most of the time their preparation procedures do not provide control over lipid compositions between the inner and outer monolayers. Partial asymmetry can nevertheless be introduced by altering the distribution of specific phospholipids using pH gradients, osmotic pressure, or molecules that promote lipid redistribution.[184] Polymersomes made from ABC-type block copolymers have introduced some intrinsic asymmetry to the biomembrane model associated with the mechanical advantages of polymer structures.[185] These polymersomes could further be modified by directed insertion of membrane proteins.[186]

Direct formation of biologically relevant polymersomes with an asymmetric membrane was recently achieved by Schlaad *et al.*.[2] A polybutadiene-*block*-poly(ethylene glycol) copolymer was glycosylated *via* thiol-ene chemistry (PB(Glc)-*b*-PEG). The resulting glucose-functionalized polymer readily formed vesicles by direct dissolution of the polymer solid in water. The study of the membrane revealed its asymmetric structure with the outside covered by glucose, the inside by poly(ethylene glycol) and a polybutadiene hydrophobic barrier (Figure 4.2). This structures proved a good primitive mimic for the asymmetry observed in cell membrane concerning the glycolipids and glycoproteins that assure cell recognition.
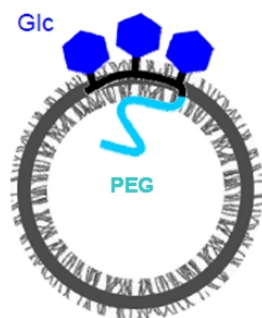
Figure 4.2: Schematic representation of the glycosome with asymmetric membrane obtained by dissolution of PB(Glb)-*b*-PEO in water. Adapted from [2].

To access the next generation of polymersomes that mimic cell membranes, we designed a copolymer also based on glycosylated polybutadiene but with a "smart" block. This structure based on a thermoresponsive block of poly(N-isopropylacrylamide) (PNIPAM) could form analogous glycosomes to the PB(Glc)-*b*-PEG ones in water at room temperature. Its behavior upon the application of a thermal stimulus was studied, and the first experiments to evaluate its potential applications in biological context are shown.

4.1   Synthesis

Polybutadiene with a high degree of 1,2-substitution (1,2-PB-OH) was prepared by living anionic polymerization as described previously.[187][188]

The chain transfer agent (CTA) used to couple to PB was synthesized by the coupling of potassium ethyl xanhogenate to 2-bromo-2-methyl propionic acid adapting a procedure described by Ladavière[189] for the synthesis of S-benzyl-O-ethyl dithiocarbonate. The CTA was subsequently coupled to the 1,2-PB-OH polymer by esterification and the resulting macro-CTA was used for the synthesis of 1,2-PB-*b*-PNIPAM block copolymers by RAFT. In initial attempts at monomer concentrations of 25 wt% in dioxane, the irreversicle precipitation of material during polymerization indicated cross-linking. Very likely double bonds of the 1,2-PB-OH block polymerized under these conditions. Under more dilute conditions (5 wt%), no precipitation was observed, indicating that the simple dilution of the reaction mixture, crosslinking could be effectively avoided. Double bonds of the 1,2-PB-OH are thus under these condition less reactive than the acryl function of the monomer in both

the initiation and propagation steps (see chapter 2.3.1). This way it was possible to afford 1,2-polybutadiene block copolymers *via* radical polymerization of an acrylamide (Scheme 4.1).
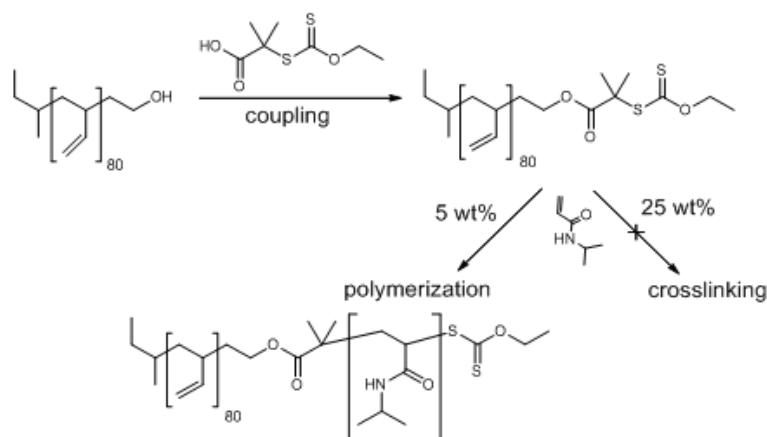
Scheme 4.1: Representation of the first synthetics steps. First the coupling of the CTA to afford a 1,2-polybutadiene macro-CTA and the subsequent polymerization under two different concentrations.

Two PNIPAM block lengths were targeted and their value was determined by ^{1}H NMR. The GPC showed remaining unreacted 1,2-PB certainly due to the incomplete coupling of the CTA in the macromononer preparation. This homopolymer was partially removed by extraction of the mixture in water with hexane. The presence of a small fraction of homopolymer was not considered a major inconvenient as the target structure was a vesicle prepared by simple dissolution of the polymer in water, and would thus incorporate the homopolymer into the membrane.

The 1,2-PB-*b*-PNIPAM copolymers were further functionalized with sugar moieties via thiol-ene (see paragraph 2.3.2.b) chemistry. 1-Thio-β-D-glucose tetraacetate was coupled to the double bonds of the 1,2-PB block in the block copolymer as previously reported.[118][119] 1.5 eq of thio-sugar to double bonds were used in THF. UV irradiation was used to produce thiyl radicals. The sugar moieties were deprotected simply by addition of a 0.5 M NaOH solution in methanol to a solution of the $PB_{80}(GlcAc_4)$-*b*-$PNIPAM_m$ in chloroform. The complete deacetylation was assessed by the disappearance of the acetyl group at δ=2.09 ppm in ^{1}H NMR. The degree of functionalization was determined using the C/S ratio of the elemental

analysis to calculate the number of sugar moieties per PB unit. The results are summarized in Table 4.1.

Table 4.1: Characteristics of glycosylated 1,2-PB-*b*-PNIPAM (*f* stands for degree of functionalization). Molar masses as calculated from the degree of polymerization determined by ^{1}H NMR

	M_n	f
PB$_{80}$(Glc)-*b*-PNIPAM$_{259}$	38500	0.26
PB$_{80}$(Glc)-*b*-PNIPAM$_{557}$	76000	0.52
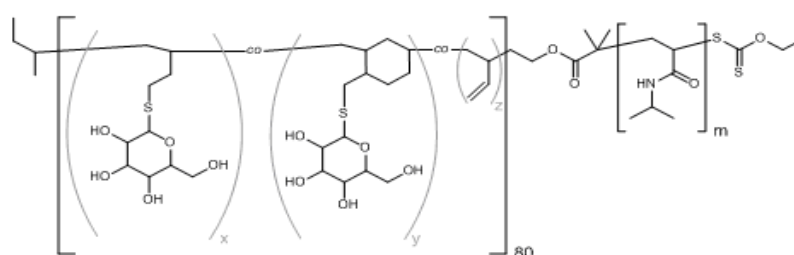
Scheme 4.2: Chemical structure of 1-thio-β-D-glucose tetraacetate-functionalized 1,2-PB-*b*-PNIPAM after deacetylation (x+y=0.51, m=259 or 557).

^{1}H NMR shows only residual amounts of non-functionalized 1,2-PB although the degree of functionalization remains relatively low. This can be explained as it has been observed before[118][119] by the side reactions upon addition of thiols to 1,2-PB leading to ring structures. The chemical structure of the polymer is represented in Scheme 4.2.

4.2   Self-assembly behavior at room temperature
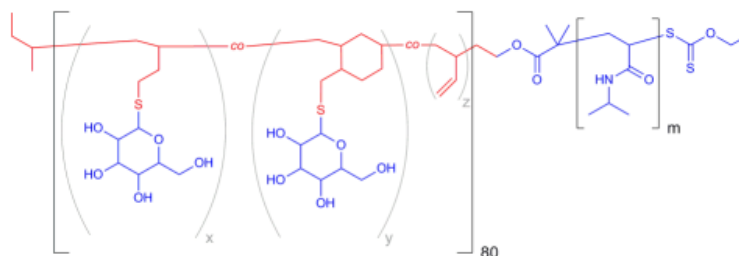
Scheme 4.3: Chemical structure of PB80(Glc)-*b*-PNIPAM$_m$. In red the hydrocarbon chain accounting for hydrophobicity in the polymer. In blue, the moeties and block contributing the hydrophilicity of the copolymer.

Glycosylation of the 1,2-PB block in the block copolymers sets the fraction of hydrophilic

moieties to around 86% in the case of $PB_{80}(Glc)$-*b*-$PNIPAM_{259}$ and to 93% the in case of $PB_{80}(Glc)$-*b*-$PNIPAM_{557}$. Basically only the hydrocarbon chain with the recurrent ring resulting from intramolecular rearrangement upon radical addition of the thiol constitutes the hydrophobic part (Scheme 4.3).

This high hydrophilic fraction allows direct dissolution of the polymer solid in water as in similar systems.[2][116][118][119][173] An iriscent-white solution formed at room temperature consistent with colloidal objects of several hundreds of nanometers in diameter (Figure 4.3).
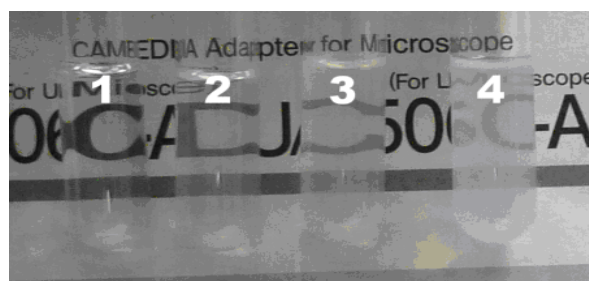
Figure 4.3: Solutions of $Pb_{80}(Glc)$-*b*-$PNIPAM_{557}$ obtained by direct dissolution of polymer in water. (1) ~1 mg/mL; (2) ~2 mg/mL; (3) ~3mg/mL; (4) ~4 mg/mL at room temperature.

A REPES[149] analysis of DLS of the solutions measured at an angle of 90° revealed a polydisperse population (Figure 4.4).
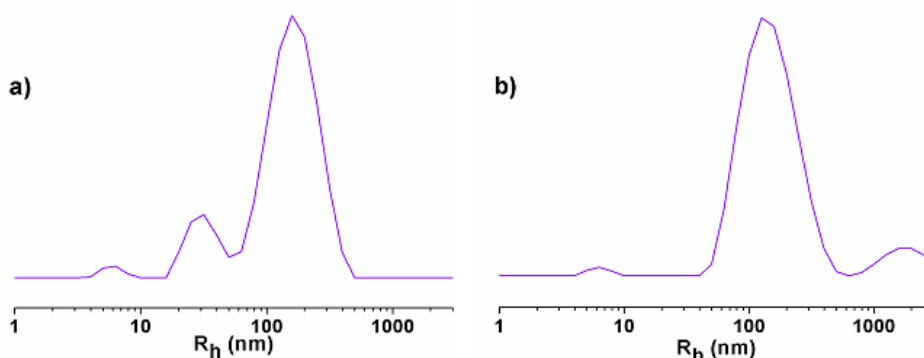
Figure 4.4: Dynamic radius distribution of (a) $PB_{80}(Glc)$-*b*-$PNIPAM_{259}$ and (b) $PB_{80}(Glc)$-*b*-$PNIPAM_{557}$ at 0.1 wt% in milliQ as determined by DLS at 90° and calculated with the REPES algorithm.

Three populations can be identified for the $PB_{80}(Glc)$-*b*-$PNIPAM_{259}$ copolymer, which reveals a non-equilibrium state. A fast mode of hydrodynamic radius of 5 ± 1 nm is present and

likely corresponds to a polymer random coil or rather an off-equilibrium association of a finite number of polymer chains. An intermediate mode of $R_h = 25 \pm 12$ nm that could be identified as micellar objects but whose relative high standard deviation is contradictory with such a usually well-defined colloidal structure and more likely is an intermediate non-equilibrium structure between the fastest and the slowest mode. The slowest mode corresponds to an aggregate of $R_h = 148 \pm 17$ nm. The size of this relatively well defined structure seems to be similar to the size of the vesicles previously obtained in glycosylated polybutadiene systems.[118][119]

The copolymer with longer PNIPAM block, $PB_{80}(Glc)$-*b*-$PNIPAM_{557,}$ shows two modes. The fastest one corresponds to an apparent hydrodynamic radius of 7 ± 1 nm and is compatible with a polymer random coil diffusion or low aggregation intermediate. The slower mode corresponds to objects with $R_h = 134 \pm 14$ nm. This diffusion is also compatible with the previously reported glycosylated polybutadiene-based vesicles. A third mode arises at a hydrodynamic radius in the micrometer order, but as the scattering intensity is strongly dependent on the radius of the particle and the proportion of big particles is always exaggerated in CONTIN and REPES analyses, this mode concerns only an extremely low percentage of particles and is actually probably due to incomplete dissolution of the polymer or simply dust particles.

A combination of SLS and negative stained TEM was used to elucidate the structure of the aggregates. In SLS measurements the intensity was acquired for a short time (typically 10 s) to make sure the scattering was mainly due to the slowest mode. A Berry plot (Figure 4.5) was used to evaluate the static parameters to overcome the angular dependence in the Zimm plot as in most spherical aggregates with $R_g > 50$ nm.[190] For the $PB_{80}(Glc)$-*b*-$PNIPAM_{259}$ copolymer the fitting delivered a gyration radius of 162 nm $\pm$ 3%. The combination of this SLS data with the R_h value delivered by DLS allows evaluating the ρ-ratio (R_g/R_h) to 1.09. This ratio is consistent with the value theoretically calculated for hollow spheres with a thin shell (ρ-ratio=1.0),[191] and suggests that the aggregates at R_h=148 nm are vesicles.

$$R_g = 162 \text{ nm} \pm 3\%$$
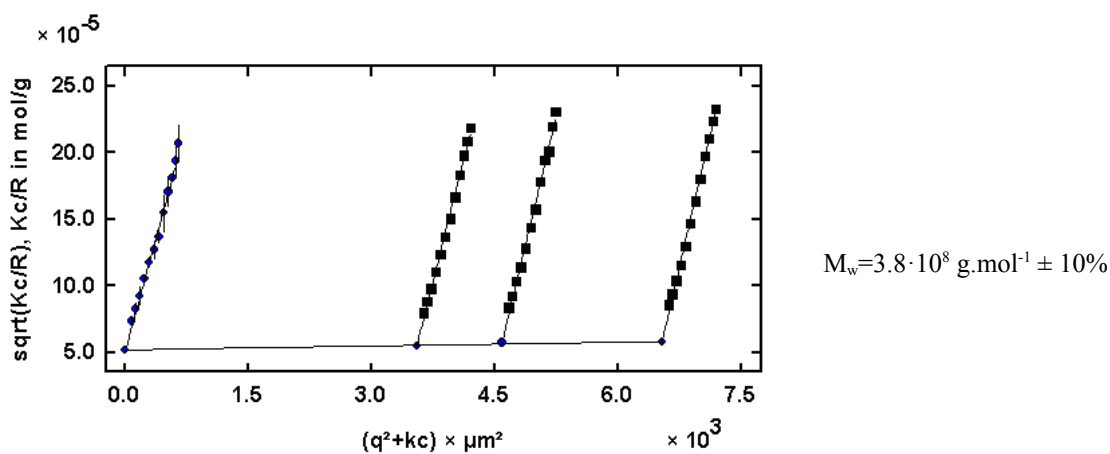
Figure 4.5: Berry plot of the SLS data of $PB_{80}(Glc)$-*b*-$PNIPAM_{259}$ obtained from 40° to 90°.

$M_w = 3.8 \cdot 10^8$ g.mol^{-1} ± 10%
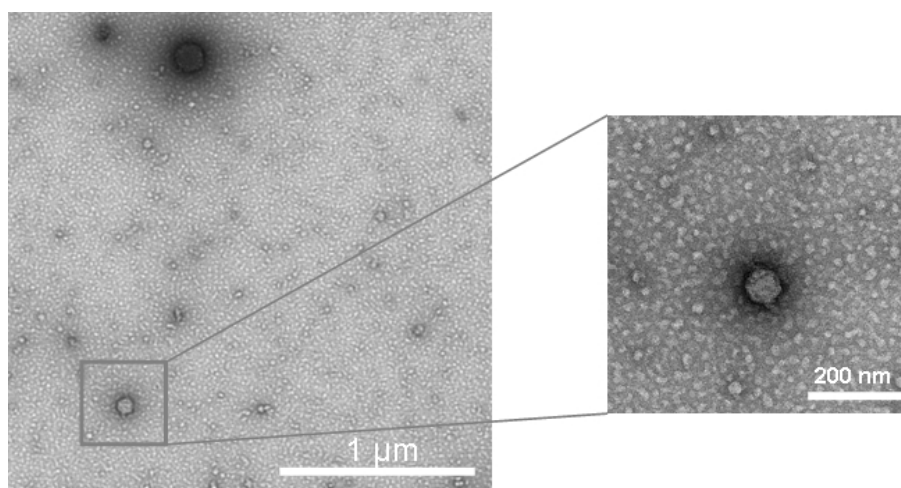
Figure 4.6: TEM images of a 1 wt% solution of $PB_{80}(Glc)$-*b*-$PNIPAM_{259}$. TEM grid prepared by drop casting and stained with uranyl acetate.

TEM images of a negatively stained air-dried sample of a 1 wt% of $PB_{80}(Glc)$-*b*-$PNIPAM_{259}$ prepared by drop casting delivered further evidence (Figure 4.6). The sample appears polydisperse, but clearly shows vesicles. Their size is compatible with the aggregate detected by DLS if we take into account the air-drying process that the TEM grid undergo before measurement tends to shrink soft matter.

The same SLS/TEM analysis performed on $PB_{80}(Glc)$-*b*-$PNIPAM_{557}$ delivers similar information (see Supporting experimental data). In this case the analysis was less straight forward certainly due to the contribution to the scattered intensity of the micrometer sized

object. A Guinier plot[191] seemed the best option in this case to minimize the angular dependence. Nevertheless, a R_g of 128 nm ± 1% was found and the ρ-ratio of 0.95 as well as the TEM images seem to agree with a vesicular structure.

Once the vesicular structure is elucidated, it is easier to understand the origin of the faster modes revealed by light scattering,. The mechanism of formation of vesicles involves intermediate structures such a disk-like micelles, for which beyond a critical size the competition between surface tension and bending energy induces the closure into vesicles.[192] However, other intermediate structures such as micelles and rod-like micelles have also been reported prior to vesicle formation.[193] In any case, as our system is not in thermodynamic equilibrium (coexistence of three species), the faster modes must correspond to membrane patches or other intermediate structures. This has consequences concerning the measured size of the vesicles, as it does not necessarily correspond to the conformational energy minimum and might evolve over time.

For a vesicle formed by $PB_{80}(Glc)$-*b*-$PNIPAM_{259}$ it seems unlikely that the membrane could be a bilayer. A mixed hydrophilic shell of PNIPAM and glucose pendant group is unlikely in terms of incompatibility and geometry. This was further confirmed by 2D-^{1}H, ^{1}H-NOESY NMR (Figure 4.7). In this spectra no correlation (intersection of the dotted blue and green lines) was found between the PNIPAM and the glucose signals confirming that there is no spatial correlation within a 5 Å length scale[2] between these two hydrophilic parts and thus the membrane is asymmetric.

The question remains whether the PNIPAM or the glucose moieties are located on the outside or the inside of the membrane. The polymer with longer PNIPAM block presents a smaller vesicle size (R_h~148 nm for $PB_{80}(Glc)$-*b*-$PNIPAM_{259}$ and R_h~134 nm for $PB_{80}(Glc)$-*b*-$PNIPAM_{557}$) which could be consistent with a interior layer of glucose and a external one constituted by the PNIPAM. But since the glucose degree of functionalization in PB_{80}-*b*-$PNIPAM_{557}$ is twice as high as in PB_{80}-*b*-$PNIPAM_{259}$ this direct comparison cannot be made. With that fact in mind, it could also be that if the glucose is on the outside, it would increase the curvature in the structure from the polymer with the highest functionalization (PB_{80}-*b*-

PNIPAM$_{557}$) when compared to PB$_{80}$(Glc)-*b*-PNIPAM$_{259}$, reducing thus its size. Further experimental results will be discussed under this perspective later in this report (see paragraph 4.4.1).
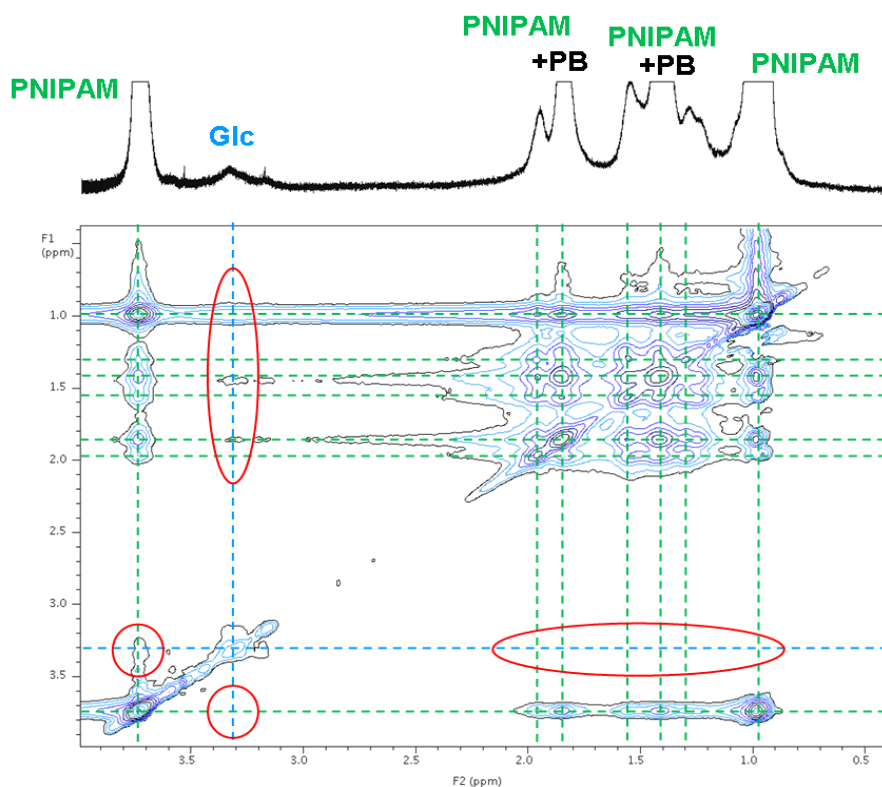
Figure 4.7: 2D-^{1}H, ^{1}H-NOESY NMR spectrum of PB$_{80}$(Glc)-*b*-PNIPAM$_{557}$ at 5 wt% in D$_2$O.

4.3 Thermo-responsive behavior

Once the solution behavior at room temperature of PB$_{80}$(Glc)-*b*-PNIPAM$_{m}$ copolymers had been studied and shown the presence of vesicles, its thermo-responsive behavior was tested. PNIPAM is a thermo-responsive polymer that shows a lower critical solution temperature (LCST) in water at around 32 °C,[194] close to the human body temperature. For this, and for its relatively low-cost and biocompatibility, it is of especial interest in systems that target biological and medical applications. The vesicles formed by PB$_{80}$(Glc)-*b*-PNIPAM$_{m}$ in water are thus expected to be thermo-responsive and undergo a transition at the critical temperature of PNIPAM.

The turbidity profile of PB$_{80}$(Glc)-*b*-PNIPAM$_{259}$ at 1 mg·mL^{-1} in water (Figure 4.8) shows a

LCST transition from around 85% of transmittance to 53%. The polymer does not precipitate. The LCST calculated at 50% of the decay of the transmittance in the transition (by derivating the heating curve and identifying the minimum) is 32.6 °C which is in good agreement with literature values for PNIPAM-based systems.[195]-[197] A similar value of 32.8 °C was found for the $PB_{80}(Glc)$-*b*-$PNIPAM_{557}$ copolymer.
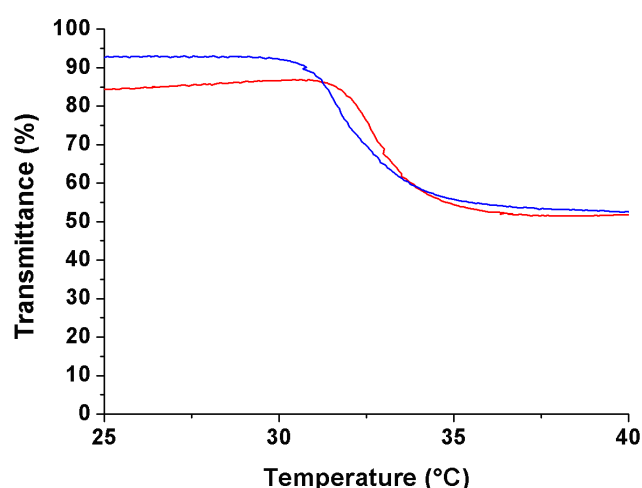
Figure 4.8: Turbidity profile of a 1 mg·mL^{-1} solution of $PB_{80}(Glc)$-*b*-$PNIPAM_{259}$ in water at 1 °C.min^{-1}. Heating curve (red) and cooling curve (blue).
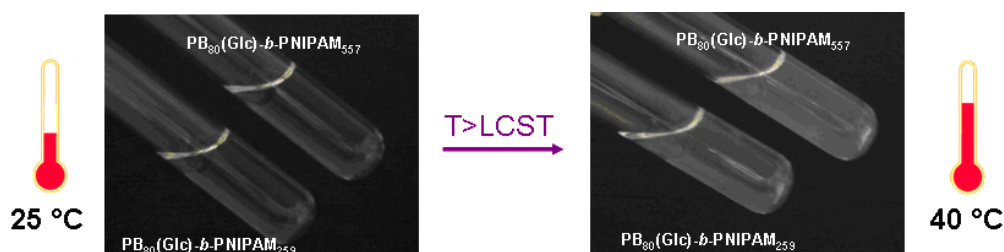
Figure 4.9: Visual aspect of $PB_{80}(Glc)$-*b*-$PNIPAM_{259}$ and $PB_{80}(Glc)$-*b*-$PNIPAM_{557}$ dilute solution (1mg·mL^{-1}) at 25 °C and 40 °C).

Visually, dilute solution of polymer go from iriscent to white-iriscent (Figure 4.9) with increasing temperature but no precipitation is observed even over days at 40 °C, meaning that stable colloidal objects are formed. This is the reason why the transmittance in Figure 4.8 never drops to 0 %. A change to a more intense white is usually consistent with objects of higher mass. A DLS measurement of these solutions at 25 °C and 40 °C shows that the transition is towards a very monodisperse objects of smaller size (Figure 4.10).
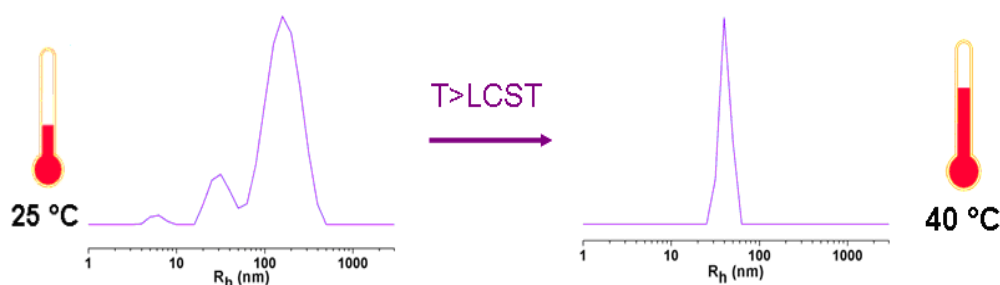
Figure 4.10: Hydrodynamic radius distribution below LCST and above the LCST of $PB_{80}(Glc)$-*b*-$PNIPAM_{259}$ as determined by a REPES analysis of the DLS data for a 1mg·mL^{-1} solution in water.

The increase in opacity can thus be explained in two terms. The first possibility is that several vesicles collapse into a single micelle accounting thus for the increase in mass revealed by the turbidity. The second possibility is that a single vesicle collapses into a single micelle. The collapse of single PNIPAM chains in its coil-to-globule transition makes the homopolymer loose around 40% of its mass by release of water changing the density from $2.5 \cdot 10^{-2}$ g·cm^{-3} to $3.4 \cdot 10^{-1}$ g·cm^{-3}.[198] It seems thus rational that this collapse could raise the optical density of the PNIPAM blocks within the colloidal objects and raise thus the turbidity of the solution. In addition, the opacity above the LCST of PNIPAM is more pronounced (Figure 4.9) in the polymer with much longer PNIPAM chain-length (557 repeating units compared to 259 repeating units) for a comparable colloidal size (41 ± 0 nm for $PB_{80}(Glc)$-*b*-$PNIPAM_{259}$ and 52 ± 2 nm for $PB_{80}(Glc)$-*b*-$PNIPAM_{557}$) meaning that collapsed PNIPAM density within the colloidal objects is greater in $PB_{80}(Glc)$-*b*-$PNIPAM_{557}$ copolymers.

The transition can also be monitored with DLS by monitoring the evolution of the hydrodynamic radius of the aggregate with temperature (Figure 4.11). Below the cloud point the R_h seems to slowly decrease certainly due to the deformation cause by the PNIPAM chains coming close together as a result of dehydration. At a temperature close to the cloud point determined by turbidity the decrease is sharp, showing that the transition from vesicles to the object of smaller size is well caused by the PNIPAM collapse and is fast. Above the LCST, the single species with narrow size distribution are formed.

Even though fitting of the SLS data at 40 °C was not possible, it seems rational that an object of that size showing colloidal stability formed after the collapse of PNIPAM chains can only

have micellar structure in which the core if formed by these hydrophobic collapsed PNIPAM chains with a hydrophilic glucose-based corona to assure stability. The geometry of the micellar structures remains nevertheless unknown. As the fast modes present below LCST (Figure 4.4) have disappeared above LCST, it seems that the micelles have incorporated the membrane patches present below the LCST.

Below the LCST, if the PNIPAM is on the outside of the vesicles, it would mean that the membrane "flips" at the LCST, revealing a very interesting collapse mechanism. If the PNIPAM is on the inside, the vesicle to micelle transition would take place by progressive shrinkage of the structure induced by the PNIPAM's collapse.
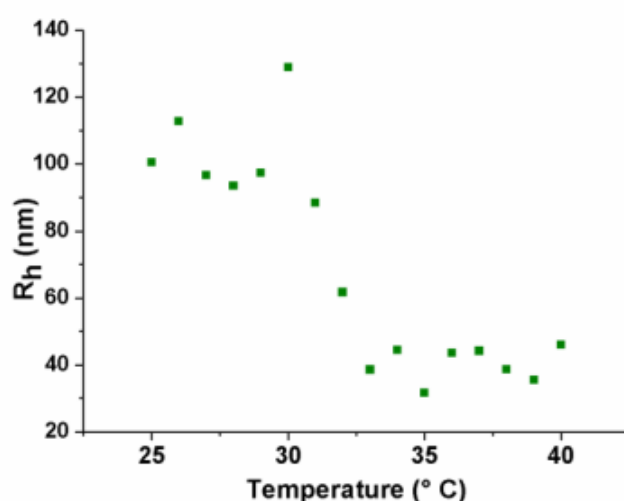
Figure 4.11: Evolution of the hydrodynamic radius with increasing temperature in the PB$_{80}$(Glc)-*b*-PNIPAM$_{259}$ copolymer. The small amplitudes below the LCST were omitted for clarity.

The reversibility of the vesicle to micelle transition was studied for the three heating/cooling cycles. The radius of gyration seems to remain invariable within the given error after each cycle. The hydrodynamic radius also remains constant within the error always slightly above R_g. This gives in all cases a ρ-ratio from 0.87 to 0.95 that can be assigned to a vesicle with finite shell thickness. Although no values are exactly the same for two different cycles, there seem to be no given tendency towards shrinkage or deformation, and the vesicle to micelle transition seems to be reversible within the three cycles limit.

Table 4.2: Gyration Radius, hydrodynamic radius, ρ-ratio and molar mass extracted from SLS and DLS data of PB$_{80}$(Glc)-b-PNIPAM$_{557}$ after successive heating cooling cycles.

Cycle	R_g (nm)	R_h (nm)	R_g/R_h	$M(q)$ (g.mol^{-1})
0	128 ± 1%	134 ± 14	0.95	1.2 10^8 g.mol^{-1} ± 3%
1	122 ± 2%	140 ± 14	0,87	2.1 10^8 g.mol^{-1} ± 9%
2	121 ± 2%	132 ± 27	0,91	2.4 10^8 g.mol^{-1} ± 9%
3	125 ± 3%	135 ± 16	0,95	0.7 10^8 g.mol^{-1} ± 9%

In addition, the DLS after every cycle shows the progressive change in the intensity of both the modes faster and slower than the vesicles mode (Figure 4.12).
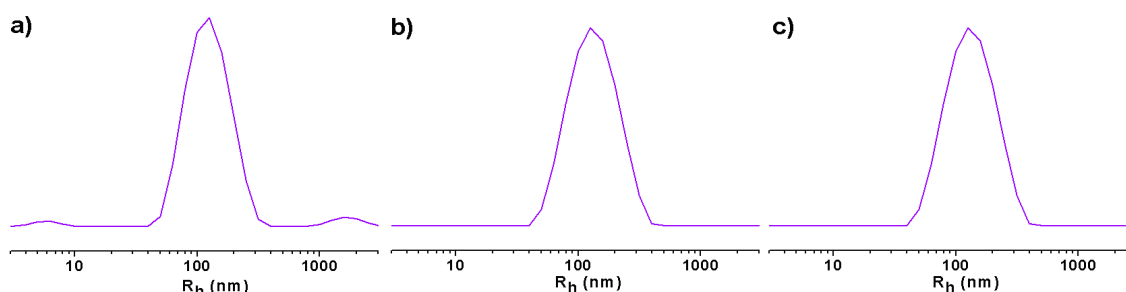
Figure 4.12: Hydrodynamic radii distribution of 1mg·mL^{-1} solution of PB$_{80}$(Glc)-b-PNIPAM$_{557}$ in water after a) Cycle 1, b) Cycle 2, c) Cycle 3 showing the progressive disappearance of the slowest and fastest mode.

The DLS were recorded in every case for 10 runs of 30 seconds. Under those conditions before any heating cycle, 3 modes were detected for PB$_{80}$(Glc)-b-PNIPAM$_{557}$ (see paragraph 4.2). Using the same fitting parameters for the data in cycles 0, 1, 2 and 3, the intensity of the fast and slower modes decreased when compared to the mode of the vesicle progressively from cycle 0 to 3. Although this decrease could not be quantified because it depended on the run, it was a general trend showing that the vesicles were progressively incorporating the intermediate structures. This can explain the progressive increase in apparent molar mass (Table 4.2) from cycle 0 to 2 from 1.16·10^8 g.mol^{-1} to 2.45·10^8 g.mol^{-1}. The exception encountered in cycle 3 seems be related to a degradation process of the vesicles as a precipitate could be observed 3 hours after the last heating/cooling cycle was applied.

4.4   Towards biological applications

The vesicles obtained with PB$_{80}$(Glc)-b-PNIPAM$_m$ copolymers by direct dilution in water

present themselves as privileged systems for biological applications. Not only all their components are biocompatible, D-glucose is also a biologically relevant molecule. Besides its value in metabolism, it plays an important role as ligand in host-pathogen interactions, targeting of proteins within cells and cell-cell interactions with lectin as its receptor.[199] From that point of view these sugar decorated vesicles are potential multivalent ligands for proteins. This interaction was studied in paragraph 4.4.1. These vesicles present also a novel reversible hydrophobic collapse that in addition to its biological value makes it a potential candidate for thermocontrolled release of hydrophilic drugs. A preliminary study of the encapsulation capabilities of organic molecules is presented in paragraph 4.4.2.

4.4.1 Lectin-carbohydrate recognition
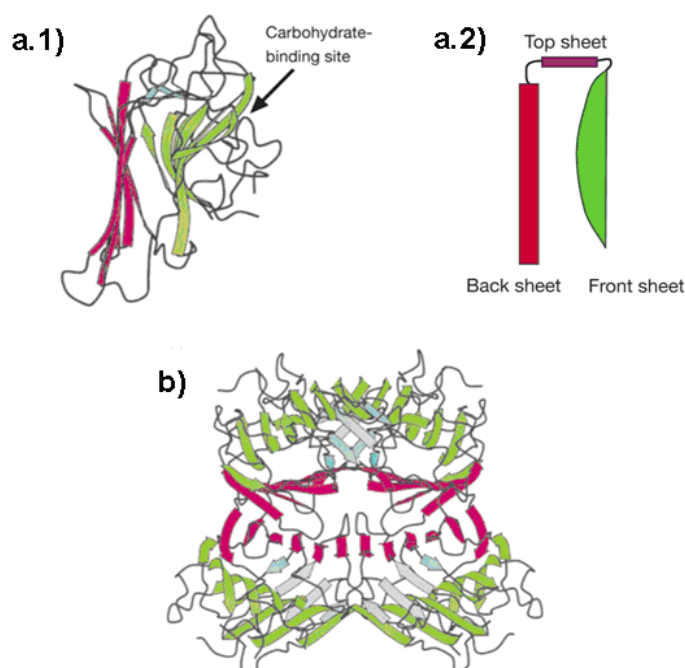
Figure 4.13: Structure of Concanavalin A (ConA), a legume seed lectin. a.1) tertiary structure of the unimer. a.2) This fold consists of a flat six-stranded antiparallel "back" β-sheet (red), a curved seven-stranded "front" β-sheet (green), and a five-stranded "top" sheet (pink) linked by loops of various lengths. b)Tetramer of Con A. Reproduced from [200].

Lectins are glycan-binding proteins and the study of their interaction with carbohydrates goes back to the end of the 19th century.[200] Concanavalin A (ConA) from jack bean (Canavalia ensiformis) is a kind of L-lectin that specifically binds to the monosaccharides glucose and

mannose. These monosaccharide-lectin interactions have low affinity constants K_a in the range of 10^3 to 10^6 M^{-1}.[201] To overcome this weak interaction and fulfill a biological activity, in nature most ligands (both carbohydrates and glycoconjugates) and lectins are multivalent.[202] For example Con A is at pH 7 a tetramer (Figure 4.11.b)) and presents thus four carbohydrate-recognition domains (CRDs) composed of antiparallel β-sheets connected by short loops and β-bends (Figure 4.11.a)).

The presence of multivalent ligands (polysaccharides, glucose functionalized polymers...) does not only enhance the binding affinity, it also might lead in some cases to the formation of crosslinked complexes,[202]-[204] depending of the structural arrangement of the carbohydrate epitopes and the CDRs of the lectins. This crosslinking ultimately leads to clustering and precipitation.

Previous works with sugar decorated vesicles[173][205][206] have already exploited lectin-carbohydrate interactions. In our case buffered solutions (HBS, pH 7.4) of polymers were studied by DLS at an angle of 30°. In that buffer and at that angle the hydrodynamic radii (Table 4.3) seems to follow the logic of the ones extracted from the DLS in water at 90° taking into account the angular dependence inherent to objects of such size. The only difference is the relative size of the object formed by both polymers although that could easily be due to a higher angular dependence of $PB_{80}(Glc)$-b-$PNIPAM_{557}$.

Table 4.3: Hydrodynamic radii (DLS, 30°) of the objects formed in HBS buffer pH 7.4 by $PB_{80}(Glc)$-b-$PNIPAM_{259}$ and $PB_{80}(Glc)$-b-$PNIPAM_{557}$ at 25 °C and 40 °C.

In HBS buffer pH 7.4	R_h (nm) at 25 °C	R_h (nm) at 40 °C
$PB_{80}(Glc)$-b-$PNIPAM_{259}$	159 ± 27	45 ± 3
$PB_{80}(Glc)$-b-$PNIPAM_{557}$	211 ± 21	52 ± 2

The evolution of the hydrodynamic radius of the vesicles after addition of a ConA solution was monitored over time at 25 °C (Figure 4.14.a)) and 35 °C (Figure 4.11.a)). At 25 °C very polydisperse objects with R_h from ~270 to ~460 nm were detected with no apparent evolution over time in the studied timeframe. Visually no precipitation was observed (Figure 4.14.b)). The absence of precipitation means that there is no crosslinking. The fluctuations of the

hydrodynamic radii could indicate short-lived non-specific interactions between the vesicles and the proteins to form vesicle dimers or even the deformation of the vesicles.
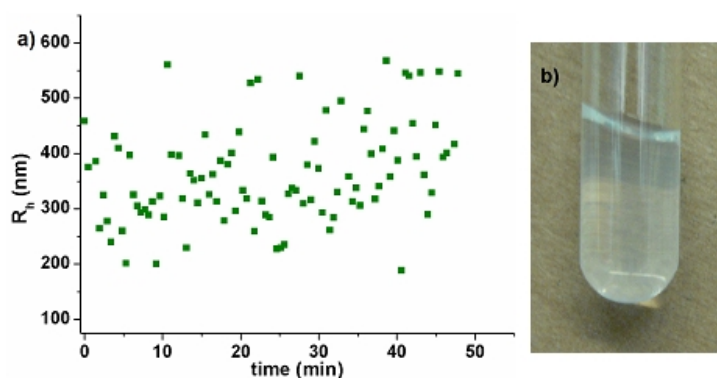
Figure 4.14: The evolution of the hydrodynamic radius after addition of Con A at 25 °C of a PB$_{80}$(Glc)-*b*-PNIPAM$_{557}$ b) Visual appearance of the solution at the end of the experiment.

This absence of clear specific interaction could be understood if the glucose is not on the outside below the LCST as previously discussed (see paragraph 4.2). In that case the PNIPAM on the outside could be engaged in non-specific short-lived interactions with the proteins giving raise to the fluctuations of the hydrodynamic radii observed in the sample. No evolution overtime or precipitation would be expected. But the absence of precipitation is not a proof of the absence of interaction. The cluster glycosidic effect leading to precipitation is a particular case of this interaction in which geometrical arrangement of the carbohydrate epitopes and the CDRs of the lectins allows the creation of 3D crosslinked networks.

To investigate further the interaction between the vesicles and the lectin, fluorescence correlation spectroscopy (FCS) experiments were carried out with fluorescein isothiocyanate (FITC)-labeled Concavalin A (FITC-ConA). Briefly, FCS performs a correlation analysis of fluctuation of the fluorescence intensity. The analysis of the correlation by fitting with the least squares method gives the average number of fluorescent particles and their diffusion time (see Appendix V.). When the FITC-ConA is not bound, a single fast diffusion time can be fitted to the correlation curve. When FITC-ConA binds to the vesicles surface, the fluorescence correlation can be fitted with a slower diffusion component corresponding to the "fluorescent vesicles".

In Figure 4.15 (*left*), the normalized autocorrelation curve of the FITC-ConA protein (in black) shows a fast diffusion that could be fitted to a single population of objects with diffusion time of 110 μs that corresponds thus to the FITC-ConA tetramers. By addition of this same quantity of FITC-ConA to a solution of PB$_{80}$(Glc)-*b*-PNIPAM$_{557}$ in HBS buffer at room temperature, after 2 h, the autocorrelation curve (in green) shows a slower diffusing object. The fitting of this curve revealed a almost unique (93%, Table 4.4) population of objects with a diffusion time of around 10000 μs and barely any free FITC-ConA. This is equivalent to particles of around 500 nm in diameter, which is similiar to the size found by DLS. This proves that indeed ConA bind to the vesicles' surface at room temperature but does not induce agglutination. After 22 hours no change is observed (red curve) showing that ConA-vesicle complex is stable and does not lead to precipitation even over time.
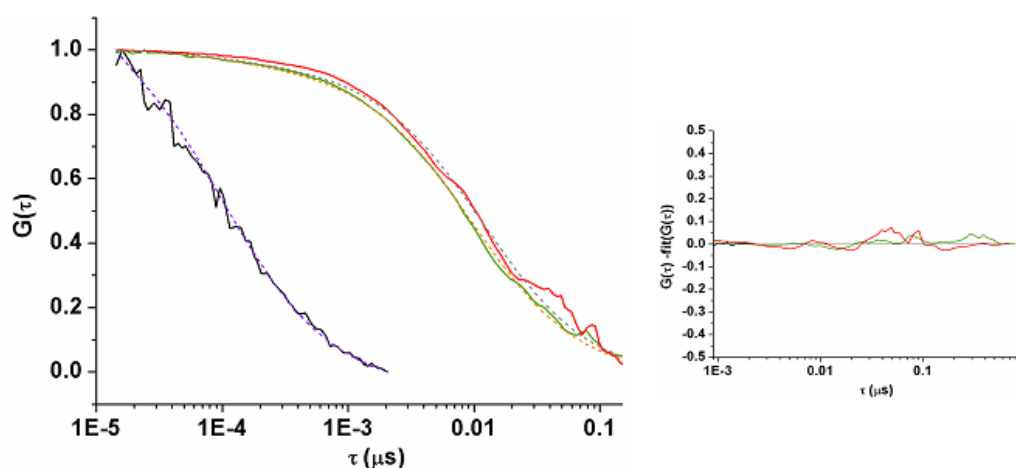
Figure 4.15: (*Left*) Normalized autocorrelation of fluctuation of the fluorescence intensity and its fittings: in black (violet fitting) FITC-ConA in HBS solution; in green (orange fitting) PB$_{80}$(Glc)-*b*-PNIPAM$_{557}$ with FITC-ConA in HBS solution after 2 h; in red (gray fitting) PB$_{80}$(Glc)-*b*-PNIPAM$_{557}$ with FITC-ConA in HBS solution after 22 h. (*Right*) Residuals of the fitting: in black FITC-ConA in HBS solution; in green PB$_{80}$(Glc)-*b*-PNIPAM$_{557}$ with FITC-ConA in HBS solution after 2 h; in red PB$_{80}$(Glc)-*b*-PNIPAM$_{557}$ with FITC-ConA in HBS solution after 22 h.

The key information that can be extracted from the experiment is not the mere existence of interaction as that was already shown by the fluctuations of the hydrodynamic radii by DLS. The key is that all the lectin (~95 %, Table 4.4) in solution is bound showing that the interaction is rather specific and proteins decorate the vesicles. That would mean that the glucose moieties should be on the outside (and therefore PNIPAM on the inside) below the LCST. The specific interaction of vesicles exhibiting an outer layer of glucose with ConA has

already been reported to show interaction without cross-linking.[173] This is presumably due to the size of the vesicles for which the geometrical arrangements of the carbohydrate epitopes and the CDRs of the lectins would not allow the creation of cross-linked networks (Figure 4.17.a)).

Table 4.4: Data extracted from the analysis in the FCS experiments.

Sample	*CR (kHz)*	*CPM (kHz)*	*N*	*Fraction 1*		*Fraction 2*	
				%	$\tau_D(\mu s)$	*%*	$\tau_D(\mu s)$
FITC-ConA	17.3	13.3	1.3	96	110	-	-
PB$_{80}$(Glc)-*b*-PNIPAM$_{557}$ + FITC-ConA after 2h	28.5	25.7	1.2	7	110	93	10000
PB$_{80}$(Glc)-*b*-PNIPAM$_{557}$ + FITC-ConA after 22h	23.5	55.3	0.4	5	110	95	11500

At 35 °C, the addition of ConA to the polymer solution induced the rapid precipitation (Figure 4.16.b)) of the solution as the monitoring of R$_h$ by DLS over time shows (Figure 4.16.a)). This means that the addition of ConA created a crosslinked 3D network, which indicates that at least 2 or 3 out of the 4 CDRs were able to interact with two or more micellar objects. By comparison with the previous experiments it seems that the size of the smaller micelle size optimizes the geometry for multiple CDRs to interact simultaneously (Figure 4.17.b)).
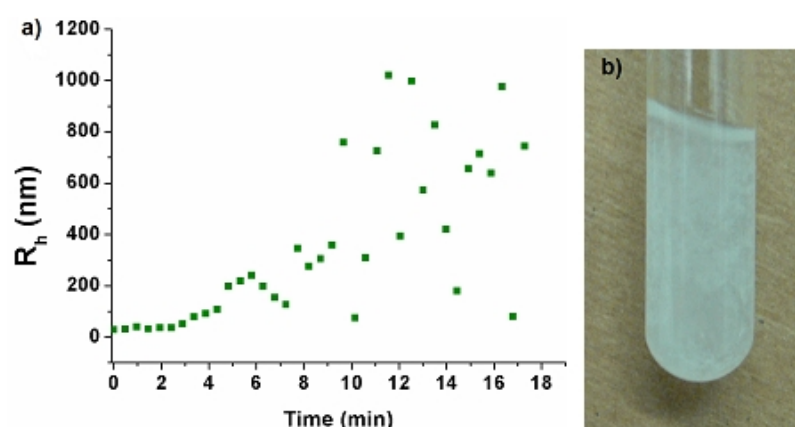
Figure 4.16: a) The evolution of the hydrodynamic radius after addition of Con A at 35 °C of a PB$_{80}$(Glc)-*b*-PNIPAM$_{557}$ b) Visual appearance of the solution at the end of the experiment

A deeper study of the interaction of the vesicles and micelles with lectins could elucidate the

number of lectins bounds per vesicle/micelle, however it is beyond the frame of this work to perform a complete biological evaluation of this system. As a preliminary conclusion, it has been shown that $PB_{80}(Glc)$-b-$PNIPAM_m$ copolymers exhibit a temperature-dependent interaction with lectins, a feature that could be exploited in potential biological and especially medical applications as it is potentially a controlled biological response.
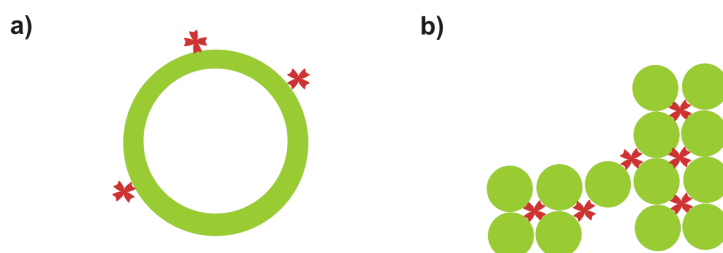
Figure 4.17: Schematic representation of the possible structure of the interacting a) vesicles/ConA at 25°C and b)micelles/ConA at 35 °C. In red the tetravalent ConA, in green vesicles and micelles. The relative size of vesicles and micelles is on scale, Con A is not.

4.4.2 Encapsulation of organic compounds

Research on the delivery of hydrophilic drugs is normally done with systems such as liposomes i.e. synthetic vesicles made of phospholipids[207] and polyelectrolyte capsules.[208] where the drug is encapsulated inside in the hollow interior. More recently, in order to take advantage of the superior mechanical performance of polymer vesicles and the special features of certain polymers (PEG antiadhesion, thermoresponsiveness...), polymersomes have gained attention as potential drug carriers.[209]

As mentioned before $PB_{80}(Glc)$-b-$PNIPAM_m$ polymersomes are interesting potential candidates for such purpose as all their components are biocompatible and the external glucose layer could be a potential vector. The encapsulation capabilities of such systems were investigated in water by means of fluorescence microscopy.

Solid polymer was dissolved in a Rhodamine B solution and subsequently dialyzed against milliQ water. The confocal fluorescence micrographs (Figure 4.18) shows bright red dots corresponding to higher fluorophore concentration zones that are superimposed onto the vesicles seen in the transmission optical micrograph. The encapsulation of Rhodamine B

inside the vesicles is thus effective. From the comparison of the transmission and the fluorescence intensity profiles, it seems that the fluorophore is inside the cavity and not located in the membrane.

Figure 4.18: Overlay micrographs (right), fluorescence intensity profile (left red scale) and transmission intensity profile (left grey scale) of vesicles formed by $PB_{80}(Glc)$-b-$PNIPAM_{557}$ with encapsulated Rhodamine B.
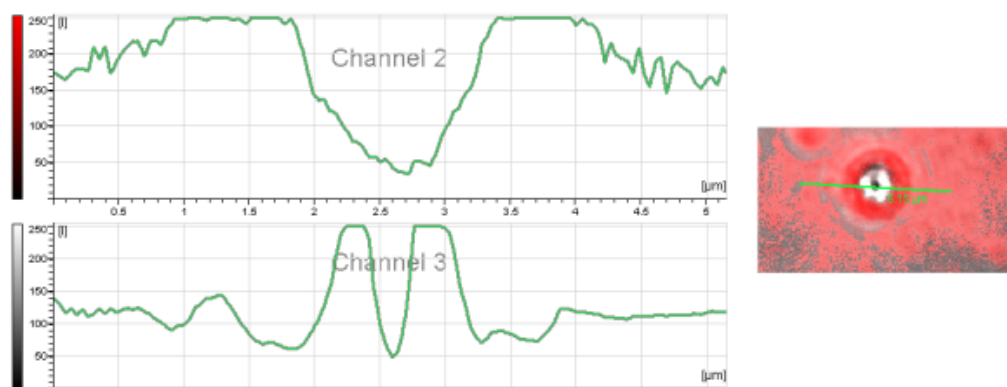
Figure 4.19: Overlay micrographs (right), fluorescence intensity profile (left red scale) and transmission intensity profile (left grey scale) of vesicles formed by $PB_{80}(Glc)$-b-$PNIPAM_{557}$ with Rhodamine B in the continuous phase.

In order to confirm that the fluorescent dye is not located in the membrane and the "fluorescent dots" were due to encapsulation, control experiments were performed by addition of Rhodamine B solution to a solution of preformed vesicles. Micrographs (Figure 4.19) show a continuous fluorescent phase with the vesicles as white dots. The transmission and fluorescence intensity profiles though suggest a concentration gradient of the fluorescent dye starting in the membrane's external boundary. This gradient is probably due to the

osmotic pressure between the vesicle's cavity and the continuous phase that tends to equilibrate the fluorophore concentration from the outside to the inside of the vesicle.This encapsulation behavior suggests thus that these asymmetric vesicles are not good candidates for the encapsulation of hydrophilic drugs as they tend to concentrate the organic molecules around the membrane.

4.5 Summary
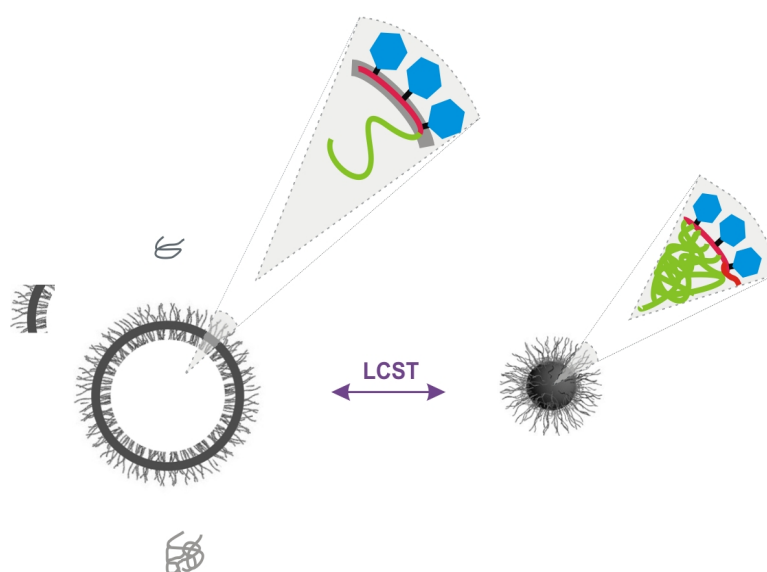
Figure 4.20: Schematization of the possible temperature-induced collapse of a vesicle into a micellar object. The two insets show the membrane structure of the vesicle, and the internal structure of the micelle. The blue hexagons are represent the D-glucose moieties, the PB segment is red and the PNIPAM chains are green

Figure 4.20 summarizes the structure of the aggregate obtained by direct dissolution of $PB_{80}(Glc)$-b-$PNIPAM_m$ copolymers in water at room temperature. The aggregate was found to be a vesicle with asymmetric membrane with an outer glycosylated exterior and PNIPAM on the inside. Above the LCST of PNIPAM, the structure collapsed into micelles with a hydrophobic PNIPAM core and glycosylated exterior. This collapse was found to be reversible at least in the three heating/cooling cycles' context. As a result, the structures showed a temperature-dependent interaction with L-lectin proteins and were shown to be able to encapsulate organic molecules.

Chapter 5: Conclusions and perspectives

In chapter 3, several DHBC systems were studied in water. They all formed structures as a consequence of microphase separation. The microphase separation was obviously not driven by *"the hydrophobic effect"* as we know it but two other reasons were accounted for it: incompatibility of the polymer pairs forming the two blocks (enthalpic) and a considerable solubility difference (enthalpic and entropic). The entropic contribution to this positive Gibbs free energy of mixing is believed to arise from the same loss of conformational entropy that is responsible for *"the hydrophobic effect"*. If the polymer is made of blocks presenting high block solubility difference, a segregation could lower even more the free energy of the system by freeing the water molecules that were trying to solubilize the "less soluble" block (loss of conformational entropy). This theory supports that to have an entropy-driven segregation, a big solubility difference is enough provided that the enthalpic contribution to the free energy does not compensate it. In that sense this is a "***hydrophilic effect***", a sort of competition for water. It is to some extend an extension of the notion of "*hydrophobic effect*"

without the sharp solubility boundary. The notion of **hydrophilic effect** is an acknowledged phenomenon in biological sciences[210] that does not have an equivalent in supramolecular and macromolecular chemistry. For example, in biological sciences, the notion of water structure near hydrophilic substrates (most notably ions) is often explained in terms of "**hydrophilic effect**". A consequence of this effect in supramolecular chemistry is that phase separation in water is ubiquitous to biomacromolecules and thus microphase separation and the subsequent formation of dilute solution phases in water is a principle well beyond hydrophobicity and amphiphilicity.

Concerning the systems developed in chapter 3, the next foci should concern for instance the study of the copolymers-water phases in semi-dilute and concentrated solutions. At those higher concentrations, the enthalpic contribution should rise and mesophases can be expected.[211] A modelization of these systems could bring detailed information of the driving forces and open doors towards a formalization of the "**hydrophilic effect**".

Chapter 4 studied the self-assembly of a glucose-modified polybutadiene-*block*-poly(N-Isopropylacrylamide). The polymer spontaneously formed vesicles by dissolution of the polymer solid in water. The structures of the micelle should still be further studied to elucidate their geometry.

Appendix I. Experimental part

A. Experimental procedures

I. Dextran-*block*-poly(ethylene glycol) polymers

I.1) Blocks prepapation

I.1.a) α-alkyne dextrans

1 eq of dextran was dissolved at 2 wt% in acetate buffer (pH=5.5, 50 mM) at 50 °C. 100 eq of propargylamine were added followed by 100 eq of sodium cyanoborohydride (NaCNBH₃). The mixture was stirred for 5 days with a daily addition of 100 eq of sodium cyanoborohydride. Purification was achieved by concentrating the solution in the rotatory evaporator and dialyzing against milliQ water (MWCO 1000) for 5 days with daily solvent change. The polymer was recovered by lyophilization.

Block	α-alkyne dextran₆	α-alkyne dextran₁₁	α-alkyne dextran₆(SO₃Na)
Quantities			
1 eq Dextran (g)	10,0	10,0	5,0
100 eq Propargylamine (mL)	9,6	9,3	5,0
100 eq NaCNBH₃ (g)	9,5	9,5	4,8
Yield			
Mass recovered (g)	5,8	7,1	3,6
Yield (%)	~58	~71	~71

α-alkyne dextran₆₅₀₀
¹H NMR (DMSO-d₆, 400 MHz): δ (ppm)= 4.91, 4.83, 4.67, 4.50 (b, 1'+6'), 3.75, 3.64, 3.48 (b, 5+6+3'), 3.36 (bs, 2+4+5), 3.20 (b, 3)
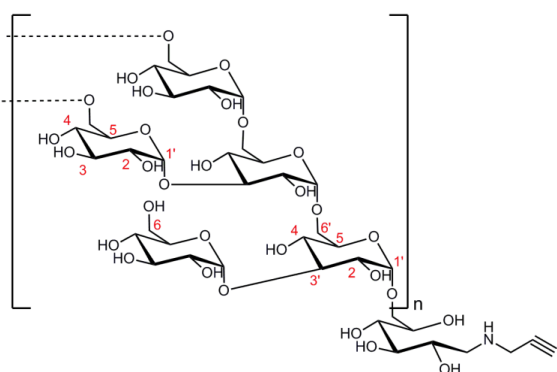
GPC (DMSO, dextran): $M_{n,app}$= 5100, PDI=1.66

α-alkyne dextran$_{11000}$
^{1}H NMR (DMSO-d$_6$, 400 MHz): δ (ppm)= δ (ppm)= 4.91, 4.83, 4.67, 4.50 (b, 1'+6'), 3.75, 3.64, 3.48 (b, 5+6+3'), 3.36 (bs, 2+4+5), 3.20 (b, 3)
GPC (DMSO, dextran): $M_{n,app}$=6500 PDI=1.75

I.1.b) α-methoxy-ω-azido-poly(ethylene glycol)

- α-methoxy-ω-p-toluenesulfonyl-poly(ethylene glycol)

1 eq of commercial poly(ethylene glycol) methyl ether (mPEG-OH) was dissolved at 25 wt % in dichloromethane. 7 equivalents of triethylamine (TEA) were added and the mixture was cooled down to 0 °C. Under stirring 5 eq of *p*-toluenesulfonyl chloride (TsCl) were added and the mixture was stirred for 2 hours at 0 °C and overnight at room temperature.
The polymers were purified by precipitation in diethylether and subsequent recrystallization twice from ethanol. The obtained solids were dried at room temperature under vacuum overnight.

Block	mPEG$_{13200}$-OTs	mPEG$_{5500}$- OTs	mPEG$_{1900}$- OTs
Quantities			
1 eq mPEG-OH (g)	4,0	20,0	20,0
7 eq TEA (mL)		4,0	10,0
5 eq TsCl (g)		4,0	10,0
Yield			
Mass recovered (g)	3,8	17,2	7,0
Yield (%)	~95	~86	~35
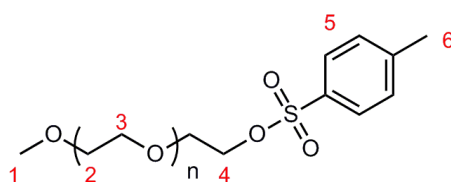
mPEG$_{13200}$-OTs
^{1}H NMR (DMSO-d$_6$, 400 MHz): δ (ppm)= δ (ppm)= 7.78 and 7.48 (4H, A$_2$B$_2$ dd, 5), 4.11 (2H, t, 4), 3.51 (bs, 2+3), 3.24 (3H, s, 1), 2.42 (3H, s, 6)
GPC (DMSO, dextran): $M_{n,app}$=11200 PDI=1.05

mPEG$_{5500}$-OTs
^{1}H NMR (DMSO-d$_6$, 400 MHz): δ (ppm)= 7.78 and 7.48 (4H, A$_2$B$_2$ dd, 5), 4.11 (2H, t, 4), 3.51 (bs, 2+3), 3.24 (3H, s, 1), 2.42 (3H, s, 6)
GPC (DMSO, PEG): $M_{n,app}$=3600 PDI=1.14

mPEG$_{1900}$-OTs
^{1}H NMR (DMSO-d$_6$, 400 MHz): δ (ppm)= 7.78 and 7.48 (4H, A$_2$B$_2$ dd, 5), 4.11 (2H, t, 4), 3.51 (bs, 2+3), 3.24 (3H, s, 1), 2.42 (3H, s, 6)
GPC (DMSO, PEG): M$_{n,app}$=1400 PDI=1.04

- α-methoxy-ω-azido-poly(ethylene glycol)

p-toluenesulfonyl terminated poly(ethylene glycol) methyl ether polymers were dissolved at 10 wt% in DMF and 10 eq of sodium azide (NaN$_3$) were added. The mixtures were heated at 60 °C under stirring for 3 days. Purification was achieved by removal of the solvent under reduced pressure and redissolving the solid in water for subsequent dialysis against bidistilled water for 4 days with 4 solvent changes. The polymer was recovered as a white solid by freeze-drying.

Block	mPEG$_{13200}$-N$_3$	mPEG$_{5500}$-N$_3$	mPEG$_{1900}$-N$_3$
Quantities			
mPEG$_y$-OTs	3,8	10,0	10,0
NaN$_3$(g)	0,2	1,3	3,3
Yield			
Mass recovered (g)	3,1	9,0	8,7
Yield (%)	~81	~90	~87
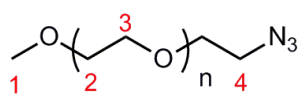
mPEG$_{13200}$-N$_3$
^{1}H NMR (DMSO-d6, 400 MHz): δ (ppm)= 3.51 (bs, 2+3), 3,37 (s, 4), 3.24 (3H, s, 1)
GPC (DMSO, PEG): M$_{n,app}$=13200 PDI=1.08

mPEG$_{5500}$- N$_3$
^{1}H NMR (CDCl$_3$, 400 MHz): δ (ppm)= 3.51 (bs, 2+3), 3,35 (s, 4), 3.25 (3H, s, 1)
GPC (DMSO, PEG): M$_{n,app}$=5500 PDI=1.03

mPEG$_{1900}$- N$_3$
^{1}H NMR (DMSO-d6, 400 MHz): δ (ppm)= 3.51 (bs, 2+3), 3,37 (s, 4), 3.24 (3H, s, 1)
GPC (DMSO, PEG): M$_{n,app}$=1900 PDI=1.05

I.1.c) α, ω-bisazido-poly(ethylene glycol)

- α, ω-bis-p-toluenesulfonyl -poly(ethylene glycol)

1 eq (10 g)of commercial poly(ethylene glycol) (HO-PEG-OH) Mw 5100 g·mol^{-1}was dissolved at 25 wt% in dichloromethane. 14 eq (4 mL) of triethylamine (TEA) were added and the mixture was cooled down to 0 °C. Under stirring 10 eq (4 g) of p-toluenesulfonyl

chloride (TsCl) were added and the mixture was stirred for 2 hours at 0 °C and overnight at room temperature.

The polymers were purified by precipitation in diethylether and subsequent recrystallization twice from ethanol. The obtained solids were dried at room temperature under vacuum overnight. m=10,01 g, Yield~ 99%

TsO-PEG$_{5100}$-OTs
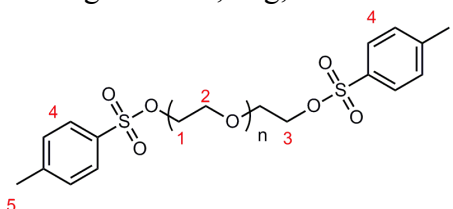^{1}H NMR (DMSO-d$_6$, 400 MHz): δ (ppm)= 7.79 and 7.48 (4H, A$_2$B$_2$ dd, 4), 4.11 (2H, t, 3), 3.51 (bs, 1+2), 2.42 (3H, s, 5)
GPC (DMSO, dextran): M$_n$= 4800 PDI=1.05

- α, ω-bisazido-poly(ethylene glycol)

1 eq (6,5 g) of bis-p-toluenesulfonyl terminated poly(ethylene glycol) polymer Mw 5000 was dissolved at 10 wt% in DMF and 20 eq (1,7 g) of sodium azide (NaN$_3$) were added. The mixtures were heated at 60 °C under stirring for 3 days. Purification was achieved by removal of the solvent under reduced pressure and redissolving the solid in water for subsequent dialysis against bidistilled water for 4 days with 4 solvent changes. The polymer was recovered as a white solid by freeze-drying. m=5,23 g, yield ~82%.
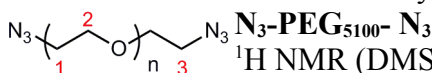
N$_3$-PEG$_{5100}$- N$_3$
^{1}H NMR (DMSO-d$_6$, 400 MHz): δ (ppm)= 3.50 (bs, 2+3), 3,38 (s, 3)
GPC (DMSO, dextran): Mn=5100 PDI=1.03

l.1.d) α-lactone-dextran

2 eq of Iodine 1N in water (6,6 mL) were added to 1 eq (5 g) of dextran (Mw 6000) at 10% in water. 8 eq (0.746 g) of KOH in water were added drop by drop under stirring. The mixture was stirred at room temperature overnight and subsequently dialyzed against milliQ water (MWCO 1000) for 3 days with 3 water changes. The solution was then stired with DOWEX 50 (sulfonic acid, H form), filtered and freeze dried. The product was recovered as a slightly yellow powder. m=4,5 g, yield~90%.
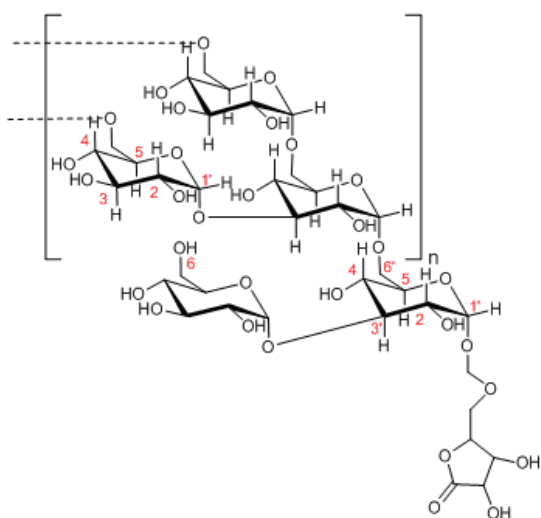
α-lactone-dextran$_{6500}$
^{1}H NMR (DMSO-d6, 400 MHz): δ (ppm)= 4.91-4.50 (b, 1'+6'), 3.75, 3.64, 3.48 (b, 5+6+3'), 3.36 (bs, 2+4+5), 3.20 (b, 3)
GPC (DMSO, dextran): M$_{n,app}$=3000 PDI=1.69

I.2) Block copolymer synthesis

I.2.a)   dextran-*block*-poly(ethylene glycol)

1 eq of α-alkyne dextran, 1.2 eq of α-methoxy-ω-azido-poly(ethylene glycol) and 1 eq of sodium L-ascorbate (NaAsc) were mixed at a 10% wt in a THF:water 3:7 (v:v) mixture. Argon was bubbled through the solution for 2 hours for degassing. 0.2 eq of copper iodide (CuI) and 10 equivalents of 1,8-Diazabicyclo[5.4.0]undec-7-ene (DBU) were added and the solution was treated under microwave irradiation (μW irradiation) for 30 minutes at 95 °C (irradiation from room temperature to 95 °C for 15 min and 15 min at 95 °C). Solutions were allowed to cool down to room temperature and were filtered. Active carbon was added to the filtrated, stirred at room temperature for 30 min and refiltrated. Purification was achieved by dialysis in milliQ water with the cut-off membrane depending on the polymer. The polymers were recovered by lyophilisation as white powders.

Polymer	dex_{6500}-b-PEG_{13200}	dex_{6500}-b-PEG_{5500}	dex_{6500}-b-PEG_{1900}	dex_{11000}-b-PEG_{5500}
Quantities				
1 eq α-alkyne dex (g)	0,24	1,00	1,00	1,00
1,2 eq mPEG-N$_3$ (g)	0,60	0,99	0,34	67,0
0,2 eq CuI (μg)	1,85	6,30	6,30	4,22
10 eq DBU (μL)	73	248	248	166
1 eq NaAsc (mg)	8,5	292	29	19
Membrane MWCO	11000	5000	3500	5000
Yield				
Mass recovered (g)	0,54	1,79	0,97	1,32
Yield (%)	73	98	76	85
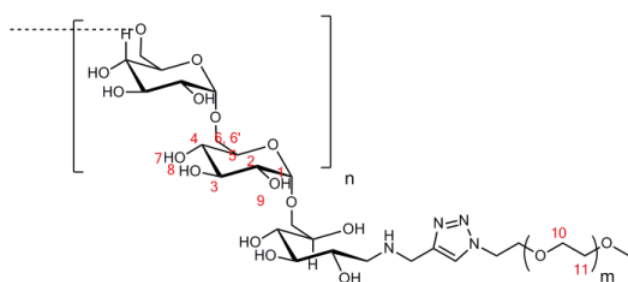
dextran$_{6500}$-*block*-PEG$_{13200}$
^{1}H NMR (DMSO-d$_6$, 400 MHz): δ (ppm)= 4.91-4.50 (b, 7+8+1+9), 3.76, 3.64, 3.48 (b, 5+6+6'), 3,51 (s, 10+11), 3.36 (bs, 2+4), 3.20 (b, 12)
GPC (DMSO, dextran): $M_{n,app}$=10800 PDI=1.85
dn/dc (25 °C)= 0.1448 mL·g^{-1}

dextran$_{6500}$-*block*-PEG$_{5500}$
^{1}H NMR (DMSO-d$_6$, 400 MHz): δ (ppm)= 4.91-4.50 (b, 7+8+1+9, 3.75, 3.64, 3.48 (b, 5+6+6'), 3,51 (s, 10+11), 3.36 (bs, 2+4), 3.20 (b, 12)
GPC (DMSO, dextran): $M_{n,app}$=8000 PDI=1.61
dn/dc (25 °C)= 0.1352 mL·g^{-1}

dextran$_{6500}$-*block*-PEG$_{1900}$
^{1}H NMR (DMSO-d$_6$, 400 MHz): δ (ppm)= 4.91-4.46 (b, 7+8+1+9), 3.75, 3.64, 3.48 (b, 5+6+6'),

3,51 (s, 10+11), 3.36 (bs, 2+4), 3.20 (b, 12)
GPC (DMSO, dextran): $M_{n,app}$=7000 PDI=1.61
dn/dc (25°C)= 0.0812 mL·g^{-1}

dextran$_{11000}$-*block*-PEG$_{5500}$
^{1}H NMR (DMSO-d$_6$, 400 MHz): δ (ppm)= 4.91-4.46 (b, 1'+6'), 3.75, 3.64, 3.48 (b, 5+6+6'),
3,51 (s, 10+11), 3.36 (bs, 2+4), 3.20 (b, 12)
GPC (DMSO, dextran): $M_{n,app}$=7600 PDI=1.44
dn/dc (25°C)= 0.1365 mL·g^{-1}

I.2.b) dextran-*block*-poly(ethylene glycol)-*block*-dextran

2.4 equivalent (0.5 g) of α-alkyne dextran, 1 equivalents (1.44 g) of α,ω-bisazido-poly(ethylene glycol) and 1 eq (35 mg) of sodium L-ascorbate were mixed at a 10% wt in a THF:water 3:7 (v:v) mixture. Argon was bubbled through the solution for 2 hours for degassing and 0.4 eq (7.6 mg) of copper iodide (CuI) and 10 eq (298 µL) of 1,8-Diazabicyclo[5.4.0]undec-7-ene (DBU) were added. The solution was treated under microwave irradiation (µW irradiation) for 30 minutes at 95 °C (irradiation from room temperature to 95 °C for 15 min and 15 min at 95 °C). Solution was allowed to cool down to room temperature and filtered. Active carbon was added to the filtrated, stirred at room temperature for 30 min and refiltrated. Purification was achieved by dialysis in milliQ water MWCO 3500 for 3 days. The polymer was recovered by lyophilisation as white powders.
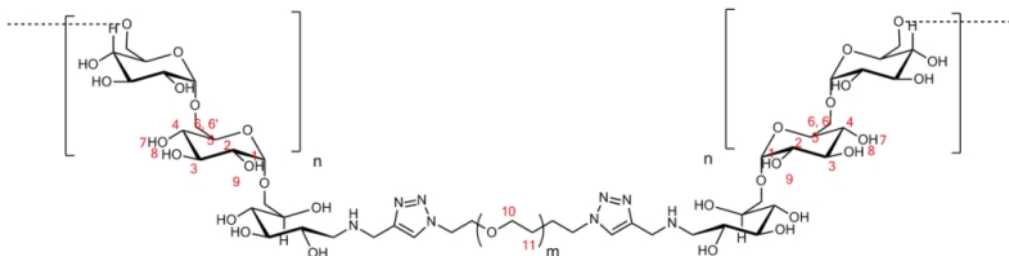
dextran$_{6500}$-*block*-PEG$_{5100}$-*block*-dextran$_{6500}$
^{1}H NMR (DMSO-d$_6$, 400 MHz): δ (ppm)= 4.91-4.47 (b, 1'+6'), 3.75, 3.64, 3.48 (b, 5+6+6'),
3,51 (s, 10+11), 3.36 (bs, 2+4)
GPC (DMSO, dextran): $M_{n,app}$=7400 PDI=1.62
dn/dc (25°C)= 0.1438 mL·g^{-1}

I.2.c) maleic anhydride-derived dextran-*block*-poly(ethylene glycol)

75 mg of dextran$_{6500}$-*b*-PEG$_{5500}$ (~9.10-4 mol OH when approximating dextran to a linear α-1,6-polyglucan) was dissolved at 3 wt% in a 0,1M LiCl/DMF at 60 °C and 5µL of TEA were added. 0.2 eq (to OH) of maleic anhydride (18,2mg) were subsequently added and the mixture was stirred at 60 °C for 24 h. The polymer was dialyzed against milliQ water in a MWCO 1000 membrane and freeze-dried. 60 mg of polymer were recovered as a slightly yellow powder.
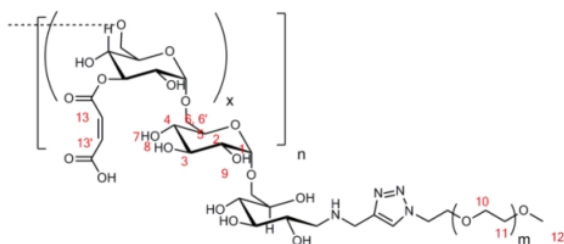
dextran_6(MA)-*block*-PEG_5000
^{1}H NMR (DMSO-d_6, 400 MHz): δ (ppm)= 6.01 (s, 13+13'), 4.91-4.50 (b, 7+8+1+9), 3.75, 3.64, 3.48 (b, 5+6+6'), 3.51 (s, 10+11), 3.36 (bs, 5+6+6'), 3.20 (b, 12)

I.2.d) dextran-*block*-poly(ethylene glycol) (amide link)

1eq (0.84 g) of dextran α-lactone-dextran6 and 5 equivalents of commercial α-methoxy-ω-amino-poly(ethylene glycol) Mw 5000 (3,48 g) were dissolved in DMSO and stirred at 60 °C for 6 days. DMSO was removed by freeze-drying and the polymer redissolved in water and dialysed against milliQ water for 3 days. The polymer was recovered as a white powder (Yield=75%).
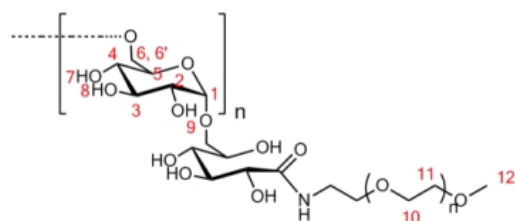
dextran_6500-*block*-PEG_5700 (amide linkage)
^{1}H NMR (DMSO-d_6, 400 MHz): δ (ppm)= 4.93-4.52 (b, 7+8+1+9), 3.75, 3.63, 3.48 (b, 5+6+6'), 3.51 (s, 10+11), 3.36 (bs, 5+6+6'), 3.20 (b, 12)
GPC (DMSO, dextran): $M_{n,app}$=8800 PDI=1.67
dn/dc (25°C)= 0.1290 mL·g^{-1}

II. Other dextran-based polymers

II.1) Dextran-CTA preparation

II.1.a) Azido-RAFT agent

The synthetic strategy was adapted from the one reported by Stenzel[146] and coworkers for the synthesis of 3-azidopropyl 2-((ethoxycarbonothioyl)thio)acetate.

• 2-azidoethanol

10 g (5.67 mL, 0.08mol) of 2-bromothanol and 8,45 g (0.13 mol) and sodium azide were mixed together at 10 wt% in a 65:10 (v:v) acetone:water mixture and stirred at 65 °C for two days. The mixture was allowed to cooled down to room temperature and the acetone was removed under reduced pressure. 100 mL of water were added and the mixture was extracted 3 times with diethyl ether. The organic phase was then dried over anhydrous magnesium sulfate and the solvent evaporated under reduced pressure. 5,60g of product were obtained as a yellow liquid (Yield=).
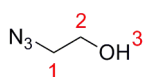
^{1}H NMR (CDCl$_3$, 400 MHz): δ (ppm)= 3.76 (2H, t, 2), 3.42 (2H, t, 1), 2.46 (1H, s, 3)

- ### 2-azidoethyl-1-bromoethanoate

5 g (57.2 mmol) of 2-azido-ethanol and TEA dried over CaH$_2$ were mixed in dry THF and cooled down to 0 °C. 9 ml (86.1 mmol) of 2-bromopropionyl bromide in 60 mL of dry THF were added drop by drop under stirring. After the addition was completed, the mixture was allowed to reach room temperature under stirring and reacted an additional hour. The solution was then filtered (removal of TEA·HCl), 20 mL of water were added drop by drop to the filtrated and the allowed to stir for 30 min. The solvent was removed under reduced pressure to dry and the solide redissolve in dichloromethane. The solution was extracted twice with a saturated ammonium chloride solution, twice with distilled water, twice with a 0.1M sodium hydroxide solution and twice with bidistilled water. The organic layer was then dried over anhydrous magnesium sulfate and filtered, and the solution concentrated under reduced pressure. Final purification was achieved by flash column chromatography with a gradient eluent CH$_2$Cl$_2$:MeOH 1:0 to 10:1 (v:v). After removal of the eluents 8,5g of pure product were isolated (Yield=).
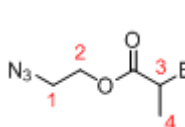
^{1}H NMR (CDCl$_3$, 400 MHz): δ (ppm)= 4.41 (1H, q, 3), 4.33 (2H, t, 2), 3.53 (2H, t, 1), 1.84 (3H, d, 4)

- ### 2-azidoethyl 2-((ethoxycarbonothioyl)thio)propanoate (CTA-N$_3$)

8,5 g (3,83.10^{-2} mol) of 2-azidoethyl-1-bromoethanoate and 6.14 g (1 eq, 3.83·10^{-2} mol) of O-ethylxantic acid potassium salt were dissolved in 80 mL of ethanol and stirred at 55 °C for 20 h. 200 mL of water were added and the solution was extracted three times with diethyl ether. The collected organic layers were dried over anhydrous magnesium sul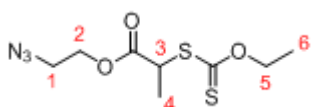fate, filtered and the product was concentrated under reduced pressure. The product was purified by column chromatography with a gradient eluent hexane:ethyl acetate 19:1 to 9:1 (v:v). 5,1 g of pure product were isolated after removal of the eluents under reduced pressure (Yield=)

^{1}H NMR (CDCl$_3$, 400 MHz): δ (ppm)= 4.65 (2H, q, 5), 4.40 (1H, q, 3), 4.22 (2H, q), 1.48(3H, d, 4), 1.44 (3H, t,), 1.29 (2H, t,)

II.1.b)   Dextran-CTA

1 equivalent (2 g) of α-alkyne dextran, 2eq (0.175 g, 160 µL) of 2-azidoethyl 2-((ethoxycarbonothioyl)thio)propanoate and 1 eq (587 mg) of sodium L-ascorbate ascorbate were mixed at a 10% wt in a THF:water 3:7 (v:v) mixture. Argon was bubbled through the solution for 2 hours for degassing and 0.2 eq (12.6 mg) of copper iodide (CuI) and 10 eq (497 µL) of 1,8-Diazabicyclo[5.4.0]undec-7-ene (DBU) were added. The solution was treated

under microwave irradiation (µW irradiation) for 30 minutes at 95 °C (irradiation from room temperature to 95 °C for 15 min and 15 min at 95 °C). Solution was allowed to cool down to room temperature and filtered. Active carbon was added to the filtrated, stirred at room temperature for 30 min and refiltrated. Purification was achieved by dialysis against milliQ water MWCO 1000 for 3 days. The polymer was recovered by lyophilisation as a white powder.
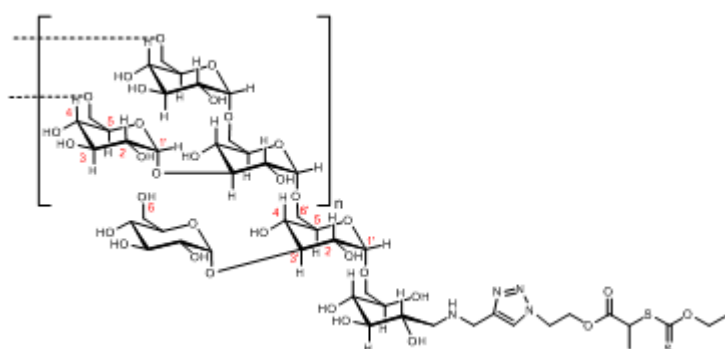
dextran$_6$-CTA
^{1}H NMR (DMSO-d$_6$, 400 MHz): δ (ppm)=
GPC (DMSO, dextran): M$_{n,app}$=3800
PDI=1.66

II.2) RAFT polymerization of dextran-based copolymers

II.2.a) General procedure

0.5g of dextran6-CTA was suspended in 40 mL of DMF 0.1 eq of Azobisisobutyronitrile (AIBN) was added. Small volumes of dry DMSO were added until the solution became clear (~2 mL). The desired amount of freshly purified (distilled or recrystallized) monomer was added and argon was bubble through the solution for 2 h. The flask was then sealed and heated to 70 °C under stirring for 4 days. The mixture was then concentrated, dialysed against milliQ water and lyophilized. The polymer was obtained as a white powder.

Polymers	*1 eq dex-CTA*	*0.1 eq AIBN*	*Monomer*
dextran-b-poly(N-vinylpyrrolidone)			N-vinylpyrrolidone
dex-*b*-PVP	0.5 g	1.43 mg	200 eq (1.87 mL)
dextran-b-polyvinyl acetate			Vinyl acetate
dex-*b*-PVAc	0.5 g	1.43 mg	200 eq (1.61 mL)
dextran-b-poly(N-isopropylacrylamide)			N-isopropylacrylamide
dex$_6$-*b*-PNIPAM$_6$	0,2	1,08	100 eq (0.75 g)
dex$_6$-*b*-PNIPAM$_{16}$	0,2	1,08	200 eq (1.50 g)
dex$_6$-*b*-PNIPAM$_{51}$	0,2	1,08	300 eq (2.26 g)
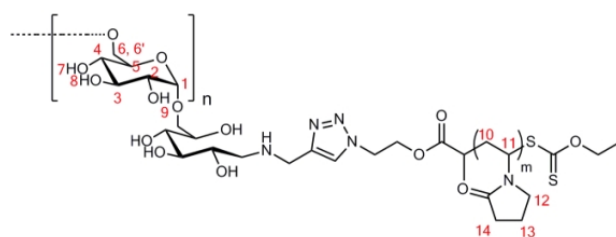
dextran$_{6500}$-*b*-PVP
^{1}H NMR (DMSO-d$_6$+ DMF-d$_7$), 400 MHz): δ (ppm)= 4.98 (s, 7), 4.87 (s, 8), 4.76 (s, 1), 4.50 (s, 9),, 3.88-3.43 (m, 5+6+6'), 3.29 (m, 2+4), 2.31 (s, 14) 2.09-1.96 (m, 10), 1.68 (b,

IX

13) *11+12 covered by DMF-d_7
GPC (DMSO, dextran): $M_{n,app}$=6500 PDI=1.79
dn/dc (25°C)= 0.1295 mL·g^{-1}
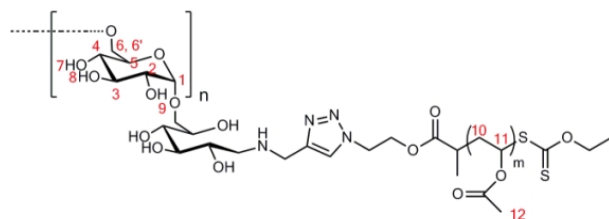
dextran$_{6500}$-b-PVAc
^{1}H NMR (DMSO-d_6, 400 MHz): δ (ppm)= 4.98 (s, 7), 4.87 (s, 8), 4.76 (s, 1), 4.50 (s, 9),, 3.88-3.43 (m, 5+6+6'), 3.29 (m, 2+4), 2.01-1.95 (m, 12), 1.68 (b, 10) *11 covered by dextran signals
GPC (DMSO, dextran): $M_{n,app}$=5200 PDI=1.64
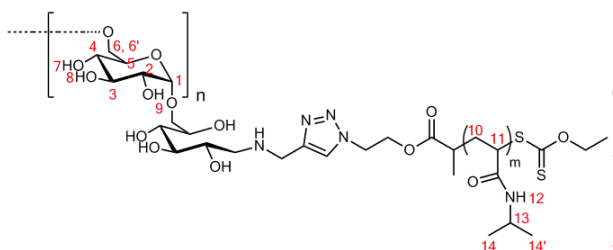
dextran$_{6500}$-b-PNIPAM$_m$
^{1}H NMR (DMSO-d_6, 400 MHz): δ (ppm)= 7.68-6.88 (b, 13), 4.91 (s, 7), 4.83 (s, 8), 4.67 (s, 1), 4.48 (s, 9). 3.83 (bs, 13), 3.63-3.43 (m, 5+6+6'), 3.19 (m, 2+4), 1.95 (bs, 11), 1.43 (bs, 10), 1.04 (s, 14+14')

dextran$_6$-b-PNIPAM$_{51}$: GPC (DMSO, dextran): $M_{n,app}$=6700 PDI=1.89
dn/dc (25°C)= 0.1494 mL·g^{-1}
dextran$_6$-b-PNIPAM$_{16}$: GPC (DMSO, dextran): $M_{n,app}$=5300 PDI=1.81
dn/dc (25°C)= 0.1626 mL·g^{-1}
dextran$_6$-b-PNIPAM$_6$: GPC (DMSO, dextran): $M_{n,app}$=4900 PDI=1.79
dn/dc (25°C)= 0.1885 mL·g^{-1}

II.2.b)   dextran-*block*-poly(vinyl alcohol)

dextran$_6$-b-PVAc was dissolved at 60 °C in a water/methanol mixture (~5:5 v:v) and 2 mL of HCl 37% percent was added. The solution was stirred for 20 hours and subsequently dialyzed against milliQ water (MWCO 1000)
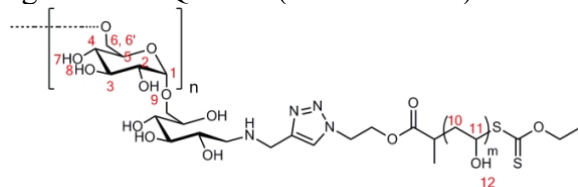
dextran$_{6500}$-b-PVOH
^{1}H NMR (DMSO-d_6 +D$_2$O, 400 MHz): δ (ppm)= 4.80-4.47 (m, 7+1+9+12), 3.83-3.63 (m, 5+6+6'), 3.57-3.44 (m, 3+11), 3.37-3.22 (2+4)
dn/dc (25°C)= 0.1300 mL·g^{-1}

III.   Poly(ethylene glycol)-*block*-poly(N-hydroxyethyl glutamine)

III.1)   γ-benzyl-glutamate N-carboxyanhydride (BLG NCA)

The synthesis was carried out adapting a procedure previously described by Daly *et al.*[212] In a typical synthesis L-Glutamic acid γ-benzylester (30 g, 126 mmol) was suspended in dry THF (300 mL) and heated to reflux under argon atmosphere. Triphosgene (13 g, 0.35 eq) was added and the mixture heated to reflux under Argon until a clear solution formed. In case the clear solution did not form after 5 hours, additional 0.5 g of triphosgene were added. The solution was cooled to room temperature under argon and precipitated with "wet" heptane. The solid was filtered out, dissolved in "dry" EtAc and filtered. The filtrate was then concentrated under vacuum at room temperature. The obtained white solid was recrystallized twice from a EtAc/heptane mixture, dried under high vacuum overnight, stored at -5 °C and used within one week. Yield was typically around 50%.
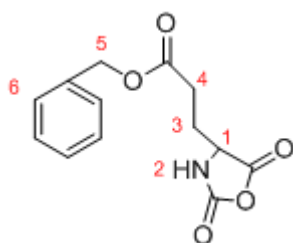
mp: (°C)= 94-97
1H NMR (CDCl$_3$, 400 MHz): δ (ppm)= 2.20 (m, 2H, 3), 2.60 (t, 2H, 4), 4.37 (t, 1H, 1), 5.14 (s, 2H, 5), 6.50(s, 0.9H, 2), 7.35 (m, 5H, 6)

III.2)   Poly(ethylene glycol)-*block*-poly(L-benzyl glutamate)

2.84 g (10.8 mmol) of γ-benzyl-glutamate N-carboxyanhydride and 0.6 g (0.12 mmol)commercial amino-functionalized poly(ethylene glycol) (M$_w$=5700 g·mol^{-1}, PDI=1.08) were dissolved at 10 wt% in NMP under argon atmosphere, and stirred in a schlenk flash equipped with an argon balloon at 40 °C for 5 days.
The polymer was precipitated with EtAc and purified by reprecipitation from CH2Cl2/EtAc twice
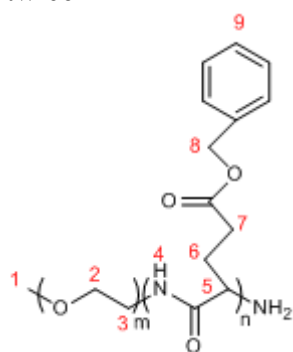
PEG-*b*-PLBG$_{24}$
^{1}H NMR (CDCl$_3$, 400 MHz): δ (ppm)= 8.34 (bs, 4), 7.24 (bs. 9), 5.03 (bs, 8), 3.93 (bs, 5), 3.64 (bs, 2+3), 3.38 (s, 1), 2.61-1.78 (b, 6+7)
GPC (NMP, PS): M$_{n,app}$=27000, PDI=1.22
GPC (NMP, PEG): M$_{n,app}$=20000, PDI=1.34

III.3)   Poly(ethylene glycol)-*block*-poly(N-hydroxyethyl-L-glutamine)

2 g of the previously synthesized poly(ethylene glycol)-*block*-poly(L-benzyl glutamate) were dissolved in 100 mL of DMF. 4.13 g (excess) of 2-hydrohypyridine and 10.41 mL (excess) of 2-aminoethanol. The solution for stirred at room temperature for 4 days. Purification was achieved by dialysis against milliQ water for 4 days with 4 solvent changes. The polymer

was recovered by lyophilization. M= 1.55 g.

PEG-*b*-PHEG$_{24}$

^{1}H NMR (DMSO-d$_6$, 400 MHz): δ (ppm)= 8,12 (bs, 4), 7,78 (bs, 8), 4.70 (b, 11), 4.12 (b, 5), 3.36 (b, 2+3), 3.23 (s, 1), 3.10 (b, 9+10), 2.24-1.70 (b, 6+7)

GPC (NMP, PEG): M$_{n,app}$=17000, PDI=1.31

dn/dc (25°C)= 0.1545 mL·g^{-1}
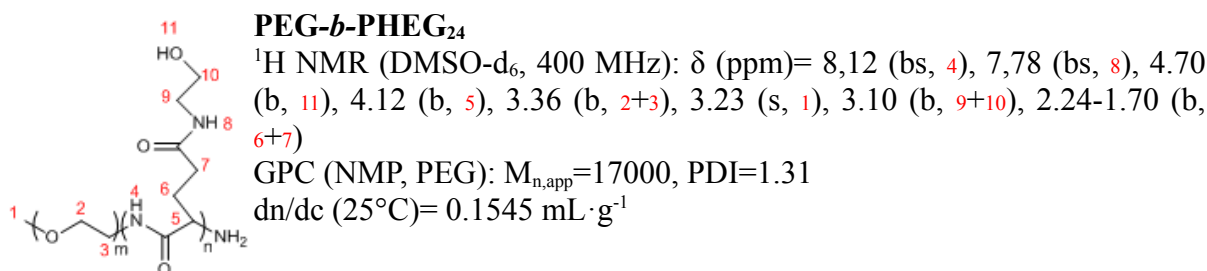
IV. glycosylated polybutadiene-*block*-poly(N-isopropyl-acrylamide) polymers

This synthesis was carried out by Ines Below-Lutz and Niels ten Brummelhuis.

IV.1) CTA synthesis

3.489 g potassium ethyl xanhogenate was dissolved at 10 wt% in ethanol and heated to 55 °C. 3.69 g of 2-bromo-2-methyl propionic acid was added to the solution and the mixture was stirred at 55 °C overnight.

130 mL of water were added to the solution and the resulting mixture was extracted with Et$_2$O three times. The collected organic layers were dried over MgSO$_4$ and filtered. The solvent was removed under reduced pressure and the product was purify by silica column chromatography with a 10:1 (v:v) hexane:ethyl acetate solvent mixture as eluent.

S-Ethoxy(thiocarbonyl)-2-mercapto-2-methylpropanoic acid

^{1}H NMR (CHCl$_3$, 400 MHz): δ □ = 1.20 (t, 3H, 3), 1.44 (s, 6H, 1+1'), 2.48 (q, 2H, 2).
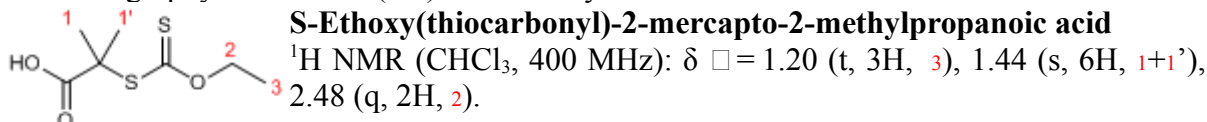
IV.2) PB macronomer synthesis and preparation

IV.2.a) 1,2-polybutadiene synthesis

Monomers and solvents were purified using conventional methods reported elsewhere in the literature.[187][188] All reactions were performed under a dry argon atmosphere. 1,2-PB(OH) was synthesized by anionic polymerization of 1,3-butadiene in tetrahydrofuran (THF) solution at -78 °C using sec-butyllithium (sBuLi) as the initiator. After 1 day, ethylene oxide was added, and the solution was stirred for 3 days at room temperature. The polymer was precipitated into methanol and dried under vacuum.

PB$_{80}$-OH

GPC (THF, PB): M$_n$=43000, PDI=1.07

96% 1,2-units

IV.2.b) α-(S-Ethoxy(thiocarbonyl)-2-mercapto-2-methylpropanoate) polybuta-1,2-diene (1,2-polybutadiene-macro CTA)

0.178 g of CTA and 95 µL oxalylchloride were dissolved in 5 mL of dry dichloromethane and stirred at room temperature for 3 hours. 1,0 g of poly(1,2-butadiene) was freeze-dried from toluene, redissolved in 10 mL of dry dichloromethane and added to the CTA/oxalylchloride solution. The solution was stirred at room temperature overnight. The end-functionalized polymer was purified by dialysis (MWCO 1000) in THF.
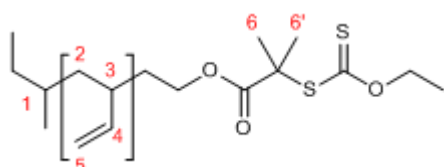
α-(S-Ethoxy(thiocarbonyl)-2-mercapto-2-methylpropanoate)-1,2-polybutadiene
^{1}H NMR (CHCl$_3$, 400 MHz): δ □= 0.7-0.9 (m, 1), 1.0-1.4 (m, 2), 1.38 (s, 6H, 6+6'), 1.9-2.3 (m, 3), 4.8-5.1 (m, 5), 5.2-5.6 (m, 4 and 1,4 substituted PB units).

IV.3) poly(1,2-butadiene)-*block*-poly(N-isopropylacrylamide)

1 eq of 1,2-polybutadiene-macro CTA, the appropriate equivalent amount of of N-isopropylacrylamide (NIPAM), and 0.1 eq of AIBN were dissolved at 5 wt% in dioxane. The solution was degassed by two freeze-thaw cycles and heated at 65 °C for 5 days after which the polymerization was terminated by rapid cooling of the reaction mixture. The polymer was purified by dialysis in THF (MWCO 1000). Left over PB homopolymer was removed by multiple extractions with hexane. The polymer was recovered as a white powder by freeze-drying.
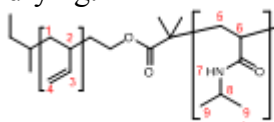
1,2-PB-*b*-PNIPAM$_m$
^{1}H NMR (CHCl$_3$,400 MHz,): δ □= 6,54 (bs, 7), 5.41 (m, 3 and 1,4 substituted PB units), 4.95 (m, 4), 4.02 (bs, 8), 2.25-1.46 (m, 1+2+5+6), 1.15 (m, 9+9').

IV.4) Glycosilation 1,2-PB-*b*-PNIPAM

IV.4.a) 1-thio-β-D-glucose tetraacetate functionalized 1,2-PB-*b*-PNIPAM

1,2-PB-*b*-PNIPAM copolymer and 1.5 eq of 1-thio-β-D-glucose tetraacetate were dissolved in freshly distilled THF at 3 wt %. The solution was degassed by two freeze-thaw cycles and placed under the UV-lamp for 24 h. Functionalized 1,2-PB-*b*-PNIPAM was purified by dialysis in THF (MWCO 1000).
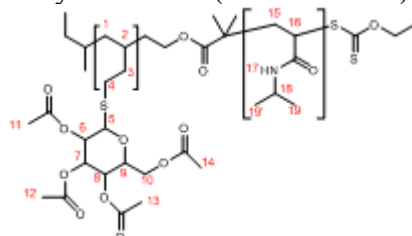
1,2-PB(GlcAc$_4$)-*b*-PNIPAM$_m$
^{1}H NMR (CHCl$_3$, 400 MHz): δ □=7.16-6.5 (m, 17), 5.35-3.78 (m, 5+ 10+ 9), 4.03 (bs, 18), 3.15-2.99 (m, 6+7+8), 2.09 (m, 11+12+13+14)2.73 (b, 4), 2.00-1.42 (m, 1+2+3+15+16), 1.05 (s, 19+19')

IV.4.b) Deacetylation

1-thio-β-D-glucose tetraacetate functionalized 1,2-PB-*b*-PNIPAM copolymer was dissolved

in chloroform (~ 100 mL·g⁻¹ polymer) and a 0.5 M NaOH solution in methanol (10 mL·g⁻¹ polymer) was added. The reaction mixture was stirred at room temperature for 48 hours after which the solvent was removed under reduced pressure and the product was redissolved in water. The pH of the solution was neutralized by addition of small amounts of 1 M HCl solution and the polymer was purified by dialysis in water (MWCO 1000).

1,2-PB(Glc)-*b*-PNIPAM$_m$
^{1}H NMR (DMSO-d$_6$, 400 MHz): δ □= 7.33-7.19 (m, 17), 4.92-3.45 (m, 11+12+13+ 14+ 5+ 10+ 9), 3.85 (bs, 18) 3.15-2.99 (m, 6+7+8), 2.73 (b, 4), 2.00-1.42 (m, 1+2+3+15+16), 1.05 (s, 19+19')

1,2-PB(Glc)-*b*-PNIPAM$_{259}$
dn/dc (25°C)= 0.1570 mL·g⁻¹
1,2-PB(Glc)-*b*-PNIPAM$_{557}$
dn/dc (25°C)= 0.1722 mL·g⁻¹
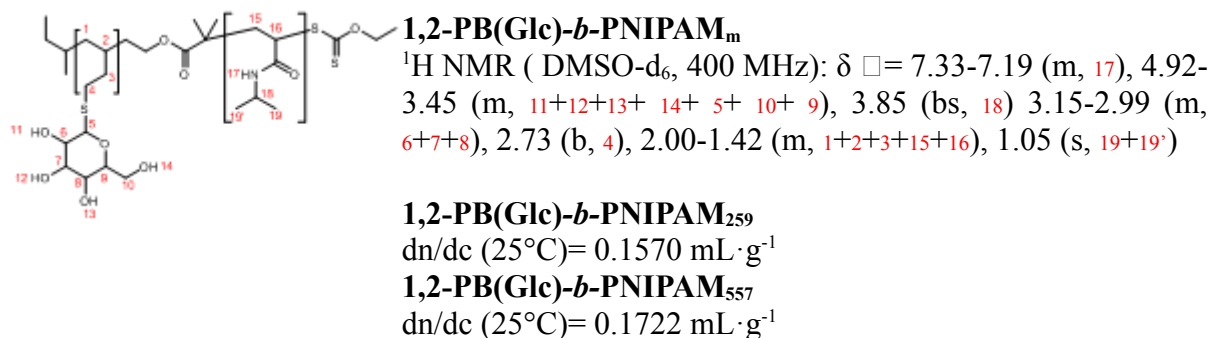
B. Analytical Instrumentation

FT-IR spectra were recorded on a BioRad 6000 FT-IR. Samples were measured in the solid state using a single reflection diamond ATR.

Elemental analysis (EA) was performed using a Vario EL Elemental Analyzer. The samples were analyzed for carbon, hydrogen and nitrogen content.

Turbidimetry was conducted on a turbidimetric photometer TP1 (Tepper Analytik, Wiesbaden) at a wavelength of 599 nm at a rate 1 °C·min⁻¹. Solutions were prepared by dissolving the polymer powder in milliQ water to afford 1 wt% solutions unless otherwise stated. Cloud points temperature (CP) were take at the 50% of the transmission drop by deriving the transmission as a function of temperature curve and identifying the minimum.

Light scattering (LS). Solutions were investigated by light scattering using ALV-7004 Multiple tau digital correlator equipped with CGS-3 Compact Goniometer system, 22 mW He-Ne laser (wavelength λ = 632.8 nm) and pair of avalanche photodiodes operated in a

pseudo-cross-correlation mode. Solution were prepared in milliQ water and filtered through 0,45 μm PVDF or 0,7 μm glass serynge filters. For **dynamic light scattering (DLS)** unless otherwise stated the measurements were made at a 90° angle and the measured intensity correlation function $g^2(t)$ was analyzed using the algorithm REPES[149] performing the inverse Laplace transformation according to Equation 11.

$$g^2(t) = 1 + \beta \left[\int A(t) \exp(-t/\tau) dt \right]^2 = 1 + \beta \left[\sum_{i=1}^{n} A_i \exp(-t/\tau_i) \right]^2 \qquad (11)$$

(where t is the delay time of the correlation function and β an instrumental parameter) and yielding distribution $A(\tau)$ of relaxation times τ. The relaxation time τ is related to the diffusion coefficient D and relaxation (decay) rate Γ by the relation in Equation 12.

$$\Gamma = \frac{1}{\tau} = Dq^2 \qquad (12)$$

where q is the scattering vector defined as q = $(4\pi n/\lambda)\sin(\theta/2)$ where n is the refractive index of the solvent and θ is the scattering angle. The hydrodynamic radius R_h of the particles can be calculated from the diffusion coefficient using the Stokes-Einstein equation 13.

$$D = \frac{k_B T}{6 \Pi \eta R_h} \qquad (13)$$

where T is absolute temperature, η the viscosity of the solvent and k_B the Boltzmann constant. **Static light scattering** was recorded in the same setup by in the angle range 30°-150° with 10° steps. Acquisition of the intensity was performed for 10 seconds with 3 consecutive runs for each angle and the intensity corrected with respect to the scattering of the solvent and toluene bath. Only measurements for which the intensity fluctuation within the 3 runs was <5% were considered. The data was plotted by means of the software ALVStat

4.48.

¹H Nuclear Magnetic Resonance (NMR) spectra were recorded at room temperature on a Bruker DPX-400 Spectrometer operating at 400.1 MHz. Calibration was carried out using signals corresponding to non-deuterated solvent traces ($CDCl_3$: 7.26 ppm; DMSO-d_6: 2.50 ppm).

¹H-¹H 2D NOESY NMR. 2D-NOESY measurements were performed on a Varian VNMRS 600 spectrometer operating at 600 MHz

Density were carried out on a density meter DMA 5000 (Anton Paar, Germany) at 25 °C. The specific density of the bulk polymer was extrapolated from the density data measured for a particular solvent and a polymer solution in that solvent of known cocentration.

Confocal laser scanning microcopy (CLSM) of the polymer vesicles were recorded with a Leica system mounted to a Leica Aristoplan and equipped with a 100xoil immersion objective with a numerical aperture of 1.4 working on simultaneous transmission and fluorescence mode.

Fluorescence correlation spectroscopy (FCS) measurements were performed at room temperature in special chambered quartz glass holders (Lab-Tek; 8-well, NUNC A/S), on a Zeiss LSM 510-META/Confcor2 laser-scanning microscope equipped with an Argon2-laser (488 nm) and a 40× water-immersion objective (Zeiss C/Apochromat 40X, NA 1.2), with pinhole adjusted to 70 μm. Spectra were recorded over 30 s, and each measurement was repeated 10 times. Excitation power of the Ar laser was PL =15 mW, and the excitation transmission at 488 nm was 5%. Diffusion times for free dye-labeled protein (FITC-ConA) was independently determined and fixed in the fitting procedure. The results were presented as a mean value of three independent measurements. The fluorescence signal was measured in real time and the autocorrelation function was calculated by a software correlator (LSM 510 META - ConfoCor 2 System). For the fitting of the autocorrelation function according to

a two component model, the following equation 14 was used:

$$G'(\tau)=1+\frac{1}{N}\left[(1-\gamma)\left(\frac{1}{1+\frac{\tau}{\tau_{D1}}}\right)\left(\frac{1}{1+\frac{\tau}{S^2\tau_{D1}}}\right)^{\left(\frac{1}{2}\right)}+\gamma\left(\frac{1}{1+\frac{\tau}{\tau_{D2}}}\right)\left(\frac{1}{1+\frac{\tau}{S^2\tau_{D2}}}\right)^{\left(\frac{1}{2}\right)}+f(T)\right] \quad (14)$$

Where N is the number of fluorescent particles, S the structural parameter determined to be 5, τ_{D1} the diffusion time of the component 1 in the assay, 1-γ the fraction of particles with diffusion time τ_{D1}, τ_{D2} the diffusion time of component 2 in the assy, γ the fraction of particles with diffusion time τ_{D2} and f(T) the funtion used for the fitting of the triplet characteristics τ_T and % τ_T of the fluorescent label within the assay. By means of an iterative least-square method, the values calculated by the algorithm are compared repeatedly to the experimentally generated autocorrelation curve and approximated until the difference between the two curves is minimized.

Raman. For Raman spectroscopy, a 532 nm Nd:YAG laser (WITec, Ulm, Germany) beam was focused down to a micrometer size spot on the sample through a confocal Raman microscope (CRM300, WITec, Ulm, Germany) equipped with piezo-scanner (P-500, Physik Instrumente, Karlsruhe, Germany). The spectra were acquired using an air-cooled CCD detector (DU401-BV, Andor, Belfast, UK) behind a grating (600 g·mm^{-1}) spectrograph (UHTS 300, WITec, Ulm, Germany). The ScanCtrlSpectroscopyPlus (version 2.02, Witec) was used for measurement setup and data processing.

Surface-enhanced Raman Spectroscopy (SERS) experiments were carried out in the same setup as the Raman but an excess of colloidal gold (Sigma-Aldrich) of 20 nm or 5 nm was added to the samples prior to measurement.

Differential refractrometer NFT-Scanref was used to determine the refractive index increment dn/dc in a thermostated cell at 25 °C.

Transmission electron microscopy (TEM) was performed with a Zeiss EM 912 Omega microscope operating at 120 kV. Samples were prepared by drop cast on carbon-coated copper grids. For negatively stained microgrphs, samples prepared by drop casting were subsenquently treated with a 2% uranyl acetate solution in water, washed with water and dried.

Appendix II.   Supporting experimental data

Paragraph 3.1.2.a
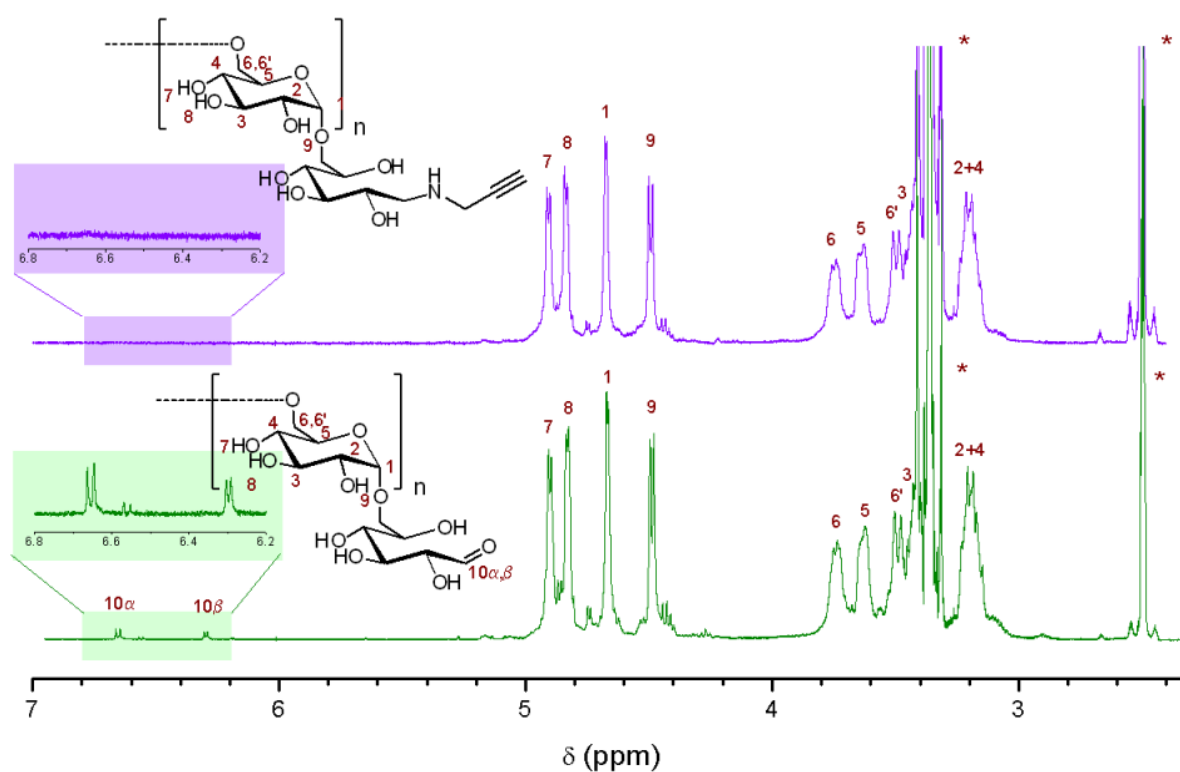
Figure II.1: ^{1}H NMR of native dextran (below) and α-alkyne-dextran (above) showing the total disappearance of the anomeric protons.

Paragraph 3.1.6.a

- dex$_{6500}$-*b*-PEG$_{1900}$

a) Dynamic light scattering
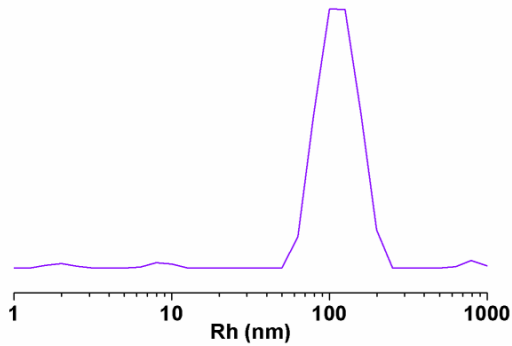
R_h=117 ±18 nm

Figure II.2: Intensity-weighted distribution of the hydrodynamic radius of the DL scattering at 90 ° for a dex$_{6500}$-b-PEG$_{1900}$

b) Static light scattering
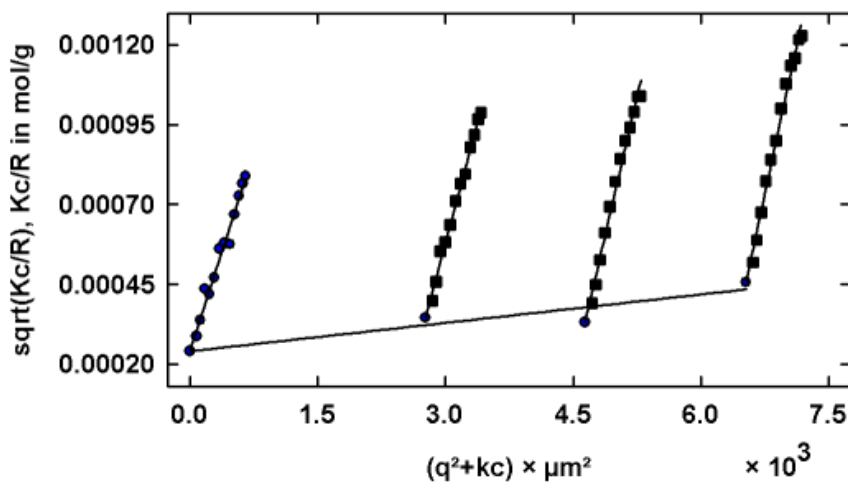
M_w= 1,73·10^7 g·mol^{-1}

R_g= 144 nm

A_2=1.08·10^{-8} mol·dm^3·g^{-2}

Figure II.3: Berry plot of the SLS data obtained between 40° and 150° at room temperature for dex$_{6500}$-b-PEG$_{1900}$ polymer solutions.

• dex$_{6500}$-b-PEG$_{13200}$

a) Dynamic light scattering

$D_z(q^2)=1.52\ \mu m^2.s^{-1}\ \pm3\%$

$R_h =164$ nm
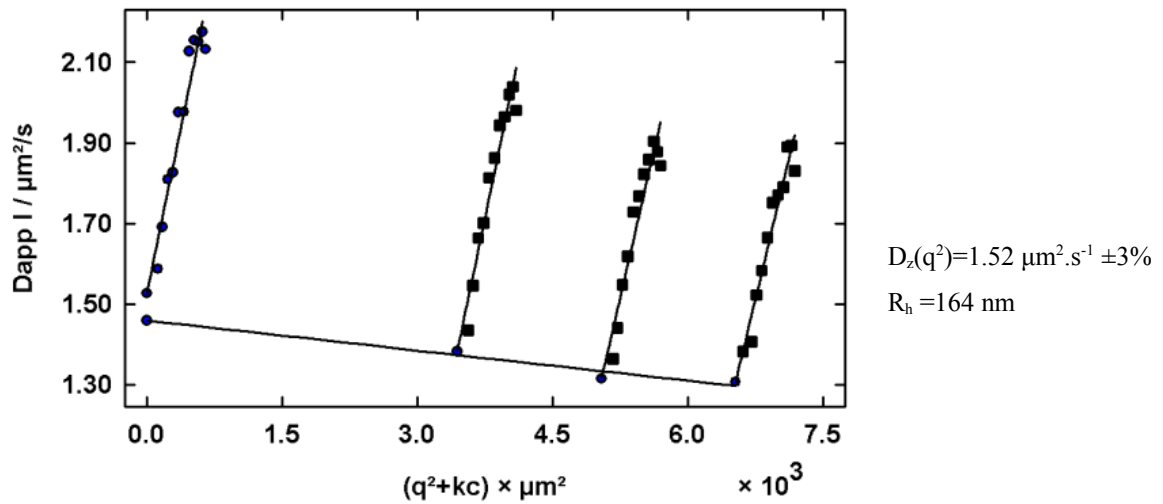
Figure II.4: Dynamic Zimm plot of the DLS recorded between 30 ° and 150 °.

b) Static light scattering

$M_w (q^2)= 4.20\cdot10^6\ g\cdot mol^{-1}$

$R_g= 134$ nm

$A_2=4.27\cdot10^{-9}\ mol.dm^3.g^{-2}$
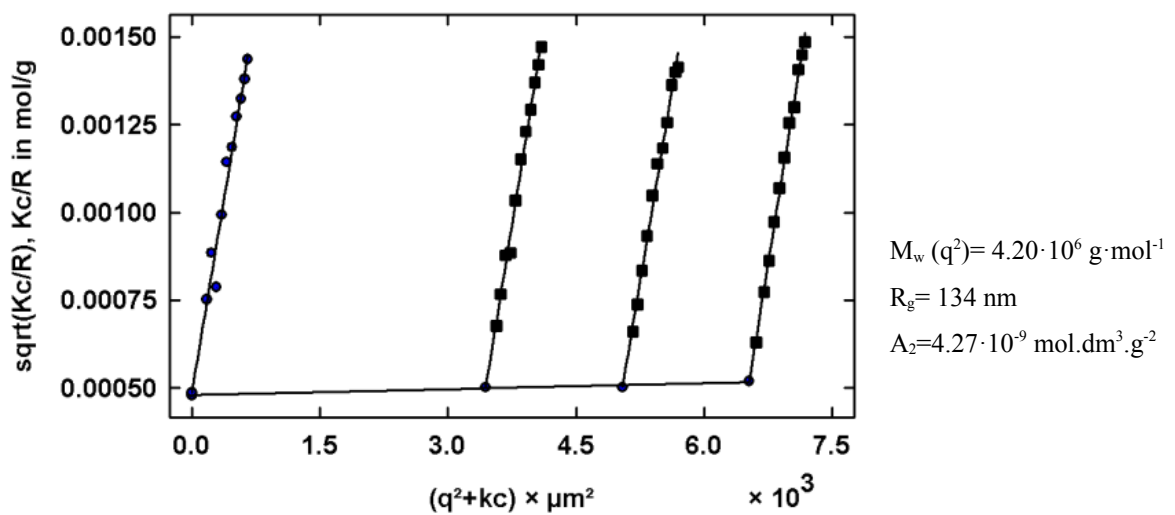
Figure II.5: Berry plot of the SLS data obtained between 40° and 150° at room temperature for dex$_{6500}$-b-PEG$_{13200}$ polymer solutions.

- dex$_{11000}$-*b*-PEG$_{5500}$

a) Dynamic light scattering
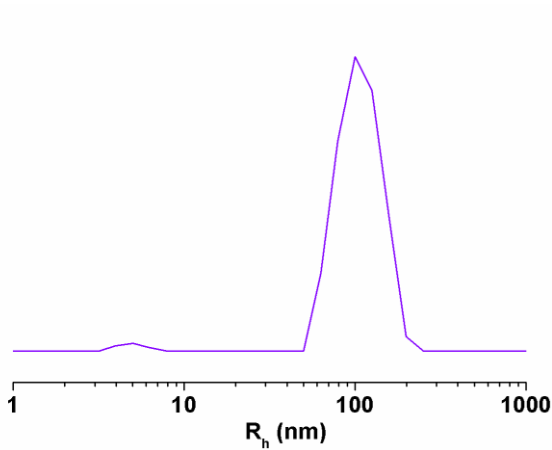
R_h=119 ±18 nm

Figure II.6: Intensity-weighted distribution of the hydrodynamic radius of the DL scattering at 90 ° for a dex$_{11000}$-b-PEG$_{5500}$

b) Static light scattering
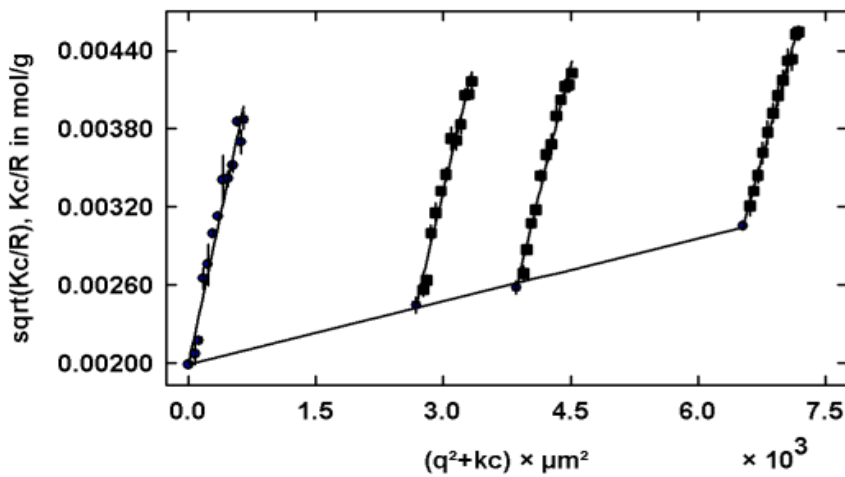
M_w= 2,53·10^5 g·mol^{-1}

R_g= 96 nm

A_2=4,35·10^{-7} mol·dm^3·g^{-2}

Figure II.7: Berry plot of the SLS data obtained between 40° and 150° at room temperature for dex$_{11000}$-b-PEG$_{5500}$ polymer solutions.

Paragraph 3.2.2.b

- dex-*b*-PNIPAM$_6$: Static light scattering
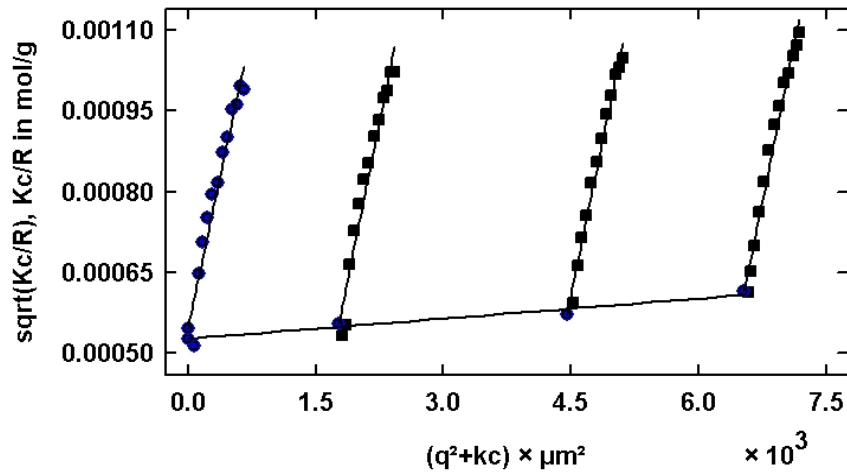
$M_w= 3,59 \cdot 10^6$ g·mol^{-1}

$R_g= 90$ nm

$A_2=9,26 \cdot 10^{-9}$ mol·dm^3·g^{-2}

Figure II.8: Berry plot of the SLS data obtained between 40° and 150° at room temperature for dex-*b*-PNIPAM$_6$ polymer solutions.

- dex-*b*-PNIPAM$_{16}$: Static light scattering
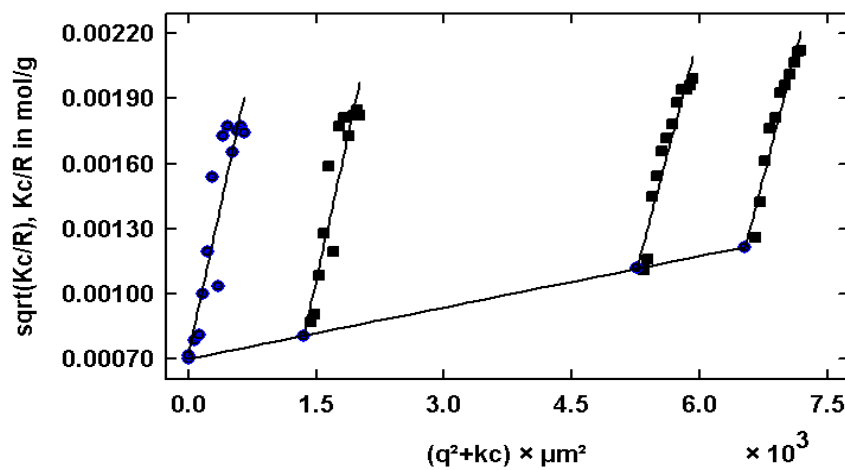
$M_w= 1,94 \cdot 10^6$ g·mol^{-1}

$R_g= 123$ nm

$A_2=8,46 \cdot 10^{-8}$ mol·dm^3·g^{-2}

Figure II.9: Berry plot of the SLS data obtained between 40° and 150° at room temperature for dex-*b*-PNIPAM$_{16}$ polymer solutions.

- dex-*b*-PNIPAM$_{51}$: Static light scattering

$M_w = 3{,}55 \cdot 10^6$ g·mol^{-1}

$R_g = 135$ nm

$A_2 = 5{,}80 \cdot 10^{-8}$ mol·dm^3·g^{-2}
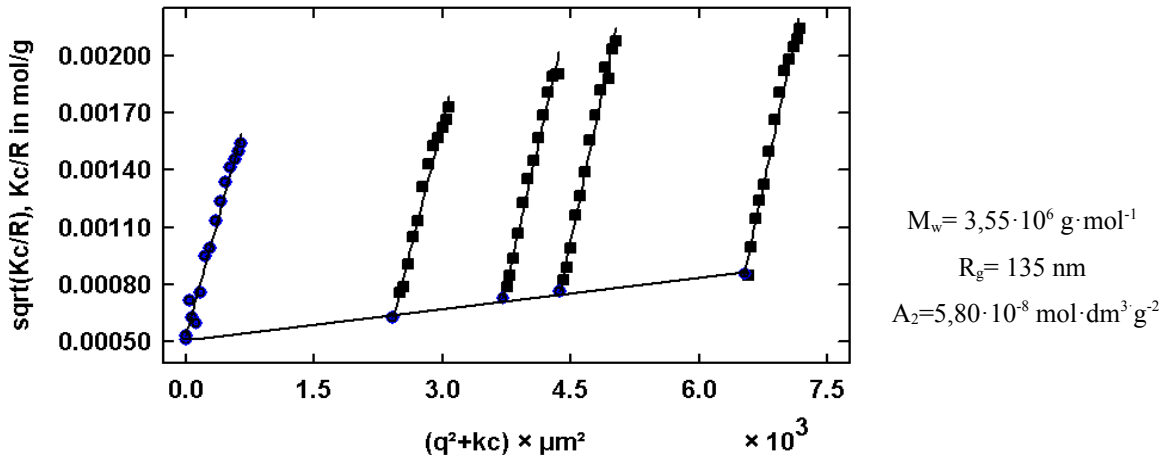
Figure II.10: Berry plot of the SLS data obtained between 40° and 150° at room temperature for dex-*b*-PNIPAM$_{51}$ polymer solutions.

Paragraph 4.2

- PB$_{80}$(Glc)-b-PNIPAM$_{557}$: Static light scattering

Mw= $1.163 \cdot 10^8$ g.mol^{-1} ±3.34%

$R_g = 128$ nm
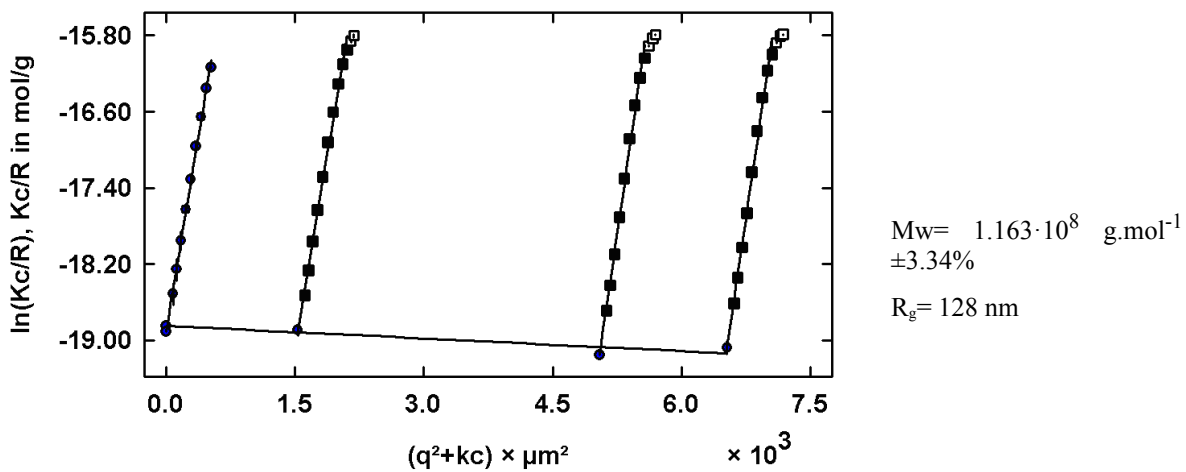
Figure II.11: Guinier plot of the SLS data obtained between 40° and 150° at room temperature for PB$_{80}$(Glc)-b-PNIPAM$_{557}$ polymer solutions.

- PB$_{80}$(Glc)-b-PNIPAM$_{557}$: TEM
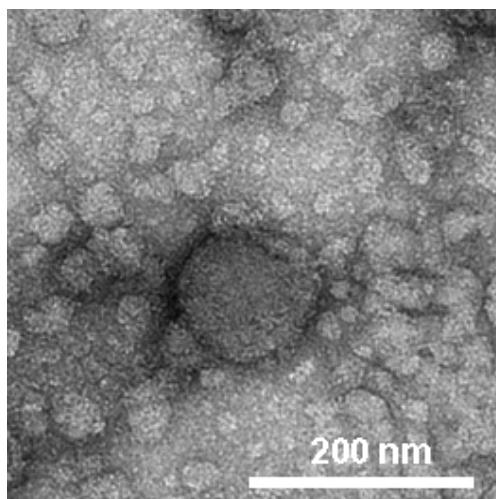
Figure II.12: TEM images of a 1 wt% solution of PB$_{80}$(Glc)-b-PNIPAM$_{557}$. TEM grid prepared by drop casting and stained with uranyl acetate.

Paragraph 4.4.1

- PB$_{80}$(Glc)-b-PNIPAM$_{259}$: Fluorescence correlation spectroscopy
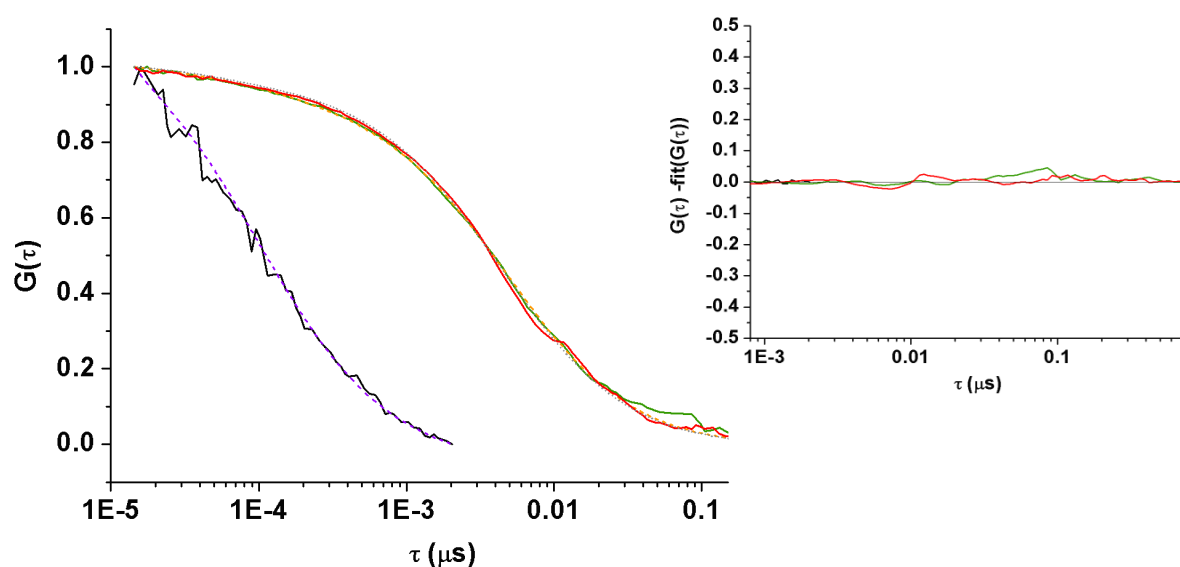
Figure II.13: (*Left*) Normalized autocorrelation of fluctuation of the fluorescence intensity and its fittings: in black (violet fitting) FITC-ConA in HBS solution; in green (orange fitting) PB$_{80}$(Glc)-b-PNIPAM$_{259}$ with FITC-ConA in HBS solution after 2 h; in red (gray fitting) PB$_{80}$(Glc)-b-PNIPAM$_{259}$ with FITC-ConA in HBS solution after 22 h. (*Right*) Residuals of the fitting: in green PB$_{80}$(Glc)-b-PNIPAM$_{259}$ with FITC-ConA in HBS solution after 2 h; in red PB$_{80}$(Glc)-b-PNIPAM$_{259}$ with FITC-ConA in HBS solution after 22 h.

Table II.1: Data extracted from the analysis in the FCS experiments.

Sample	CR (kHz)	CPM (kHz)	N	Fraction 1		Fraction 2	
				%	$\tau_D(\mu s)$	%	$\tau_D(\mu s)$
FITC-ConA	17.3	13.3	1.3	96	110	-	-
PB$_{80}$(Glc)-b-PNIPAM$_{259}$ + FITC-ConA after 2h	30.9	12.1	3	10	110	90	5500
PB$_{80}$(Glc)-b-PNIPAM$_{259}$ + FITC-ConA after 22h	27.5	20.4	1.4	1	110	99	4700

Appendix III. Review on the self-assembly of DHBCs in water

The classical view on amphiphilic self-assembly in which a typical surfactant with hydrophilic head and hydrophobic tails self-assembles above a critical concentration into well-define monodisperse micelles has long been insufficient to describe the behavior of more complex systems e.g. copolymers. Although the behavior of an amphiphile block copolymer constituted of a hydrophobic non-soluble block and a hydrophilic soluble block in water follows a similar pattern, the wider range of parameters that polymers allow to tune (chemical composition, block lengths, architecture, specific interactions, polydispersity…) gives raise to much more complex phenomena. Association of blocks copolymers in non-selective solvent outside stimulus are included in this list of systems without a low-molecular weight equivalent and this rare phenomenon lacks of a solid bibliography account that could give a good general picture of the phenomenon.

The most studied case is the association of PEG-*b*-PNIPAM or PNIPAM-g-PEG copolymers. At least six publications report the presence of aggregation below the LCST of poly(isopropylacrylamide).[54][213]-[217] The explanations for this unexpected large aggregates vary. Motokawa *et al.*[214] reported an onset temperature of the decrease in the ratio I_1/I_3 on the emission spectra of pyrene in the presence of PEG-*b*-PNIPAM copolymers at 16 °C to 28 °C depending on the concentration but always far below the LCST (Figure III.1.a)). The phase diagram (Figure III.1.b)) of the block copolymer in water could show the existence of two different transparent sol regions, (I) corresponding to the non solubilization of pyrene in the

core ("neutral solvent state") and one that the authors attribute to a "selective solvent state" (II) but still below the collapsed regions (cloud point) (III), (IV) and (V) . The authors suggest that in this region (II) the PEG chains are more swollen with water than the PNIPAM chains, and such asymmetrically swollen state might be responsible for this decrease in I_1/I_3. In other words, the difference in the solubilization of the two blocks may lead to the formation of less hydrated regions in associates that could stabilized the excitation state of pyrene thus rising the quantum yield of the fluorescence. In those terms "selective solvent state" might not be the most accurate description, as it is rather a non-selective but yet preferential solvation state.
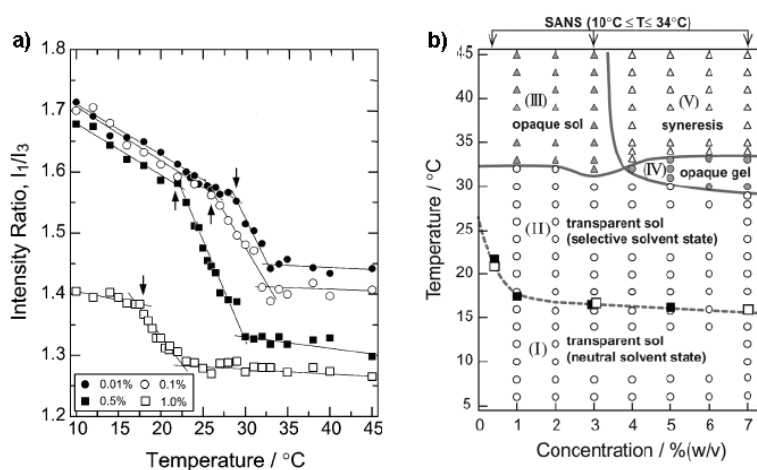
Figure III.1: (a) Changes in the ratio of intensities (I1/I3) of the vibrational bands in the fluorescence spectrum as a function of temperature for various concentration of mPEG114-*b*-PNIPAM228. Lines are guides for the eyes. (b) Phase diagram of mPEG114-*b*-PNIPAM228 observed in water. (I) and (II): transparent sol; (III): opaque sol; (IV): opaque gel; (V): syneresis; region (VI): transparent gel. Adapted from [2].

Complementarely by a light scattering study, Yan *et al.*[215] proposed an illustration for the temperature behavior of a PEG$_{44}$-*b*-PNIPAM$_{95}$ copolymer that makes the difference between an associated state, an aggregated state and a micellar state (Figure III.2). The region (I) in Motokawa's work correspond to the associated state described by Yan. In that state $R_{g,app}$ was larger than $R_{h,app}$, which could be consistent with a loose aggregate with a very hydrated shell.

Tenhu, H. *et al.*[213] attributed it in PNIPAM-*g*-PEG systems to an interchain association leading to the formation of clusters. Nedelcheva et *al.*[216] rationalized the phenomenon by the assumption that PNIPAM, which is quite hydrophobic at ambient temperature forms

hydrophobic domains stabilized by the more hydrophilic PEG. Whatever the driving for the association and its thermodynamic characteristics might be, two patterns seem to influence it. First Topp *et al.*[217] detected this association only for block copolymers with a $M_{n,PNIPAM}/M_{n,PEG}$ ratio exceeding 1/3. Secondly, Berlinova *et al.*[54] stated that the propensity of the copolymers for aggregation increased with a decrease of the molecular weight of both thermosensitive and PEG blocks. This two findings show the importance of the balance between the two blocks and suggest that the driving force for the association might be a difference of behavior in water e.g. solubility difference, which would be in accordance with Motokawa's model.
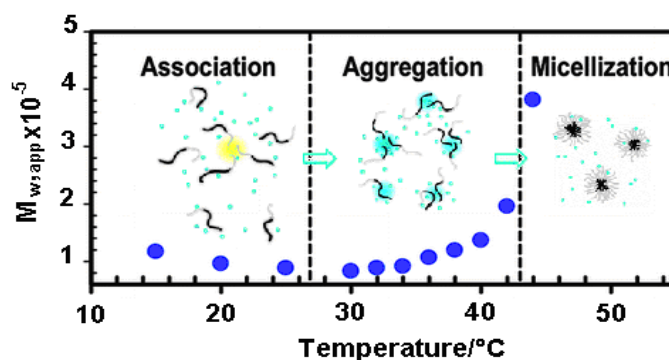
Figure III.2: Temperature dependence of the average apparent molecular weight (Mw,app) of PEO44-*b*-PNIPAm95 at 0.1 mg/mL and illustration of the three different stages, associated, aggregated and micellar. Adapted from [3].

A similar behavior was detected by Huang *et al.*[218] in poly(ethylene glycol)-*block*-poly-trans-N-(2-ethoxy-1,3-dioxan-5-yl)acrylamide (PEG-*b*-PtNEA) block copolymers. Below LCST, the polymer showed a bimodal distribution in DLS indicating the occurrence of association. The PtNEA block was held responsible for this association as the authors reported its association below LCST even as homopolymer. It was qualitatively stated by the appreciation of the scattered intensity that the weight percentage of these associates was very small when compared to the single chains.

Non-stimuli responsive polymers have also been found to be able to forms aggregates. The most prominent work on it was carried out and published recently by Ke *et al.*[169], where they focused on the study of the loose aggregates formed in water by a poly(ethylene glycol)-

block-poly(N,N-dimethylacrylamide) (PEO-*b*-PDMA) copolymer. This aggregates showed weak concentration and temperature dependence as well as opposite salt effect and were in equilibrium with the unimers. The study of these aggregates in different conditions (additives,..) led the authors to the conclusion that the driving force for the association was the incompatibility between the two blocks, mainly caused by their different capacity to interact with water.
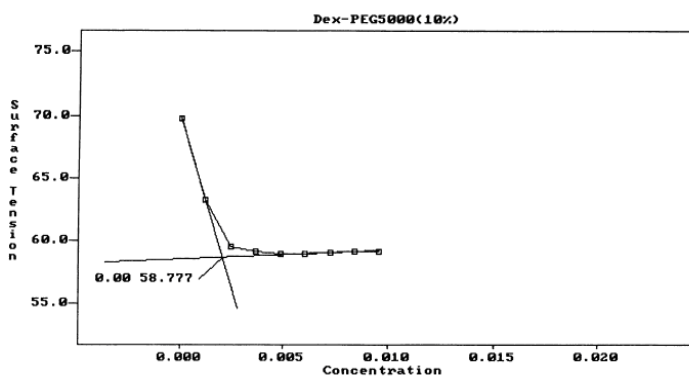
Figure III.3: Surface tension of a solution of PEG(10%)-dextran as a function of the concentration. Reproduced from [12]

Previously some publications on the synthesis of biocompatible and biodegradable polymers had reported a similar behavior for two other poly(ethylene glycol)-based graft and block copolymers. De Marre and coworkers[219] synthetised a Poly(ethylene glycol)-*block*-poly[N-hydroxyethyl-L-glutamine) copolymer (PEG-*b*-PHEG) . Emulsification studies and DSC analysis showed the phase separation occurred at in solution and in the solid state. J.M. Duval *et al.*[220] reported the synthesis and characterization of dextran-*graft*-poly(ethylene glycol) copolymers (dex-*g*-PEG). The authors claimed to obtain amphiphilic polymers that due to incompatible structures undergo phase separation at the molecular level. This was proven by GPC where the copolymer was eluted in the void volume indicating high molecular weight species, probably aggregates. Shortly after K. Hoste *et al.*[221] confirmed this findings and reported the trapping of free PEG inside the core of the aggregates. It was later rationalized[176] that as PEG is soluble in water and organic solvents, both systems dex-*g*-PEG and PEG-*b*-PHEG may act tensioactives and form aggregates with the "more" hydrophilic polymer in the outer shell and the "less" hydrophilic PEG as the core. A critical concentration aggregation could be determined for every system in the range from 1.0 to 3.5 mg·L^{-1} (Figure III.3) showing that even at low concentration stable aggregates

spontaneously form.

Non-amphiphilic self-assembly has already been studied in semi-dilute/concentrated solution when referred to liquid crystal phases and water-in-water emulsions of liquid crystals. The group of Luk[222] first studied a water-in.water emulsion consisting of dispersed droplets of water-soluble liquid crystal disodium cromoglycate (DSCG) (.Figure III.4.a)) in a continuous phase of water-soluble polymers (Figure III.4.1)).
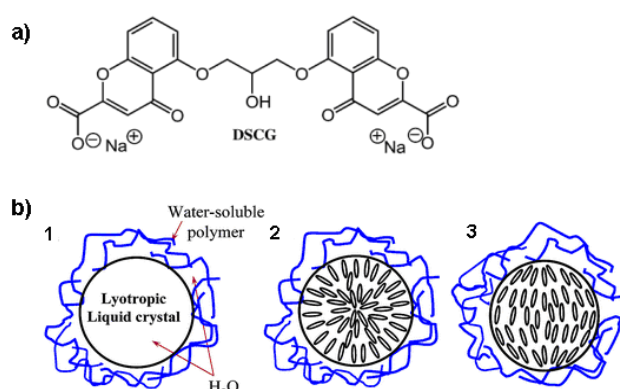
Figure III.4: a) Disodium cromoglycate (DSCG) b.1) Model of emulsions of water-solvated liquid crystal (LC) droplets stabilized from coalescence by the adsorption of polymers in a continuous aqueous medium. Two possible droplet configurations: b.2) radial configuration in b.3) tangential configuration. Reproduced from [13].

Depending on the polymer in the continous phase, the droplets can be spherical and the LC adopt a radial configuration in which they are aligned perpendicular to the interface (Figure III.4.b.2)), or be ellipsoidal and the LC adopt a tangential configuration in which they align parallel to the interface (Figure III.4.b.3)) which suggests a direct interaction between the polymer's functional groups and the LC molecules. The same group later reported[223] the nonamphipilic assembly in water of the so-called chromonic liquid crystal phases. These water-soluble aromatic molecules self-assemble above 11 wt% in thread-like structures rather than molecular stacks (as the usual amphiphilic LC) and are very sensitive to small variations in the structural details. Interestingly, the mixing of these molecules with slightly different structure in water can result in a macro-phase separation, each phase solvating one type of LC molecule. This thermodynamic incompatibility is surprising but supports the model of threads of molecules acting as a pair of incompatible polymers.

Also in concentrated solution, Taubert *et al.*[211] reported the mesophases formed by a DHBC of poly(ethylene glycol)-*block*-poly(2-methyl oxazoline) (PEG-*b*-PMOXA) in water. Below 55% wt of polymer the polymer solution is isotropic but above that concentration two mesophases can be formed (Figure III.5.a)): one presumably hexagonal (H1) and a lamellar one (Lα). This implies the existence of distinct water domains separated only by hydrophilic copolymers. The authors explained the phase separation in terms of incompatibility between the two blocks, that would microphase-separate and give raise two those water-rich domains (Figure III.5.b)).
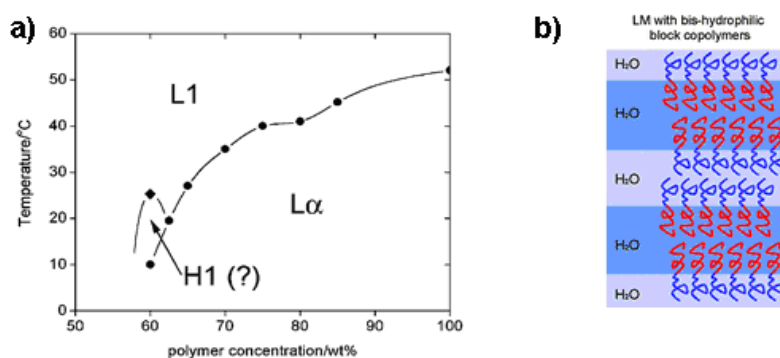
Figure III.5: a) Phase diagram of PEG-*b*-PMOXA in water showing three regions. Lα lamellar LM. L1 isotropic. H1 presumably hexagonal. b) Schematic representation of a water-in-water LM where the separation between water layers is due to the phase separation of the block copolymer. Reproduced from [15].

The formation of associates, aggregates, and mesophases in non-selective solvent does not appear exclusively in water. Several examples are available in organic media. The most prominent and studied ones are the formation of aggregates in toluene of polystyrene-*b*-poly(methyl methacrylate) and poly(ethylene glycol)-*b*-poly(methyl methacrylate) copolymers. Strategieszielle *et al.*[224] studied the dynamic of a of polystyrene-*b*-poly(methyl methacrylate) (PS-*b*-PMMA) diblock copolymer in toluene and reported the apparition of a slow mode above c*. The frequency of this mode was very low and decreased with increasing copolymer concentration. It was attributed to the formation of aggregates. Similarly, poly(ethylene glycol)-poly(methyl methacrylate) diblock copolymers (PEG-*b*-PMMA).in toluene and other organic solvents have been found to form aggregates.[225][226] Often mistaken by a classic self-assembly in selective solvent,[226] these polymers show bimodal distribution by dynamic light scattering in toluene. The deviations

from the hard-sphere model suggested that the aggregates responsible for the slow mode were not compact but rather loosely packed, globular structures formed by strongly fluctuating chains.[225]

Appendix IV.   Nomenclature

ΔGm	Gibbs free energy change of mixing
ΔHm	Enthalpy of mixing
ΔSm	Entropy of mixing
χ$_{AB}$	Polymer-Polymer interaction parameter
χ$_{AS}$	Polymer-Solvent interaction parameter
χ$_{eff}$	Effective interaction parameter
φ	Volume concentration
ρ	Packing parameter
ρ-ratio	R_g/R_h
ATPS	Aqueous two-phase system
ATRP	Atom transfer radical polymerization
C	C-parameter as in $D_{app}=D_z\cdot(1+C\cdot R_g)$
CONTIN	Constrained regularization algorithm[150]
CP	Cloud point
CRD	Carbohydrate-recognition domain
CTA	Chain transfer agent
CuAAC	Copper-catalyzed azide-alkyne cycloaddition

DCM	Dichloromethane
DHBC	Double hydrophilic block copolymer
DMF	Dimethylformamide
DMSO	Dimethyl sulfoxide
DNA	Deoxyribonucleic acid
EA	Elemental analysis
ƒ	Volume fraction
FCS	Fluorescence correlation spectroscopy
FITC	Fluorescein isothiocyanate
FITC-ConA	Fluorescein isothiocyanate-labeled Concavalin A
Glc	D-Glucose
GPC	Gel permeation chromatography
GV	Giant vesicle
HBS	(4-(2-hydroxyethyl)-1-piperazineethanesulfonic acid) saline buffer
LCST	Lower critical solution temperature
MADIX	Macromolecular design *via* interchange of xanthanes
M$_n$	Number average molecular weight
M$_w$	Weight average molecular weight
MWCO	Molecular weight cut-off
N	Degree of polymerization
NCA	N-Carboxyanhydride
NMP	N-methylpyrrolidone
NMR	Nuclear magnetic resonance spectroscopy
NOESY	Nuclear Overhauser Enhancement Spectroscopy

ODT	Order-disorder transition
OOT	Order-order transition
P(q)	Form Factor
PB	Polybutadiene
PEG	Poly(ethylene glycol)
PDI	Polydispersity index
PNIPAM	Poly(N-isopropylacrylamide)
PPG	Poly(propylene glycol)
PVAc	Poly(vinyl acetate)
PVOH	Poly(vinyl alcohol)
PVP	Poly(vinyl pyrrolidone)
RAFT	Reversible addition-fragmentation chain transfer
REPES	Regularized positive exponential sum algorithm[149]
R_g	Radius of gyration
R_h	Hydrodynamic radius
RNA	Ribonucleic acid
RT	Room temperature
SANS	Small-angle neutron scattering
SAXS	Small-angle X-ray scattering
SERS	Surface-enhanced Raman spectroscopy
SLS	Static light scattering
SSL	Strong segregation limit
SSSL	Super strong segregation limit
TEA	Triethylamine
TEM	Transmission electron microscopy

THF	Tetrahydrofuran
_p_-TsCl	_para_-Toluenesulfonyl chloride
UCST	Upper critical solution temperature
UV	Ultraviolet
VOC	Volatile organic compound
WSL	Weak segregation limit

Appendix V.   Selected Analytical Methods

A.   Light scattering

The light scattering[191] phenomenon happens when an incident light beam interacts with the charges constituting a given molecule and remodel the spatial charge distribution. The molecule acts then as a oscillating dipole and emits in all directions an electromagnetic wave of same wavelength as the incident one (elastic scattering).

For molecules or particles larger than 20 nm, several oscillating dipoles are created simultaneously. The interference of the simultaneously emitted scattered waves is characteristic for the size and shape of the scattering particle.

I. Static light scattering

Static light scattering (SLS) is a technique used to determine the mass, size and shape of particles. In experiments the intensity $I(\theta)$ of the elastically scattered light is measured at different angles with respect to the incident beam. The ratio of the scattered light intensity $I(\theta)$ over the incident beam intensity I_0 is given by equation (15).

$$\frac{I(\theta)}{I_0} = \frac{16\pi^2\alpha^2}{\lambda_0^4 r^2}$$

(15)

where α is the polarizability of the molecule, λ_0 the vacuum wavelength of the incident beam

and r is the distance between the sample and the detector. Debye related the scattered light intensity to the osmotic pressure by considering that additional scattering results from local fluctuation of the concentration (equation (16)).

$$\frac{Kc}{R(\theta)} = \frac{1}{RT}\left(\frac{\partial \Pi}{\partial c}\right)_T \tag{16}$$

where R(θ) is the Rayleigh ratio, Π is the osmotic pressure, c is the concentration, R the ideal gaz constant, T the temperature and K an optical constant given by equation (17).

$$K = \frac{4\pi^2}{\lambda_0^4 N_A} n_0^2 \left(\frac{\partial n}{\partial c}\right)^2 \tag{17}$$

with n_0 the refractive index of the solvent, N_A Avogadro's number and n the refractive index of the sample.

By extending the osmotic module into a power series (equation (18)), equation (16) can be expressed as equation (19).

$$\left(\frac{\partial \Pi}{\partial c}\right) = RT\left(\frac{1}{M_w} + 2A_2 c + 3A_3 c + \dots\right) \tag{18}$$

where M_w is the weight-averaged molar molecular mass and A_x virial coefficients.

$$\frac{Kc}{R(\theta)} = \frac{1}{M_w} + 2A_2 c + \dots \tag{19}$$

For particles of diameter above $\lambda/20$ nm, the interference pattern of intraparticular scattered light has to be taken into account as the scattering becomes sensitive to the particle's anisotropy. The dependence is expressed in the Mie theory as the angle dependent form factor $P(q)$ (equation (20)) and the expression of the Rayleigh ratio is expressed as in

equation (22).

$$P(q) = 1 - \frac{1}{3}\langle R_g^2 \rangle q^2 + \dots \tag{20}$$

with q the module of the scattering vector $\vec{q}$ (difference of the scattered and incident wave vectors)

$$q = \frac{4\pi}{\lambda_0} n_0 \sin\left(\frac{\theta}{2}\right) \tag{21}$$

$$\frac{Kc}{R(\theta)} = \frac{1}{M_w} + \frac{1}{P(\theta)} + 2A_2 c = \frac{1}{M_w}\left(1 + \frac{q^2\langle R_g^2 \rangle}{3}\right) + 2A_2 c \tag{22}$$

Equation (22) is used for data evaluation of the static light scattering in the form of a Zimm plot. $Kc/\Delta R(\theta)$ is plotted against $q^2 + kc$ (k is an arbitrary constant) for a series of concentrations and angles. The extrapolation to 0 concentration and 0 q allows the determination of M_w, A_2 and $\langle R_g \rangle$. When the scattering intensity does not depend on the angle linearly for a given concentration, which is the case for particles of diameter over 50 nm, alternative plots can be build. For example, Guinier's approximation plots the logarithm of the scattered intensity *vs.* q^2 and the Berry plot plots the square root of the scattered intensity *vs.* q^2.

Static light scattering can also be used to study the morphology of particles *via* the fitting of the form factor with known models. Widely used plots are Holtzer's that plots the z-averaged form factor $P_z(u) \cdot q$ *vs* q or Kratky's that plots the $P_z(u) \cdot q^2$ *vs* q and that is typically used to analyze the conformation of proteins.

II. Dynamic light scattering

If static light scattering averages the scattered intensity, dynamic light scattering (DLS) studies its fluctuations over time. The intensity fluctuates because the change in the interparticle position as a result of Brownian motion changes the interference pattern. Correlation of the intensities I at time intervals τ can be expressed by a normalized intensity autocorrelation function (equation (23)).

$$g_2(q,\tau) = \frac{\langle I(t)I(t+\tau)\rangle}{\langle I(q,\tau)^2\rangle} \tag{23}$$

The dynamic structure factor $g_1(q,\tau)$ can be derived *via* the Siegert relation (equation (24)).

$$g_1(q,\tau) = \sqrt{g_2(q,\tau)-1} \tag{24}$$

For diluted monodisperse particle samples with $qR_g<1$, $g_1(t)$ can be expressed as a single exponential (equation (21)).

$$g_1(q,\tau) = \exp(D_t q^2 \tau) \tag{25}$$

where D_t is the translational diffusion coefficient. For particle with $qR_g>1$ the $g_1(t)$ function has a multiexponential decay and can be expressed as a sum of several single exponentials weighted by different diffusion coefficients (equation (26)).

$$g_1(q,\tau) = \langle \exp(-\Gamma\tau)\rangle = \int_0^\infty \exp(-\Gamma\tau)G(\Gamma).d\Gamma \tag{26}$$

where $\Gamma = D_{app}(q) \cdot q^2$. In dilute solution, when the interparticular interactions can be neglected,

the hydrodynamic radius of particles can be obtained from the Stokes-Einstein equation (equation (25)).

$$R_h = \frac{kT}{6\pi\eta D}$$

(27)

Data analysis of the dynamic light scattering can be performed with different mathematical approaches. The simplest method is the fitting of the first order autocorrelation function $g_1(q,\tau)$ with a single exponential decay but it is only valid for monodisperse samples (situation in equation (21)). Other methods are more sophisticated and adapted to the study of polydisperse samples. Two examples are the cumulant method where the experimental data points are fitted to a polynomial series expansions and the nonnegatively least square method which calculates a histogram of the particle size by minimizing an expression.

A very popular method is the one based on the CONTIN algorithm, that delivers a solution of the Laplace inverse of $g_1(q,\tau)$. Similarly to CONTIN, the REPES algorithm also solves the Laplace inverse of $g_1(q,\tau)$ but avoids certain artifacts and is therefore more adapted than CONTIN for the study of polydisperse samples. Both these analyses deliver the intensity-weighted size distribution of the samples.

B.   Fluorescence correlation spectroscopy

Fluorescence correlation spectroscopy[227] (FCS) is a correlation analysis of the fluorescence intensity fluctuations. Similarly to DLS, the intensity fluctuations are the result of the Brownian motion of the fluorescent particles, in other words the number of the particles in the sub-space defined by the optical system is randomly changing around the average number. Correlation of the intensities I at time intervals τ can be expressed by a normalized intensity autocorrelation function $G(\tau)$ (equation (28)).

$$G(\tau) = \frac{\langle \delta I(t)\delta I(t+\tau)\rangle}{\langle I(t)\rangle^2} = \frac{\langle I(t)I(t+\tau)\rangle}{\langle I(t)\rangle^2} - 1$$

(28)

where δI(t) is the deviation from the mean intensity.

The analysis of this function gives the average number of fluorescent particles and average diffusion time, when the particle is passing through the confocal volume. Eventually, both the concentration and size of the particle are determined. The most common method for the data analysis is the use of a nonlinear least square algorithm to fit the expression of the autocorrelation curve expressed without baseline G'(τ).

For a unique monodisperse population G'(τ) has the form expressed in equation (29).

$$G'(t) = \frac{1}{N} \frac{1}{\left(1+\dfrac{t}{\tau_D}\right)\sqrt{1+\dfrac{t}{S^2\tau_D}}} \tag{29}$$

where N is the average number of fluorescents present at any given moment in the focal volume, τ_D is the average diffusion time of a single fluorescent and S is the structural parameter of the focal volume.

Multiple monodisperse populations can be simultaneously detected when the autocorrelation time is fitted with the general form of G'(τ) (equation (30)).

$$G'(t) = \frac{1}{N} \sum_{i=1}^{n} \frac{F_i}{\left(1+\dfrac{t}{\tau_{Di}}\right)\sqrt{1+\dfrac{t}{S^2\tau_{Di}}}} \tag{30}$$

with F_i the fraction of number of fluorescents of the *i*-th population (N_i/N).

From the diffusion time τ_D the diffusion coefficient D can be calculated and this can later be related to the hydrodynamic radius of the molecule/particle *via* the Stokes-Einstein (equation (25)).

Appendix VI.   Bibliography

[1]   A. Napoli, D. Sebök, A. Senti, W. Meier, in *Block Copolymers in Nanoscience*, Wiley-vch Verlag Gmbh & Co. Kgaa, **2008**.

[2]   H. Schlaad, L. You, R. Sigel, B. Smarsly, M. Heydenreich, A. Mantion, A. Masic, *Chemical Communications* **2009**, 1478-1480.

[3]   M. E. Silva, T. T. Franco, *Brazilian Journal of Chemical Engineering* **2000**, *17*, 1-17.

[4]   R. Hatti-Kaul, *Molecular Biotechnology* **2001**, *19*, 269-277.

[5]   R. Hatti-Kaul, in *Aqueous Two-Phase Systems: Methods and Protocols*, **2000**, pp. 1-10.

[6]   J. Benavides, O. Aguilar, B. Lapizco-Encinas, M. Rito-Palomares, *Chemical Engineering & Technology* **2008**, *31*, 838-845.

[7]   B. Y. Zaslavsky, *Aqueous Two-Phase Partitioning : Physical Chemistry and Bioanalytical Applications*, C R C Press Llc, **1994**.

[8]   P. G. Mazzola, A. M. Lopes, F. A. Hasmann, A. F. Jozala, T. C. Penna, P. O. Magalhaes, C. O. Rangel-Yagui, A. Pessoa Jr, *Journal of Chemical Technology & Biotechnology* **2008**, *83*, 143-157.

[9]   A. D. Diamond, J. T. Hsu, *Biotechnology Techniques* **1989**, *3*, 119-124.

[10]   S. B. Zimmerman, A. P. Minton, *Annual Review of Biophysics and Biomolecular Structure* **1993**, *22*, 27-65.

[11]   S. B. Zimmerman, S. O. Trach, *Journal of Molecular Biology* **1991**, *222*, 599-620.

[12]   H. M. R. Brij M. Mitruka, *Clinical Biochemical and Hematological Reference Values in Normal Experimental Animals and Normal Humans*, Masson Pub. Usa, New York, **1981**.

[13]   R. J. Ellis, *Trends in Biochemical Sciences* **2001**, *26*, 597-604.

[14]   R. J. Ellis, *Current Opinion in Structural Biology* **2001**, *11*, 114-119.

[15]   D. S. Goodsell, *The Machinery of Life*, Springer, New York, **1993**.

[16]   K. Sasahara, P. McPhie, A. P. Minton, *Journal of Molecular Biology* **2003**, *326*, 1227-1237.

[17]   S. L. Flaugh, K. J. Lumb, *Biomacromolecules* **2001**, *2*, 538-540.

[18]   J. Ovádi, V. Saks, *Molecular and Cellular Biochemistry* **2004**, *256-257*, 5-12.

[19]   J. S. Clegg, *American Journal of Physiology: Regulatory, Integrative and Comparative Physiology* **1984**, *246*, R133-151.

[20]   K. R. Porter, M. C. Beckerle, M. A. McNiven, in *Modern Cell Biology*, Alan R. Liss Inc., New York, **1983**, pp. 259-302.

[21]   N. D. Gershon, K. R. Porter, B. L. Trus, *Proceedings of the National Academy of Sciences of the United States of America* **1985**, *82*, 5030-5034.

[22]   M. Al-Habori, *The International Journal of Biochemistry & Cell Biology* **1995**, *27*, 123-132.

[23]   M. E. Campanella, H. Chu, P. S. Low, *Proceedings of the National Academy of Sciences of the United States of America* **2005**, *102*, 2402-2407.

[24]   H. Walter, *International Review of Cytology* **1999**, *192*, 331-343.

[25]   G. J. Pielak, *Proceedings of the National Academy of Sciences of the United States of America* **2005**, *102*, 5901-5902.

[26]   M. S. Long, C. D. Jones, M. R. Helfrich, L. K. Mangeney-Slavin, C. D. Keating, *Proceedings of the National Academy of Sciences of the United States of America* **2005**, *102*, 5920-5925.

[27]   Y. Li, Phase Separation in Giant Vesicles, phD Thesis, Potsdam Universität, **2008**.

[28]   M. Stamm, D. W. Schubert, *Annual Review of Materials Science* **1995**, *25*, 325-356.

[29]   S. Förster, T. Plantenberg, *Angewandte Chemie International Edition* **2002**, *41*, 688-714.

[30]   M. W. Matsen, F. S. Bates, *Macromolecules* **1996**, *29*, 1091-1098.

[31]   F. S. Bates, G. H. Fredrickson, *Annual Review of Physical Chemistry* **1990**, *41*, 525-557.

[32]   L. Leibler, *Macromolecules* **1980**, *13*, 1602-1617.

[33]   I. A. Nyrkova, A. R. Khokhlov, M. Doi, *Macromolecules* **1993**, *26*, 3601-3610.

[34]   V. V. Vasilevskaya, L. A. Gusev, A. R. Khokhlov, O. Ikkala, G. ten Brinke, *Macromolecules* **2001**, *34*, 5019-5022.

[35]   Y. Li, X. Wang, I. C. Sanchez, K. P. Johnston, P. F. Green, *The Journal of Physical Chemistry B* **2006**, *111*, 16-25.

[36]   J. H. Kenneth, P. L. Timothy, *Journal of Polymer Science Part B: Polymer Physics* **1998**, *36*, 3101-3113.

[37]   C. Tanford, *Science* **1978**, *200*, 1012-1018.

[38]   G. H. Findenegg, *Berichte der Bunsengesellschaft für physikalische Chemie* **1986**, *90*, 1241-1242.

[39]   D. A. Hajduk, M. B. Kossuth, M. A. Hillmyer, F. S. Bates, *The Journal of Physical Chemistry B* **1998**, *102*, 4269-4276.

[40]   M. Lazzari, G. Liu, S. Lecommandoux, *Block Copolymers in Nanoscience*, Wiley, **2006**.

[41]   D. Schmaljohann, *Advanced Drug Delivery Reviews* **2006**, *58*, 1655-1670.

[42]   C. de las H. Alarcon, S. Pennadam, C. Alexander, *Chemical Society Reviews* **2005**, *34*, 276-285.

[43]   P. Bawa, V. Pillay, Y. Choonara, L. du Toit, *Biomedical materials* **2009**, *4*, 022001.

[44]   J. Rodríguez-Hernández, F. Chécot, Y. Gnanou, S. Lecommandoux, *Progress in Polymer Science* **2005**, *30*, 691-724.

[45]   V. Aseyev, S. Hietala, A. Laukkanen, M. Nuopponen, O. Confortini, F. E. Du Prez, H. Tenhu, *Polymer* **2005**, *46*, 7118-7131.

[46]   R. Koningsveld, L. A. Kleintjens, H. M. Schoffeleers, *Pure and Applied Chemistry* **1974**, *39*, 1-35.

[47]   S. B. Allin, in *Polymer Science and Technology* (Ed.: J.R. Fried), American Chemical Society, **2004**, p. 809.

[48]   S. Saeki, N. Kuwahara, S. Konno, M. Kaneko, *Macromolecules* **1973**, *6*, 246-250.

[49]   C. Wohlfarth, in *Polymers, Polymer Solutions, Physical Properties and Their Relations 1:Thermodynamic Properties andPhase Equilibria*, Springer-verlag Berlin Heidelberg, **2009**.

[50]   R. Liu, M. Fraylich, B. Saunders, *Colloid & Polymer Science* **2009**, *287*, 627-643.

[51]   J.-F. Lutz, Ã. Akdemir, A. Hoth, *Journal of the American Chemical Society* **2006**, *128*, 13046-13047.

[52]   M. Almgren, W. Brown, S. Hvidt, *Colloid & Polymer Science* **1995**, *273*, 2-15.

[53]   G. Wanka, H. Hoffmann, W. Ulbricht, *Colloid & Polymer Science* **1990**, *268*, 101-117.

[54]   I. Berlinova, N. Iliev, P. Vladimirov, C. Novakov, *Journal of Polymer Science Part A: Polymer Chemistry* **2007**, *45*, 4720-4732.

[55]   M. Prabaharan, J. J. Grailer, D. A. Steeber, S. Gong, *Macromolecular Bioscience* **2009**, *9*, 744-753.

[56]   N. Hadjichristidis, M. Pitsikalis, H. Iatrou, G. Sakellariou, in *Controlled and Living Polymerizations: From Mechanisms to Applications*, Wiley-vch Verlag Gmbh & Co. Kgaa, **2010**.

[57]   C. Tsitsilianis, in *Controlled and Living Polymerizations: From Mechanisms to Applications*, Wiley-vch Verlag Gmbh & Co. Kgaa, **2010**.

[58]   N. Hadjichristidis, H. Iatrou, M. Pitsikalis, G. Sakellariou, *Chemical Reviews* **2009**.

[59]   H. Leuchs, W. Manasse, *Berichte der Deutschen Chemischen Gesellschaft* **1907**, *40*, 3235-3249.

[60]   R. Wilder, S. Mobashery, *The Journal of Organic Chemistry* **1992**, *57*, 2755-2756.

[61]   D. S. Poche, M. J. Moore, J. L. Bowles, *Synthetic Communications* **1999**, *29*, 843 - 854.

[62]   J. R. Kramer, T. J. Deming, *Biomacromolecules* **2010**, *11*, 3668-3672.

[63]   I. Dimitrov, H. Schlaad, *Chemical Communications* **2003**, 2944-2945.

[64]   T. J. Deming, *Nature* **1997**, *390*, 386-389.

[65]   T. Aliferis, H. Iatrou, N. Hadjichristidis, *Biomacromolecules* **2004**, *5*, 1653-1656.

[66]   K. Matyjaszewski, in *Controlled and Living Polymerizations: From Mechanisms to Applications*, Wiley-vch Verlag Gmbh & Co. Kgaa, **2010**.

[67]   J.-S. Wang, K. Matyjaszewski, *Journal of the American Chemical Society* **1995**, *117*, 5614-5615.

[68]   T. E. Patten, K. Matyjaszewski, *Advanced Materials* **1998**, *10*, 901-915.

[69]   R. J. Spontak, S. D. Smith, *Journal of Polymer Science Part B: Polymer Physics* **2001**, *39*, 947-955.

[70]   G. Moad, E. Rizzardo, S. H. Thang, *Polymer* **2008**, *49*, 1079-1131.

[71]   E. Rizzardo, J. Chiefari, R. Mayadunne, G. Moad, S. Thang, *Macromolecular Symposia* **2001**, *174*, 209-212.

[72]   J.-F. Lutz, H. Schlaad, *Polymer* **2008**, *49*, 817-824.

[73]   C. K. Hartmuth, M. G. Finn, K. B. Sharpless, *Angewandte Chemie International Edition* **2001**, *40*, 2004-2021.

[74]   J.-F. Lutz, *Angewandte Chemie International Edition* **2007**, *46*, 1018-1025.

[75]   A. Dondoni, *Angewandte Chemie International Edition* **2008**, *47*, 8995-8997.

[76]   C. E. Hoyle, T. Y. Lee, T. Roper, *Journal of Polymer Science Part A: Polymer Chemistry* **2004**, *42*, 5301-5338.

[77]   C. E. Hoyle, A. B. Lowe, C. N. Bowman, *Chemical Society Reviews* **2010**, *39*, 1355-1387.

[78]   R. M. Hensarling, V. A. Doughty, J. W. Chan, D. L. Patton, *Journal of the American Chemical Society* **2009**, *131*, 14673-14675.

[79]   B. D. Fairbanks, T. F. Scott, C. J. Kloxin, K. S. Anseth, C. N. Bowman, *Macromolecules* **2008**, *42*, 211-217.

[80]   J. A. Opsteen, J. C. M. van Hest, *Chemical Communications* **2005**, 57-59.

[81]   H. B. Wolfgang, S. Robert, *Macromolecular Rapid Communications* **2007**, *28*, 15-54.

[82]   H. B. Wolfgang, S. Robert, *Macromolecular Rapid Communications* **2008**, *29*, 952-981.

[83]   M. Morten, *Macromolecular Rapid Communications* **2008**, *29*, 1016-1051.

[84]   C. Barner-Kowollik, F. E. Du Prez, P. Espeel, C. J. Hawker, T. Junkers, H. Schlaad, W. Van Camp, *Angewandte Chemie International Edition* **2011**, *50*, 60-62.

[85]   M. Arthur, *Journal für Praktische Chemie* **1893**, *48*, 94-95.

[86]   R. Huisgen, *Angewandte Chemie International Edition* **1963**, *2*, 633-645.

[87]   R. Huisgen, *Angewandte Chemie International Edition* **1963**, *2*, 565-598.

[88]   C. W. Tornøe, C. Christensen, M. Meldal, *The Journal of Organic Chemistry* **2002**, *67*, 3057-3064.

[89]   M. Meldal, C. W. Tornøe, *Chemical Reviews* **2008**, *108*, 2952-3015.

[90]   V. R. Vsevolod, G. G. Luke, V. F. Valery, K. B. Sharpless, *Angewandte Chemie International Edition* **2002**, *41*, 2596-2599.

[91]   V. D. Bock, D. Speijer, H. Hiemstra, J. H. van Maarseveen, *Organic & Biomolecular Chemistry* **2007**, *5*, 971-975.

[92]   Y. L. Angell, K. Burgess, *Chemical Society Reviews* **2007**, *36*, 1674-1689.

[93]   J. P. Roland, T. S. R. Dirk, M. J. L. Rob, *QSAR & Combinatorial Science* **2007**, *26*, 1181-1190.

[94]   F. Amblard, J. H. Cho, R. F. Schinazi, *Chemical Reviews* **2009**, *109*, 4207-4220.

[95]   B. Le Droumaguet, K. Velonia, *Macromolecular Rapid Communications* **2008**, *29*, 1073-1089.

[96]   S. Dedola, S. A. Nepogodiev, R. A. Field, *Organic & Biomolecular Chemistry* **2007**, *5*, 1006-1017.

[97]   D. B. Aaron, L. K. Kristi, *Peptide Science* **2009**, *94*, 128-140.

[98]   R. Gruškienė, G. Čiuta, R. Makuška, *Chemija* **2009**, *20*, 241-249.

[99]   C. Schatz, S. Louguet, J.-F. Le Meins, S. Lecommandoux, *Angewandte Chemie International Edition* **2009**, *48*, 2572-2575.

[100] B. Mareike, G. Nina, R. Helmut, *Macromolecular Chemistry and Physics* **2008**, *209*, 25-31.

[101] P. Appukkuttan, W. Dehaen, V. V. Fokin, E. Van der Eycken, *Organic Letters* **2004**, *6*, 4223-4225.

[102] D. T. S. Rijkers, G. W. van Esse, R. Merkx, A. J. Brouwer, H. J. F. Jacobs, R. J. Pieters, R. M. J. Liskamp, *Chemical Communications* **2005**, *36*, 4581-4583.

[103] C. Bouillon, A. Meyer, S. Vidal, A. Jochum, Y. Chevolot, J.-P. Cloarec, J.-P. Praly, J.-J. Vasseur, F. Morvan, *The Journal of Organic Chemistry* **2006**, *71*, 4700-4702.

[104] T. Posner, *Berichte der deutschen chemischen Gesellschaft* **1905**, *38*, 646-657.

[105] A. B. Lowe, *Polymer Chemistry* **2010**, *1*, 17-36.

[106] B. Holmberg, *Berichte der deutschen chemischen Gesellschaft (A and B Series)* **1932**, *65*, 1349-1354.

[107] G. E. Serniuk, F. W. Banes, M. W. Swaney, *Journal of the American Chemical Society* **1948**, *70*, 1804-1808.

[108] K. L. Killops, L. M. Campos, C. J. Hawker, *Journal of the American Chemical Society* **2008**, *130*, 5062-5064.

[109] L. M. Campos, K. L. Killops, R. Sakai, J. M. J. Paulusse, D. Damiron, E. Drockenmuller, B. W. Messmore, C. J. Hawker, *Macromolecules* **2008**, *41*, 7063-7070.

[110] L. Herczynska, L. Lestel, S. Boileau, J. Chojnowski, S. Polowinski, *European Polymer Journal* **1999**, *35*, 1115-1122.

[111] U. Gorski, E. Klemm, *Die Angewandte Makromolekulare Chemie* **1995**, *224*, 125-131.

[112] F. Ciardelli, M. Aglietto, E. Passaglia, F. Picchioni, *Polymers for Advanced Technologies* **2000**, *11*, 371-376.

[113] F. Romani, E. Passaglia, M. Aglietto, G. Ruggeri, *Macromolecular Chemistry and Physics* **1999**, *200*, 524-530.

[114] J. Justynska, Z. Hordyjewicz, H. Schlaad, *Macromolecular Symposia* **2006**, *240*, 41-46.

[115] J. Justynska, H. Schlaad, *Macromolecular Rapid Communications* **2004**, *25*, 1478-1481.

[116] Y. Geng, D. E. Discher, J. Justynska, H. Schlaad, *Angewandte Chemie International Edition* **2006**, *45*, 7578-7581.

[117] N. ten Brummelhuis, C. Diehl, H. Schlaad, *Macromolecules* **2008**, *41*, 9946-9947.

[118] L. You, H. Schlaad, *Journal of the American Chemical Society* **2006**, *128*, 13336-13337.

[119] Z. Hordyjewicz-Baran, L. You, B. Smarsly, R. Sigel, H. Schlaad, *Macromolecules* **2007**, *40*, 3901-3903.

[120] J. Justynska, Z. Hordyjewicz, H. Schlaad, *Polymer* **2005**, *46*, 12057-12064.

[121] A. Gress, A. Voelkel, H. Schlaad, *Macromolecules* **2007**, *40*, 7928-7933.

[122] H. Cabezas, *Journal of Chromatography B: Biomedical Sciences and Applications* **1996**, *680*, 3-30.

[123] P. A. Pessôa Filho, R. S. Mohamed, *Process Biochemistry* **2004**, *39*, 2075-2083.

[124] R. J. H. Stenekes, O. Franssen, E. M. G. van Bommel, D. J. A. Crommelin, W. E. Hennink, *International Journal of Pharmaceutics* **1999**, *183*, 29-32.

[125] S. Kavlak, H. K. Can, A. Güner, *Journal of Applied Polymer Science* **2004**, *94*, 453-460.

[126] R. L. Scott, *The Journal of Chemical Physics* **1949**, *17*, 268-279.

[127] H. Tompa, *Polymer Solutions*, Academic Press, New York, **1956**.

[128] A. E. Nesterov, I. S. Lipatov, *Thermodynamics of Polymer Blends, Volume I*, Crc Pr Inc, **1997**.

[129] A. Robard, D. Patterson, G. Delmas, *Macromolecules* **1977**, *10*, 706-708.

[130] C. Tanford, *The Hydrophobic Effect: Formation of Micelles and Biological Membranes*, John Wiley & Sons, New York, **1973**.

[131] M. Naessens, A. Cerdobbel, W. Soetaert, E. J. Vandamme, *Journal of Chemical Technology & Biotechnology* **2005**, *80*, 845-860.

[132] L. H. Derek, H. Boualem, R. K. Steven, *Journal of Polymer Science Part B: Polymer*

Physics **2003**, *41*, 135-138.

[133] S. Han, B. Jhun, *Archives of Pharmacal Research* **1984**, *7*, 1-9.

[134] E. I. Fedin, V. G. Tsitsishvili, V. Y. Grinberg, T. I. Bakari, V. B. Tolstoguzov, *Carbohydrate Research* **1975**, *39*, 193-199.

[135] P. Cernoch, H. Schlaad, H. Coelfen, *submitted* **2011**.

[136] É. Kalutskaya, *Chemistry of Natural Compounds* **1990**, *26*, 621-625-625.

[137] K.-J. Liu, J. L. Parsons, *Macromolecules* **1969**, *2*, 529-533.

[138] V. Mank, I. Solomentseva, A. Baran, O. Kurilenko, *Ukrainian Chemistry Journal* **1974**, *40*, 1035.

[139] H. Yoshioka, *The Journal of Physical Chemistry* **1978**, *82*, 2736-2739.

[140] C. Branca, S. Magazù, G. Maisano, F. Migliardo, P. Migliardo, G. Romeo, *The Journal of Physical Chemistry B* **2002**, *106*, 10272-10276.

[141] R. Kjellander, E. Florin, *Journal of the Chemical Society, Faraday Transactions 1: Physical Chemistry in Condensed Phases* **1981**, *77*, 2053-2077.

[142] K. Serap, C. Hatice Kaplan, G. Ali, *Journal of Applied Polymer Science* **2004**, *94*, 453-460.

[143] M. Hillmyer, *Current Opinion in Solid State and Materials Science* **1999**, *4*, 559-564.

[144] R. F. Borch, M. D. Bernstein, H. D. Durst, *Journal of the American Chemical Society* **1971**, *93*, 2897-2904.

[145] S. L. Ng, P.-Y. Yang, K. Y. T. Chen, R. Srinivasan, S. Q. Yao, *Organic & Biomolecular Chemistry* **2008**, *6*, 844-847.

[146] D. Quemener, T. P. Davis, C. Barner-Kowollik, M. H. Stenzel, *Chemical Communications* **2006**, 5051-5053.

[147] T. Zhang, R. E. Marchant, *Macromolecules* **1994**, *27*, 7302-7308.

[148] O. S. Hernandez, G. M. Soliman, F. M. Winnik, *Polymer* **2007**, *48*, 921-930.

[149] J. Jakeš, *Collection of Czechoslovak Chemical Communications* **1995**, *60*, 1781-1797.

[150] S. W. Provencher, *Computer Physics Communications* **1982**, *27*, 213-227.

[151] R. Sigel, M. Łosik, H. Schlaad, *Langmuir* **2007**, *23*, 7196-7199.

[152] W. Burchard, M. Schmidt, W. H. Stockmayer, *Macromolecules* **1980**, *13*, 1265-1272.

[153] Y. Zhang, F. Wu, W. Yuan, T. Jin, *Journal of Controlled Release* **2010**, *147*, 413-419.

[154] Cheng, T. Hui, Megha undefined London, , and , Erwin, *The Journal of Biological Chemistry* **2009**, *284*, 6079-6092.

[155] E. Le Ru, P. Etchegoin, *Principles of Surface-Enhanced Raman Spectroscopy and Related Plasmonic Effects*, Elsevier, **2008**.

[156] D. Lide, *CRC Handbook of Chemistry and Physics, 88th Edition (Crc Handbook of Chemistry and Physics)*, Crc, **2007**.

[157] Z. Lu, J. Goebl, J. Ge, Y. Yin, *Journal of Materials Chemistry* **2009**, *19*, 4597-4602.

[158] R. G. Zhbankov, S. P. Firsov, E. V. Korolik, P. T. Petrov, M. P. Lapkovski, V. M. Tsarenkov, M. K. Marchewka, H. Ratajczak, *Journal of Molecular Structure* **2000**, *555*, 85-96.

[159] H. Matsuura, T. Miyazawa, *Journal of Polymer Science Part A-2: Polymer Physics* **1969**, *7*, 1735-1744.

[160] J. L. Koenig, *Journal of Polymer Science: Macromolecular Reviews* **1972**, *6*, 59-177.

[161] J. L. Koenig, A. C. Angood, *Journal of Polymer Science Part A-2: Polymer Physics* **1970**, *8*, 1787-1796.

[162] E. Sabadini, T. Cosgrove, F. do C. Egídio, *Carbohydrate Research* **2006**, *341*, 270-

274.

[163] L. Whistler Roy, in *Carbohydrates in Solution*, American Chemical Society, **1973**, pp. 242-255.

[164] M. R. Gittings, L. Cipelletti, V. Trappe, D. A. Weitz, M. In, C. Marques, *The Journal of Physical Chemistry B* **2000**, *104*, 4381-4386.

[165] G. Battaglia, A. J. Ryan, *Journal of the American Chemical Society* **2005**, *127*, 8757-8764.

[166] B. M. Discher, Y.-Y. Won, D. S. Ege, J. C. M. Lee, F. S. Bates, D. E. Discher, D. A. Hammer, *Science* **1999**, *284*, 1143-1146.

[167] L. J. M. Vagberg, K. A. Cogan, A. P. Gast, *Macromolecules* **1991**, *24*, 1670-1677.

[168] F. Szoka, D. Papahadjopoulos, *Annual Review of Biophysics and Bioengineering* **1980**, *9*, 467-508.

[169] F. Ke, X. Mo, R. Yang, Y. Wang, D. Liang, *Macromolecules* **2009**, *42*, 5339-5344.

[170] W. Zhang, L. Shi, K. Wu, Y. An, *Macromolecules* **2005**, *38*, 5743-5747.

[171] S. Koizumi, H. Hasegawa, T. Hashimoto, *Makromolekulare Chemie. Macromolecular Symposia* **1992**, *62*, 75-91.

[172] G. W. Gokel, K. Arnold, T. Cleary, R. Friese, V. Gatto, D. Goli, Hanlon C. undefined Kim M. undefined Miller S. undefined Ouchi M. undefined Posey I. undefined Sandler A. undefined Viscariello A. undefined White B. undefined Wolfe J. undefined , and undefined Yoo H.in *Phase-Transfer Catalysis*, American Chemical Society, **2011**, pp. 24-37, .

[173] P. George, A. Cameron, *Angewandte Chemie International Edition* **2008**, *47*, 4847-4850.

[174] P.-A. Albertsson, *Partition of Cell Particles and Macromolecules*, Wiley, New York, **1986**.

[175] M. Destarac, D. Taton, S. Z. Zard, T. Saleh, Y. Six, in *Advances in Controlled/Living Radical Polymerization*, American Chemical Society, **2011**, pp. 536-550.

[176] E. H. Schacht, K. Hoste, in *Poly(ethylene Glycol)* (Ed.: S.Z. J. Milton Harris), American Chemical Society, **1997**, pp. 297-315.

[177] A. De Marre, H. Soyez, E. Schacht, J. Pytela, *Polymer* **1994**, *35*, 2443-2446.

[178] G. Bokias, I. Iliopoulos, D. Hourdet, G. Staikos, *Trends in Colloid and Interface Science XV* **2001**, *118*, 48.

[179] H. Friedrich, P. M. Frederik, G. de With, N. A. J. M. Sommerdijk, *Angewandte Chemie International Edition* **2010**, *49*, 7850-7858.

[180] Z. Li, Y.-H. Kim, H. Min, C.-K. Han, K. Huh, *Macromolecular Research* **2010**, *18*, 618-621-621.

[181] NIST Center for Neutron Research, "Cell Membrane," can be found under http://www.ncnr.nist.gov/programs/reflect/cnbt/

[182] J. Arimatti, Lateral Heterogeneity in Model Membranes - Inducements and Effects, phD Thesis, University of Helsinki, **2001**.

[183] R. Garrett, C. Grisham, *Biochemistry*, Brooks Cole, **1999**.

[184] J. M. Boon, B. D. Smith, *Medicinal Research Reviews* **2002**, *22*, 251-281.

[185] R. Stoenescu, W. Meier, *Chemical Communications* **2002**, 3016-3017.

[186] R. Stoenescu, A. Graff, W. Meier, *Macromolecular Bioscience* **2004**, *4*, 930-935.

[187] H. Kukula, H. Schlaad, J. Falkenhagen, R.-P. Krueger, *Macromolecules* **2002**, *35*, 7157-7160.

[188] H. Schlaad, H. Kukula, J. Rudloff, I. Below, *Macromolecules* **2001**, *34*, 4302-4304.

[189] C. Ladavière, N. Dörr, J. P. Claverie, *Macromolecules* **2001**, *34*, 5370-5372.

[190] R. Borsali, R. Pecora, W. Burchard, in *Soft Matter Characterization*, Springer Netherlands, **2008**, pp. 463-603.

[191] W. Schärtl, *Light Scattering from Polymer Solutions and Nanoparticle Dispersions*, Springer Laboratory, **2007**.

[192] M. Antonietti, S. Förster, *Advanced Materials* **2003**, *15*, 1323-1333.

[193] M. Gradzielski, *Current Opinion in Colloid & Interface Science* **2003**, *8*, 337-345.

[194] M. Heskins, J. E. Guillet, *journal of Macromolecular Science, Part A: Pure and Applied Chemistry* **1968**, *2*, 1441 - 1455.

[195] K. Skrabania, L. Wen, A. Laschewsky, *Macromolecular Chemistry and Physics* **2008**, *209*, 1389-1403.

[196] D. Roy, J. N. Cambre, B. S. Sumerlin, *Chemical Communications* **2009**, *16*, 2106-2108.

[197] L. Guiying, G. Lei, M. Songmei, *Journal of Applied Polymer Science* **2009**, *113*, 1364-1368.

[198] C. Wu, X. Wang, *Physical Review Letters* **1998**, *80*, 4092.

[199] S. Elgavish, B. Shaanan, *Trends in Biochemical Sciences* **1997**, *22*, 462-467.

[200] A. Varki, *Essentials of Glycobiology*, Cold Spring Harbor Laboratory Press, Cold Spring Harbor, N.Y., **2009**.

[201] T. K. Dam, R. Roy, S. K. Das, S. Oscarson, C. F. Brewer, *The Journal of Biological Chemistry* **2000**, *275*, 14223-14230.

[202] J. C. Sacchettini, L. G. Baum, C. F. Brewer, *Biochemistry* **2001**, *40*, 3009-3015.

[203] W. I. Weis, K. Drickamer, *Annual Reviews of Biochemistry* **1996**, *65*, 441-473.

[204] J. J. Lundquist, E. J. Toone, *Chemical Reviews* **2002**, *102*, 555-578.

[205] J. Voskuhl, M. C. A. Stuart, B. J. Ravoo, *Chemistry – A European Journal* **2010**, *16*, 2790-2796.

[206] H.-K. Lee, K. M. Park, Y. J. Jeon, D. Kim, D. H. Oh, H. S. Kim, C. K. Park, K. Kim, *Journal of the American Chemical Society* **2005**, *127*, 5006-5007.

[207] V. P. Torchilin, *Nature Reviews Drug Discovery* **2005**, *4*, 145-160.

[208] B. G. De Geest, N. N. Sanders, G. B. Sukhorukov, J. Demeester, S. C. De Smedt, *Chemical Society Reviews* **2007**, *36*, 636-649.

[209] D. E. Discher, F. Ahmed, *Annual Review of Biomedical Engineering* **2006**, *8*, 323-341.

[210] B. Ratner, *Biomaterial Science: An Introduction to Materials in Medecine*, Academic Press, **2004**.

[211] A. Taubert, E. Furrer, W. Meier, *Chemical Communications* **2004**, 2170-2171.

[212] W. H. Daly, D. Poché, *Tetrahedron Letters* **1988**, *29*, 5859-5862.

[213] A.-L. Kjøniksen, B. Nyström, H. Tenhu, *Colloids and Surfaces A: Physicochemical and Engineering Aspects* **2003**, *228*, 75-83.

[214] R. Motokawa, K. Morishita, S. Koizumi, T. Nakahira, M. Annaka, *Macromolecules* **2005**, *38*, 5748-5760.

[215] J. Yan, W. Ji, E. Chen, Z. Li, D. Liang, *Macromolecules* **2008**, *41*, 4908-4913.

[216] N. N. Ana, G. V. Nikolay, P. N. Christo, V. B. Iliyana, *Journal of Polymer Science Part A: Polymer Chemistry* **2004**, *42*, 5736-5744.

[217] M. D. C. Topp, P. J. Dijkstra, H. Talsma, J. Feijen, *Macromolecules* **1997**, *30*, 8518-8520.

[218] X. Huang, F. Du, J. Cheng, Y. Dong, D. Liang, S. Ji, S.-S. Lin, Z. Li, *Macromolecules* **2009**, *42*, 783-790.

[219] A. De Marre, K. Hoste, D. Bruneel, E. Schacht, F. De Schryver, *Journal of Bioactive and Compatible Polymers* **1996**, *11*, 85-99.

[220] J. Marc Duval, C. Delestre, M.-C. Carré, P. Hubert, E. Dellacherie, *Carbohydrate Polymers* **1991**, *15*, 233-242.

[221] K. Hoste, D. Bruneel, A. D. Marre, F. D. Schrijver, E. Schacht, *Macromolecular Rapid Communications* **1994**, *15*, 697-704.

[222] K. A. Simon, P. Sejwal, R. B. Gerecht, Y.-Y. Luk, *Langmuir* **2006**, *23*, 1453-1458.

[223] L. Wu, J. Lal, K. A. Simon, E. A. Burton, Y.-Y. Luk, *Journal of the American Chemical Society* **2009**, *131*, 7430-7443.

[224] L. Ould-Kaddour, C. Strazielle, *Polymer* **1992**, *33*, 899-908.

[225] K. Edelmann, M. Janich, E. Hoinkis, W. Pyckhout-Hintzen, S. Höring, *Macromolecular Chemistry and Physics* **2001**, *202*, 1638-1644.

[226] Z. Lei, L. Zhang, *Colloids and Surfaces A: Physicochemical and Engineering Aspects* **2008**, *312*, 166-171.

[227] E. Haustein, P. Schwille, in *Soft Matter Characterization*, Springer Netherlands, **2008**, pp. 637-675-675.

Declaration/Erklärung

I herewith declare that I have made this existing work single-handedly. I have only used the stated utilities and references.

Ich erkläre hiermit, dass ich die vorliegende Dissertation selbst verfasst habe und keine anderen als die angegebenen Quellen und Hilfsmittel benutzt habe.

Potsdam, Mai 2011

Clara Valverde Serrano

Acknowledgments

Zoe, Alfonso, Filipe, Hiro, Robin, Jéjé, Camillo, Li, Yael, Silke, Nicole, Caro, Cécile, Yuan, Nicola, Micha, Johannes, Dim, Caro, John, Marek, Daniel Pussak, Camillo's electric expresso …and a long etcetera.

To my friends in Berlin for their infinite patience over my "I'm too tired" sentence and for the music-related fun and to the brunch crew (Boitel, Steffan, Jana, ♥**Dana** ♥, Kazka, Sonne, Asja).

I would like to thank my father, my sister and my mother for their support along the years even when I took decisions that they could not understand. Last I would like to thank my grandmother to whom I would also like to dedicate this work, may all that wax not have burnt in vain. You are a model of intelligence, strength and generosity and I admire and love you dearly for it.

Me gustaría agradecer a mi padre, mi hermana y a mi madre su apoyo a lo largo de los años, incluso cuando he tomado decisiones que no siempre han sido fáciles de entender, os quiero. Y ya por último me gustaría dar la gracias a mi abuela, a quien también quisiera dedicar este trabajo, espero que toda esa cera no se haya quemado en vano. Eres un modelo de inteligencia, fuerza y generosidad, y por ello te quiero y admiro profundamente.

Clara.